Review Article

SCC Publishing
Michelets vei 8 B
1366 Lysaker Norway

ISSN: 2703-9072

Correspondence:
patrice.poyet.science@gmail.com

Vol. 5.3 (2025)
pp. 135-185

Revisiting the Carbon Cycle

Camille Veyres[1], Jean-Claude Maurin[2], Patrice Poyet[3]

[1]Engineer, [2]Professor of Physics, [3]Docteur d'État ès Sciences

Abstract

The stock-to-outflow ratio of CO_2 molecules in the atmosphere is about five years. Accordingly, only about 5.5% of the atmospheric CO_2 stock comes from fossil fuel emissions not yet absorbed by vegetation or oceans, while 94.5% originates from natural outgassing of oceans and soils. This interpretation is supported by the $\delta^{13}C$ record at Mauna Loa Observatory (MLO). The 50% increase in vegetation productivity since 1900 can be attributed to higher atmospheric CO_2 concentrations and a longer growing season. Decarbonization policies may therefore affect only 5.5% of atmospheric CO_2. Moreover, the strong month-by-month correlation, over nearly 800 months, between the increments of the CO_2 stock at MLO (altitude 3.4 km) and the sea-surface temperature (SST) anomaly in the inter-tropical zone shows that 94.5% of atmospheric CO_2 reflects the time-integrated effect of past surface temperatures, themselves determined by surface insolation. ARIMA time-series modeling further supports the correlation between 12-month increments of MLO CO_2 and SST. By contrast, there is no correlation ($R^2 = 0.01$) between the detrended 12-month CO_2 increments and fossil-fuel emissions. Simple models of carbon fluxes and stocks for the oceans, atmosphere, and vegetation & soils, assuming ocean degassing driven by inter-tropical SST, reproduce the observed time series atmospheric CO_2, $\delta^{13}C$ and vegetation productivity since 1900. In this context, IPCC theories and models based on concepts such as the Airborne Fraction, the Bern function, an adjustment time, the supposed persistence of 15–50% of fossil emissions in the atmosphere after 1000 years, a bottleneck between atmosphere and ocean, very low fluxes between surface and deep ocean, and Revelle's buffer factor, appear to be misleading constructs.

Keywords: Climate; CO_2; carbon cycle; ARIMA; ocean out-gassing; ^{13}C; ^{14}C; airborne fraction; Bern function; simple carbon cycle models

Submitted 2025-08-26, Accepted 2025-11-13. https://doi.org/10.53234/scc202510/10

1. Introduction

This contribution follows on from several important articles on the carbon cycle that have given rise to argumentative discussions (Salby & Harde, 2021a, 2021b, 2022a, 2022b; Berry, 2021; Harde, 2017, 2019; Köhler et al., 2018), after (Beenstock et al., 2012; Cawley, 2011; Essenhigh, 2009; Hocker, 2010; Pretis & Hendry, 2013). It incorporates results from (Campbell et al., 2017; Haverd et al., 2020; Koutsoyiannis, 2024a, 2024b; Lai et al., 2024; Levy et al., 2013; Segalstad, 1998) and of (Munshi, 2015, 2016a, 2016b, 2016c, 2017). A complete list of symbols and abbreviations used in this paper is provided in Appendix A.

2. Water, Carbon and Latent and Sensible Heat Cycles

Differences in insolation and temperature between the inter-tropical zone and the high latitudes result in the transfer of latent heat (evaporation, then condensation) and sensible heat (water, water

vapor and CO_2) from the warm surface oceans to the cold surface oceans and to the continents, thanks to the turbulent motion of air and of surface oceans; the ocean is the main reservoir of water, of mobile carbon and of heat. The partial pressure of CO_2 in seawater varies as the power of 12.5 of the absolute temperature (in Kelvin) of this water (Sec. 8) and, for the same quantity of inorganic carbon per kg of seawater is, at 32°C, about 3.2 times greater than at 5°C. The contrast in sea surface temperatures means that there is an oceanic carbon degassing zone and an absorption zone separated by several thousand kilometers.

These out-gassing and absorption of the order of 100 Gt-C/yr between the atmosphere and the surface oceans are extensions of fluxes between the surface ocean and the deep ocean, as expressed by (Levy et al., 2013): "*We find that climatological physical fluxes of dissolved inorganic carbon (DIC) are two orders of magnitude larger than the other carbon fluxes and vary over the globe at smaller spatial scale. At temperate latitudes, the subduction of DIC and to a much lesser extent (< 10%) the sinking of particles maintain CO_2 undersaturation, whereas DIC is obducted back to the surface in the tropical band (75%) and Southern Ocean (25%). At the global scale, these two large counter-balancing fluxes of DIC amount to +275.5 Gt-C/yr for the supply by obduction and –264.5 Gt-C/yr for the removal by subduction which is 3 to 5 times larger than previous estimates*". These fluxes maintain the under-saturation or the supersaturation of surface seawater with respect to the air. These 275 Gt-C/yr have (finally!) been taken up by IPCC AR6 WG1, (Fig. 5.12, p. 700).

For a reservoir, as for a bank account, the inflow over 12 months equals the sum of the outflow and the change in the reservoir's content over that period. For atmospheric CO_2, the outflow is taken as one-fifth of the stock, consistent with the IPCC's estimate of a mean residence time of roughly 5 years (≈ 5 yr when the biospheric outflow is taken as NPP = GPP/2, versus ≈ 4 yr when using GPP, here GPP denotes gross primary production, i.e. total photosynthetic uptake before vegetation respiration): the natural degassing is therefore:

$$\text{degas}(t) = \frac{X(t)}{5\ yr} + \frac{\mathrm{d}X(t)}{\mathrm{d}t} - f_{\text{fossil}}, \text{ i.e. in ppm} \quad (1)$$

thus: 315/5 + 1 – 1 = 63 ppm/year in 1959 and 425/5 + 3.3 – 5 = 83.3 ppm/year in 2024. Over 66 years, +20.5 ppm/year for natural degassing versus +4 ppm/year for the inflow from fossil fuels; end 2024: 83.3 / (83.3 + 5) = 94.3% is the contribution of the natural degassing to the total inflow.

3. Tropical SSTs (20°S–20°N) Account for 83% of Post-1958 CO_2 Growth

The autotrophic respiration of plants is invisible from observatories at Mauna Loa (altitude 3397 m) or at South Pole (altitude 2837 m) far from any vegetation; at the surface on land 24-hour fluctuations in CO_2 air content of up to 100 ppm are common, e.g. in July in Luxembourg (Massen et al., 2005; Massen & Beck, 2011) with a diurnal minimum and a nocturnal maximum.

Table 1: The stock-to-outflow ratio, $X(t)$/absorb(t), has been about five years since pre-industrial times.

Carbon flows in Gt-C/year and atmospheric stocks in Gt-C			
	Pre-industrial	1990	2024
Absorption by ocean, i.e. $\text{absorb}_{\text{oce}}$	70 (IPCC, 2007)	92 (IPCC, 2007)	103
Absorption by vegetation, i.e. $\text{absorb}_{\text{veg}}$	50 (Haverd et al., 2020)	61 (IPCC, 2007)	77 (Lai et al., 2024), 73 in 2016 (Haverd et al., 2020)
Atmospheric stock Gt-C (ppm in air), i.e. X(t)	590 ? (278 ppm ?)	754 (356 ppm)	902 (425.3 ppm)
Stock-to-outflow ratio, i.e. $X(t)$ / absorb (t)	4.9 years	4.9 years	5 years

The area between 20°S and 20°N is three-quarters oceanic. Fig. 7.3.5 of (IPCC, 2007) for the year 1990 (360 ppm at MLO) and for the pre-industrial period suggests an average residence time of

a CO_2 molecule in the atmosphere of about 5 years, i.e. a half-life of 3.5 years, since each year 20% of the CO_2 in the atmosphere is absorbed. IPCC (2001) §1.3 suggests a net carbon uptake by vegetation NPP (Net Primary Productivity) of the order of GPP/2, where GPP is Gross Primary Productivity. Haverd et al. (2020) estimate global GPP at 104 Gt-C/yr in 1900 and 146 Gt-C/yr in 2016, hence a "pre-industrial" NPP of 50 Gt-C/yr, 52 Gt-C/yr in 1900, 63 Gt-C/yr in 1990 and 73 Gt-C/yr in 2016, and according to Lai et al. (2024) 77 Gt-C/yr recently. These indications overlap with those of (Donohue et al., 2013; H. D. Graven et al., 2013; Nemani et al., 2003; Pretzsch et al., 2014; Zhu et al., 2016). Cawley (2011) adopts 5 years as did Essenhigh (2009) and Bolin (1960).

The total mass $X(t) = X_{natural}(t) + X_{fossil}(t)$ of carbon in the air, solution of $dX(t)/dt = f(t) - X(t)/5yr$, where $f(t)$ is the sum of the $f_{fossil}(t)$ in-flux from fossil fuels and of the $f_{natural}(t)$ in-flux from natural out-gassing by oceans and soils. This differential equation is linear, hence:

$$\frac{dX_{\text{fossil}}(t)}{\mathrm{d}t} = f_{\text{fossil}}(t) - \frac{X_{\text{fossil}}(t)}{5\ yr} \tag{2}$$

$$X_{\text{fossil}}(t) = \int_{t_0}^{t} e^{\frac{-(t-t')}{5}} f_{\text{fossil}}(t')dt' \tag{3}$$

$$X_{\text{natural}}(t) = X(t) - X_{\text{fossil}}(t) \tag{4}$$

where $X(t)$ is based on X_{MLO}, series measured at the Mauna Loa Observatory since March 1958. Although $f_{natural}(t)$ is poorly known, $X_{natural}(t)$ is the difference between two precisely known quantities.

$f_{fossil}(t)$ comes from economic series: the CDIAC dataset (Boden et al., 2013) from 1751 to 2010 and, since 1965, the BP Statistical Review of World Energy (British Petroleum, annual editions) (with values increased by 5% to account for cement production), adjusted so as to coincide with the last 45 years of CDIAC. Emissions for a given year are dated to the middle of that year (e.g. emissions of the year 2020, recorded at date 2021.0, are to be dated 2020.5) or interpolated month by month between the dates 2020 and 2021. A +/– 5% seasonal modulation may be added (see carbonmonitor.org).

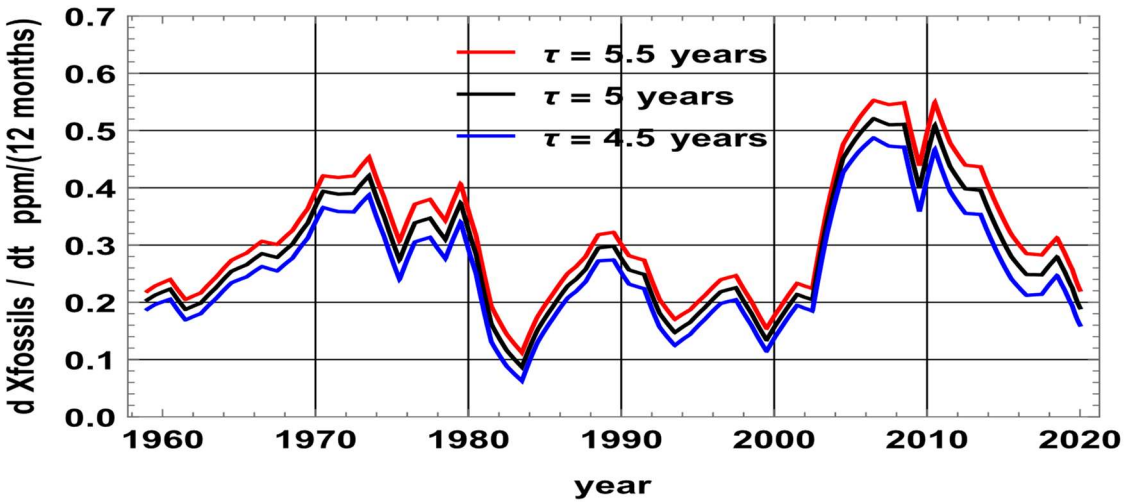

Figure 1: Anthropogenic contribution $dX_{fossil}(t)/dt$ in ppm/yr to the annual atmospheric CO_2 increase computed for three residence times τ of the carbon dioxide in the atmosphere: 5.5 years, 5 years and 4.5 years.

Figure 1 shows that carbon dioxide atmospheric residence times of 4.5 years or 5.5 years have almost no effect on the increments $dX_{fossil}(t)/dt$, which differ by less than 0.1 ppm / (12 months). Uncertainty over lifetime will therefore have little effect on the calculation of:

$$\frac{dX_{\text{natural}}(t)}{dt} = \frac{dX(t)}{dt} - \frac{dX_{\text{fossil}}(t)}{dt} \tag{5}$$

Figure 1 also shows the 1973-1974 crisis, the growth of natural gas in the 1980s and 1990s, and the growth of coal use in China and South-East Asia between 2000 and 2012; for the three lifetimes 5.5, 5 and 4.5 years, the 1959-2020 averages of $dX_{\text{fossil}}(t)/dt$ are 0.315 ppm/year, 0.287 ppm/year and 0.26 ppm/year.

To de-seasonalize the variations in atmospheric stock $X(t)$, we take 12-month increments centered in the middle of the 12 months: $dX(t)/dt$ is close to $X(t + 6 \text{ months}) - X(t - 6 \text{ months})$. Figure 2 shows that the two stationary series MLO increments minus the fossil fuel stock increments (the black curve) and the blue curve[1] 3.17 (AT(t) + 0.25°C) where AT(t) is the sea surface temperature anomaly of the HadISST series between 20°S and 20°N correlate: between the dates 1958.7 and 2024.63, the correlation coefficient R of these series smoothed by a 3-month moving average is $R^2 = 0.795$, despite disturbances induced by several major volcanic eruptions (red curve in Figure 2) and a few mid-latitudes SST anomalies. Smoothing by a 12-month moving average yields $R^2 = 0.83$, but at the cost of losing some of the strength of the statistical test (Munshi, 2016c).

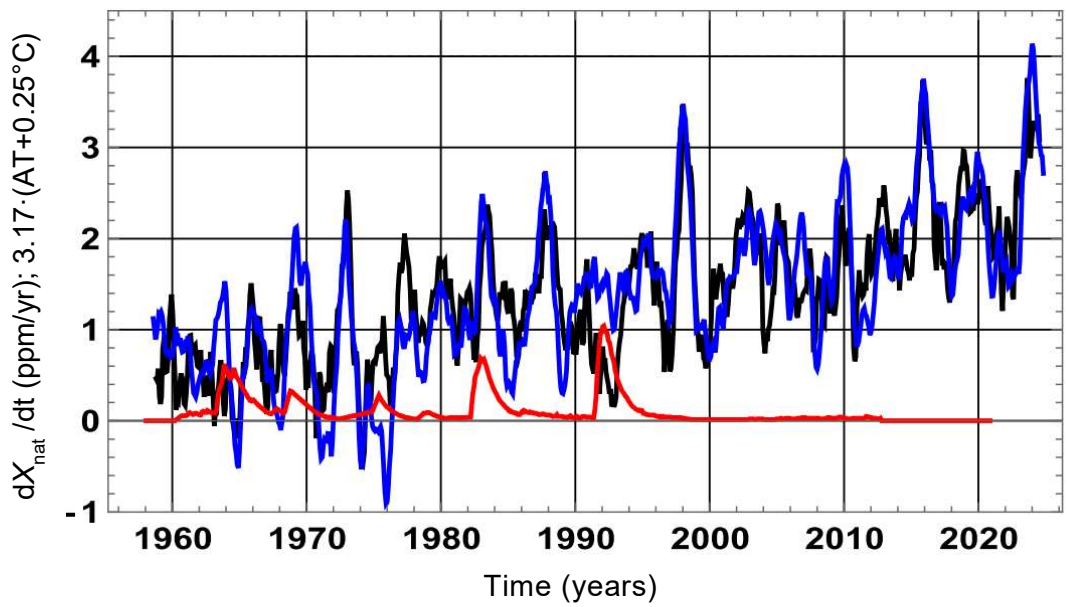

Figure 2: Black curve: increments $X_{natural}(t + 6 \text{ months}) - X_{natural}(t - 6 \text{ months})$ from the MLO series. Blue curve: 3.17 (AT(t) + 0.25°C) where AT(t) is the anomaly of the HadISST 20°S to 20°N series (Rayner et al., GRL), downloaded from knmi-climate explorer. The red curve shows 7× the stratospheric aerosol optical thickness at 550 nm, illustrating the cooling/insolation-reduction episodes associated with volcanic aerosols. Smoothing with a 3-month moving average has been applied. This figure independently confirms the relationship reported by Salby & Harde (2022a), i.e. see their Fig. 8.

Between those dates X_{MLO} went from 313.3 ppm to 422.9 ppm (+109.5 ppm), X_{fossil} from 4.6 to 22.9 (+18.4 ppm), the sum of the monthly natural increments (the black curve) is 91.2 ppm, and the sum of the temperature effects (blue curve) is 91.7 ppm. Contributions to the total increase of X_{MLO} are 16.7% (+18.4 ppm) for fossil fuel and 83.3%.for the Sea Surface Temperature controlled X_{natural} increase.

With the whole HadISST series 1870 to end of 2024 the addition of the 1860 monthly increments

[1] This coefficient is the result of the ratio between the variation in the growth rate and the corresponding variation in temperature: 3.17 = Δ (increment over 12 months) / Δ temperature. An extended discussion of how the parameters of this type of equation are obtained is available in Maurin (2022), see Figure 3d.

given by: 3.17 (AT_{SST} + 0.25°C) is 122.8 ppm, which added to the 280.2 ppm assumed at t = 1870 derived from a logistic approximation of observations at MLO:

$$X_{MLOlogis}(t) = 275 + \frac{555.7}{1 + e^{\frac{(2067-t)}{42.2\,yr}}} \quad \text{in ppm} \tag{6}$$

and to the 23 ppm from fossil fuels yields the 426 ppm observed at MLO at time 2025.0. The discrepancies between the blue and black curves of Figure 2 are small compared with the seasonal fluctuations, which at MLO are +9 ppm between September and April and –7 ppm from May to September.

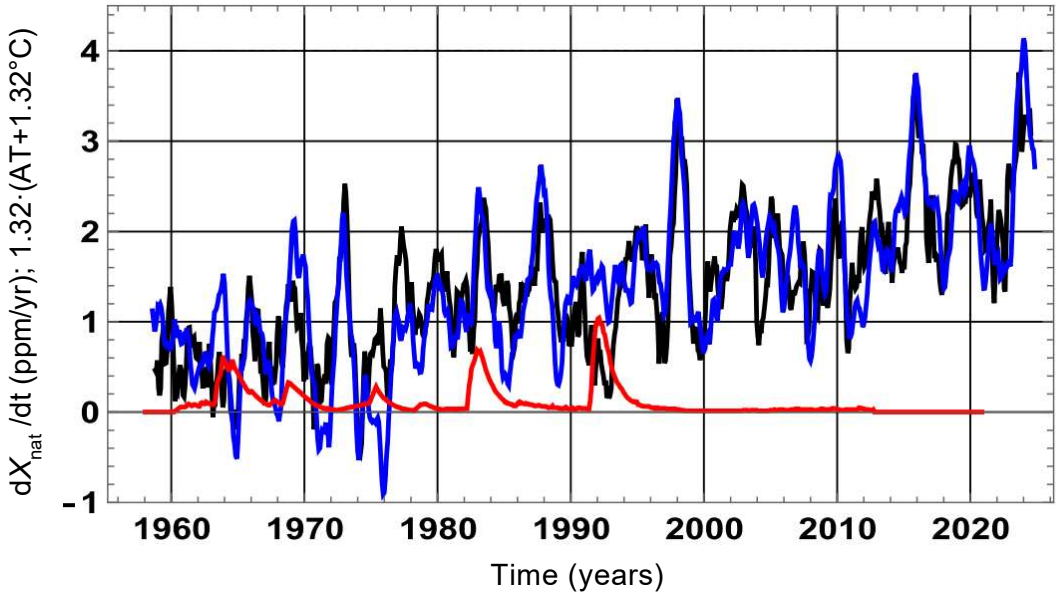

Figure 3: As in Figure 2, but the blue curve here is 1.321 (AT(t) + 1.318°C), with AT(t) anomaly of the temperatures in the lower inter-tropical troposphere UAH MSU series starting in December 1978. No smoothing applied.

With the UAH (University of Alabama in Huntsville) MSU (Microwave Sounding Unit) lower-troposphere temperature anomaly series for the inter-tropical band (20° S–20° N) (Spencer et al., 2017) UAH Version 6.0, shown here un-smoothed in Figure 3 , the correlation coefficient is R^2 = 0.66 and R^2 = 0.75 with a 4-month moving average. See also (Hocker, 2010). Between 1978.9 and 2024.0, the integral of the blue curve gives 77.3 ppm, added to the +12.6 ppm increase in the anthropogenic stock, is 89.9 ppm, close to the +90.5 ppm observed at MLO.

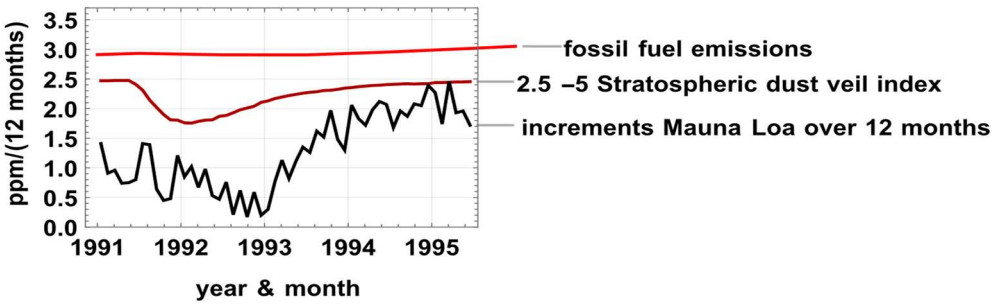

Figure 4: Top red curve: $f_{fossil}(t)$ emissions in ppm/year. Bister (brownish) curve: 2 – 5 × stratospheric dust veil index. Black curve: ppm increments at MLO: 0.5 ppm/(12 months) during the 9 months centred on October 1992 and 2.2 ppm/(12 months) during the 9 months centred on October 1994.

Figure 4 underlines the role of sea surface temperatures: from 1991 to end 1995, anthropogenic

emissions were constant, but the 12-month increments of $X_{MLO}(t)$ were 0.48 ppm/(12 months) over the 9 months centered on October 1992 (the eruption of Mount Pinatubo occurred in 1991), four times less than the 2.1 ppm/(12 months) over the 9 months centered on October 1994, after the end of the cooling brought by volcanic dust, which may have reduced inter-tropical out-gassing and increased mid-latitude absorption.

4. No Correlation Between Anthropogenic Emissions and $X(t)$ Increments

$f_{fossil}(t)$ may be approximated by $f_{logis}(t)$ = 17.92 Gt-C/yr / (1 + exp((2011–t)/29 yr)) and over 1950-2024 by $f_{fossil\ linear}$(t) = 1.39 Gt-C/yr + 0.118 (–1950+ t) = 0.1183 (t – 1938.23) Gt-C/yr, that is a linear trend b = +0.056 ppm/yr. With linearly increasing emissions $b\ (t - t_0)$, a residence time of τ = 5 years for CO_2 molecules, $t - t_0$ large enough for $X\ (t_0)\ \exp(-\ (t-t_0)\ /\tau)$ to be negligible, $X_{fossil}(t)$ is:

$$\int_{t_0}^{t} b\,(t' - t_0)\, e^{\frac{-(t-t')}{\tau}} \mathrm{d}t' = \tau \cdot b\left(t - t_0 - \tau + \tau \cdot e^{\frac{-(t-t_0)}{\tau}}\right) \approx \tau \cdot b \cdot (t - t_0 - \tau) \qquad (7)$$

The increment $X_{fossil}(t) - X_{fossil}(t–1)$ is $\tau \cdot b$ = 5 yr · 0.056 ppm/yr = 0.28 ppm or 0.59 Gt-C, this is the difference between the emissions of year t and those of year t – 5 yr.

The grey curve in Figure 5 shows the 12-month increments of $X_{MLO}(t)$ observed since 1958; their average after 1995 is + 2.2 ppm/year, 7.9 times the + 0.28 ppm/year growth of the stock from fuels (average of the lower black curve of Figure 5).

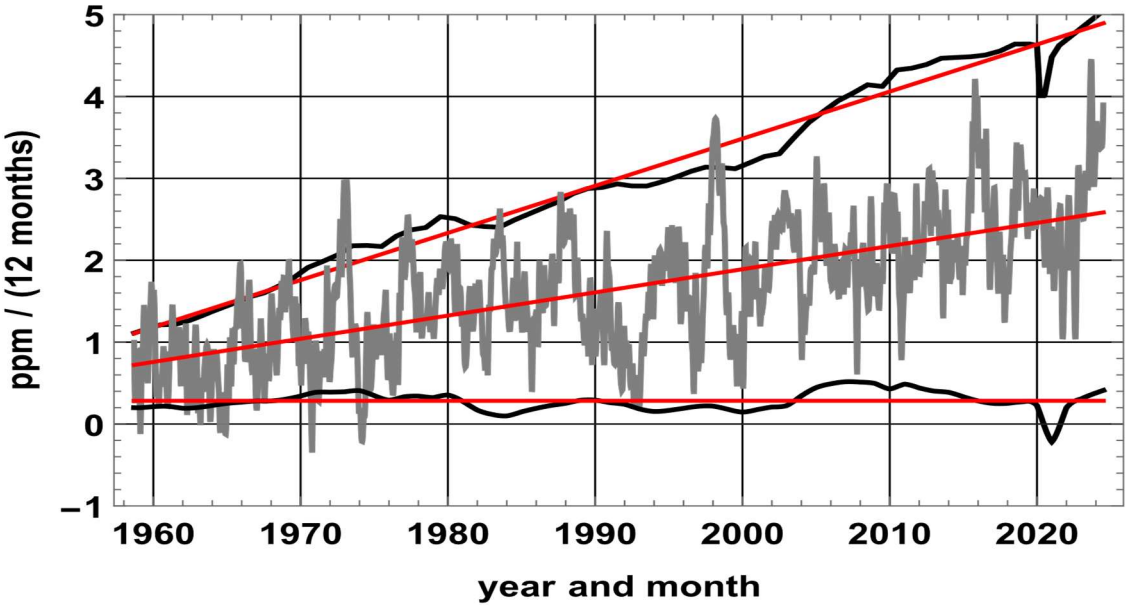

Figure 5: From top to bottom, in ppm/(12 months): series of emissions from fossil fuels and cement plants (in black, an in-flow), series of ppm increments at MLO (in grey) and in black at bottom the time series of atmospheric stock increments $dX_{fossil}(t)/dt$ from fossil fuels and cement plants; the red lines are the linear trends in ppm with t=date: emissions from fossil fuels and cement plants = 0.0575 (t – 1939.45); increases in ppm at MLO = 2.57 – 0.028 (2024 – t); increases in atmospheric stocks dXfossil(t)/dt =0.283 + 0.000013 (t – 1959).

A correlation can be sought only between weakly stationary series; to make a series stationary it may be derived with respect to time or its linear trend may be subtracted (Munshi, 2015, 2017; Podobnik & Stanley, 2008); Figure 6 shows the non-correlation between the series of the increments of annual averages of $X(t)$ and the series $f_{fossil}(t)$ after subtraction from each series of its linear trend: the coefficient of determination R^2 is 0.026!

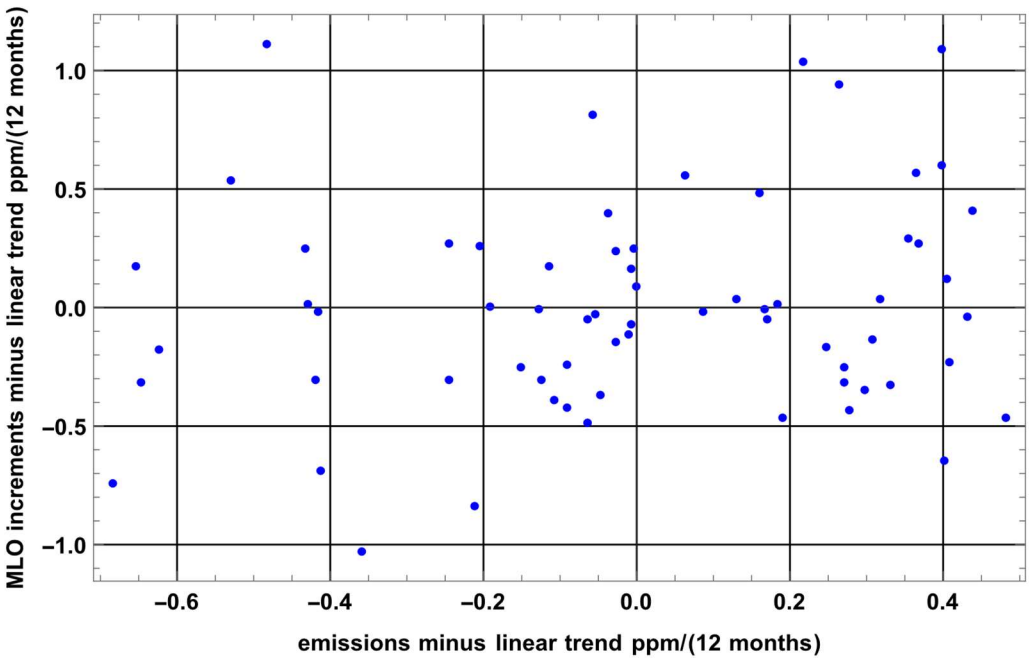

Figure 6: Correlation between the year-on-year increments of the annual means at MLO (vertical axis) and the annual emissions $f_{fossil}(t)$ (horizontal axis), on series made stationary by subtracting their linear trend (detrended series). Coefficient of determination $R^2 = 0.026$.

Munshi (2017) has shown that even with moving averages taken over 1, 2, 3, 4 and 5 years, the atmospheric CO_2 concentration is unresponsive to fossil fuel emissions. This is supported by the autocorrelations of the three series (Figure 7) fossil fuel emissions, increments $X_{MLO}(t + 6 \text{ months}) - X_{MLO}(t - 6 \text{ months})$ and inter-tropical sea surface temperatures anomaly.

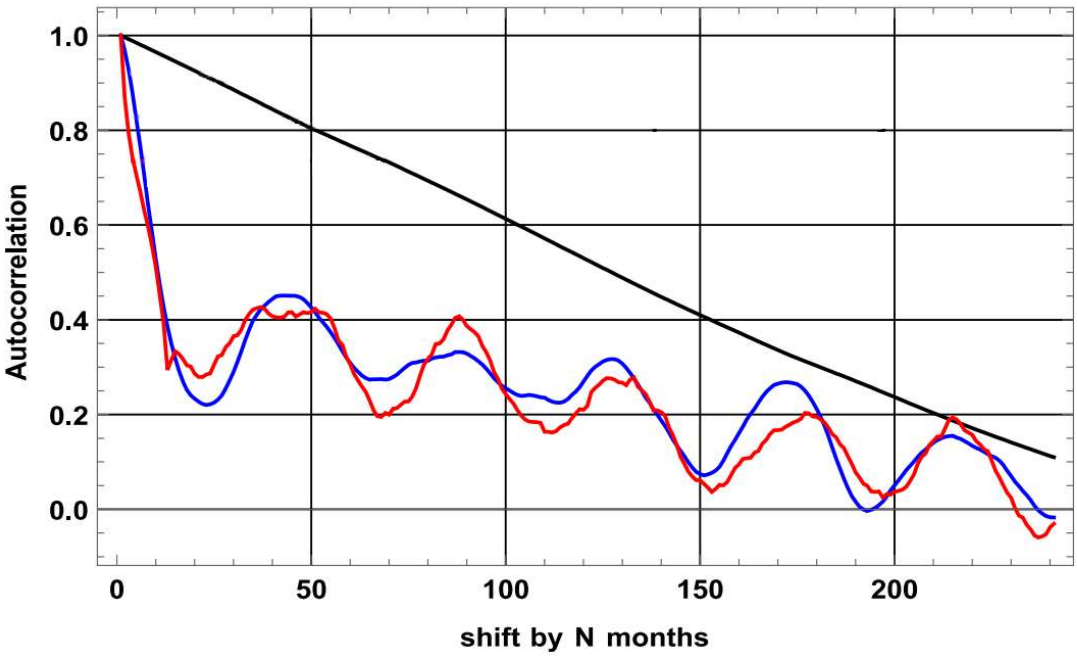

Figure 7: Autocorrelations of the three time series: fossil fuel emissions (black curve), sea surface temperature anomaly of the inter-tropical degassing zone (blue curve) and ppm increments at MLO (red curve) X(t + 6 months) – X(t – 6 months).

The uncertainties of the natural carbon fluxes (Table 1) are of the same order of magnitude as the fossil-fuel emissions. This alone should invite caution in drawing firm conclusions about the

partitioning of sources and sinks. In addition, some budget closures, such as the balanced flux diagram in (IPCC, 2013) Fig. 6.1, rely on inferred fluxes that are adjusted to satisfy mass balance. It introduces a logical circularity[2], since the agreement is partly imposed rather than independently demonstrated. Thus, because the IPCC budget relies in part on inferred fluxes that are adjusted to close the mass balance, the resulting equilibrium is imposed by construction. As a consequence, the reported carbon budget does not independently demonstrate the underlying dynamics.

5. ARIMA Time Series : $X(t)$, $\Delta X(t)$, $f_{fossil}(t)$, SST Anomalies

5.1 ARIMA Time Series

Understanding the dynamics of atmospheric CO_2 requires methods capable of distinguishing genuine causal structure from spurious correlations in trending data. In climatological and geophysical time series, non-stationarity and autocorrelation can easily produce misleading statistical relationships if not properly treated. Standard tools from econometrics and signal processing, including differencing, autocorrelation modeling, and ARIMA[3] (Autoregressive Integrated Moving Average) processes, are therefore essential for rigorous analysis of CO_2 records. These techniques explicitly account for persistence, serial dependence, and stochastic variability, ensuring that apparent associations are not artifacts of trend and memory in the data. Techniques for avoiding false correlations and for modeling time series are well known[4] e.g. (Maddala & Kim, 1998; Wolfram Research, 2012) and (Box et al., 2016).

Monthly CO_2 ppm series at MLO and SPO are ARIMA, I = 1. Modeling gives for SPO:

ARIMAProcess[0.109, {0.472, 0.079, 0.020, –0.126, –0.162, –0.177}, 1,{–0.478}, 0.042].

The equation for SPO is:

$(1 - L_1)\ (1 - 0.472\ L_1 - 0.079\ L_2 - 0.02\ L_3 + 0.126\ L_4 + 0.162\ L_5 + 0.177\ L_6)\ X(n) = 0.109 + e(n) - 0.478\ e(n-1)$

with Lm the shift operator by m months, $L(m)\ X(n) = X(n-m)$, e(n) a white noise of variance 0.042

Modeling gives for MLO:

ARIMAProcess[0.101, {0.772, –0.155, –0.219, –0.0248, –0.0129, –0.177}, 1, {–0.534}, 0.652]

Figure 8-a shows in blue and black the $X(t)$ series observed at MLO and SPO and their extensions, and as a curiosity, random draws in orange and red starting at the last historical point. Note that the increments $(1 - L_1)\,X(n) = X(n) - X(n-1)$ are ARMA stationary series.

Modeling MLO and SPO data as SARIMA, I=1, with seasonal variations gives for SPO: $(1-L_1)(1-L_{12})\,X(n) = 0.00096 + (1 - 0.222\ L_{12})\ e(n)$, e(n) of variance 0.057 and a close equivalent for MLO: those random walks are plotted in Figure 8-b with blue and black forecasts and illustrative, non-significant random draws starting at the last historical point.

---

[2] When a system of fluxes is adjusted so that inflows and outflows balance by definition, the resulting "closure" does not constitute independent empirical verification. It reflects a *tautology*: the conclusion (balanced fluxes) is embedded in the premise (fluxes are inferred and adjusted to balance). This corresponds to the classical logical fallacy *petitio principii*, assuming what one seeks to prove. True empirical validation requires that mass balance emerge from independently measured fluxes and stocks, rather than from parameters tuned so that the balance necessarily holds.

[3] The ARIMA framework (Box et al., 2016) generalizes autoregressive and moving-average models to non-stationary series via differencing. It is a standard tool in econometrics and geophysical data analysis to separate signal from trend-driven pseudo-correlation.

[4] An introduction is given here: https://en.wikipedia.org/wiki/Autoregressive_integrated_moving_average

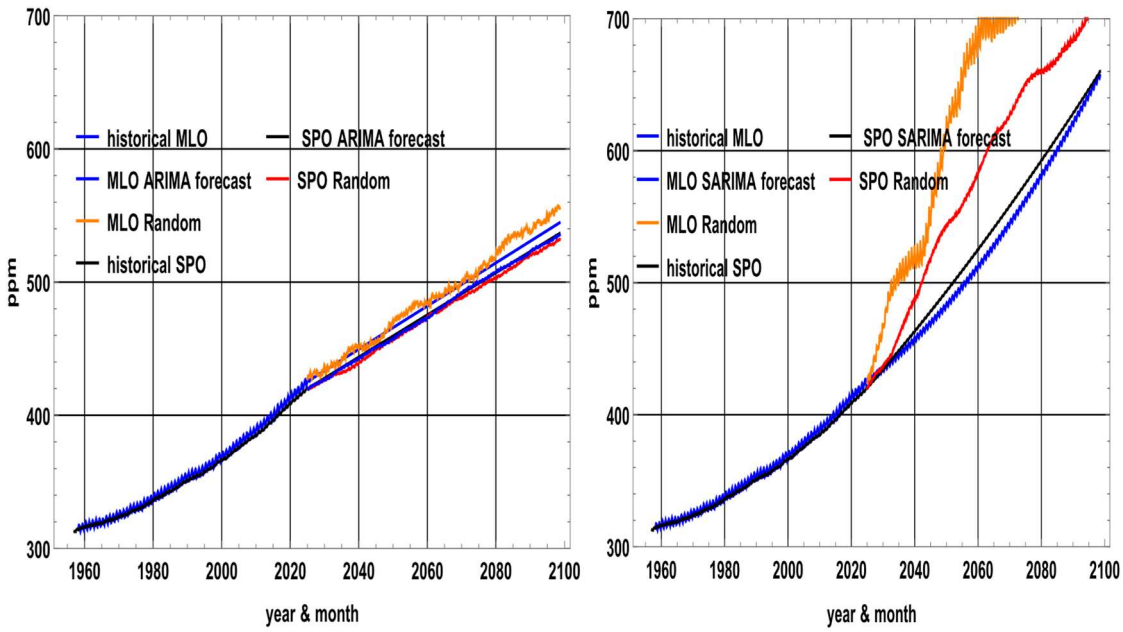

Figure 8 a-b: Historical time series, forecasts and illustrative random draws of no predictive value. a) left: X(t) series at MLO and SPO as ARIMA I=1; b) right: ditto as SARIMA I=1 with seasonal variations.

The series of increments X(t + 6 months) – X(t – 6 months) at MLO plotted on Figure 9-a is an autoregressive stationary moving average process ARMAProcess[0.214, {0.525, 0.346}, {0.255},0.162] that is $(1 - 0.525\ L_1 - 0.346\ L_2)\ X(n) = 0.214 + e(n) + 0.255\ e(n-1)$; the blue line forecast is the average of historical values; illustrative random draw is in orange.

Plotted in Figure 9-b are the annual emissions $f_{\text{fossil}}(t)$ since 1958; they are an I = 1, ARIMAProcess[0.124, {}, 1,{}, 0.0262] with e(n) of variance 0.026, $(1 - L_1)\ X(n) = 0.124 + e(n)$; plotted are a forecast, illustrative random draws from the last historical point and a logistic approximation of the series of emissions.

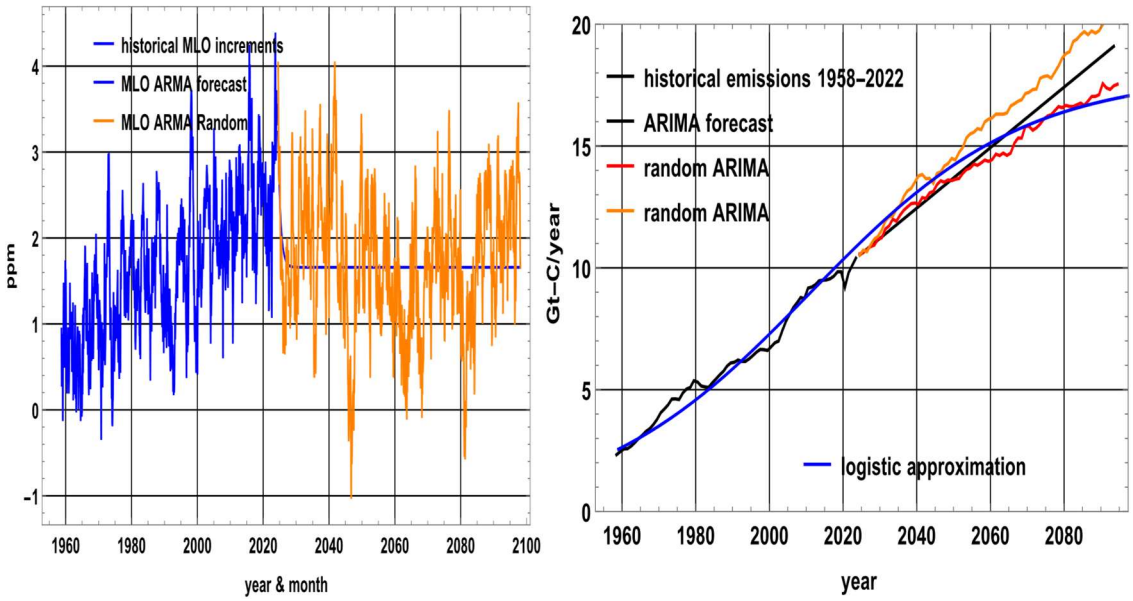

Figure 9 a-b: Historical time series, forecasts and illustrative random draws of no predictive value. a) left: series of the X(t) increments at MLO as ARMA; b) right: series of fossil fuel and cement emissions since 1958 (I=1) as ARIMA I=1 and a logistic approximation of the historical series.

The sea surface temperature (SST) anomaly between 20°S and 20°N (Figure 10-a since 1958 and 10-b since 1870, blue curve) is, since 1958 an ARMAProcess[–0.0, {0.971}, {–0.072, 0.051},

0.0053] with a strong correlation from one month to the previous month but is not a random walk. $AT_{SST}(n) = 0.971\ AT_{SST}(n–1) + e(n) – 0.072\ e(n–1) + 0.051\ e(n–2)$ with e(n) variance 0.0053.

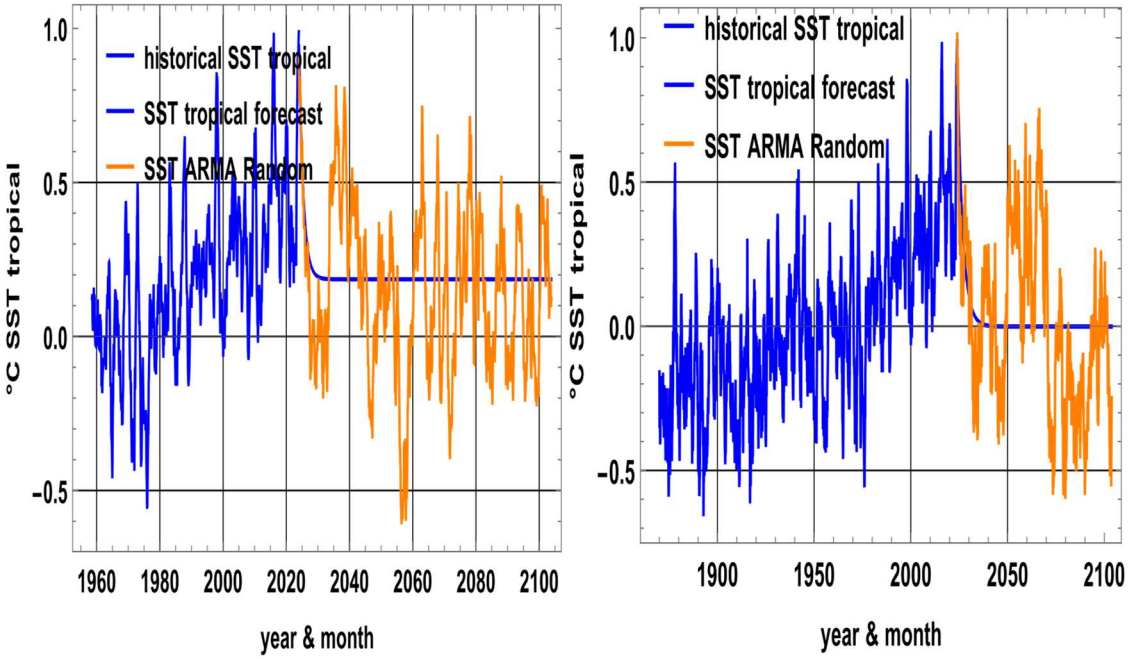

Figure 10 a-b: a) left: AT_{SST} temperature series as ARMA since mid-1958 with its "best forecast" (blue line) and illustrative random draws of no predictive value; b) right: AT_{SST} ARMA series since 1870 with best forecast (blue line) and illustrative random draws of no predictive value.

These exercises also show that the stationary series of CO_2 ppm increments (ARMA Figure 9-a) can be correlated with the stationary series of inter-tropical sea surface temperatures (Figure 2 and Figures 10-a-b) or with the inter-tropical lower troposphere temperature series (Figure 3), but not with the ARIMA I=1 series of fuel emissions (Figure 9-b) which must be detrended before a correlation with the stationary ARMA AT_{SST} anomaly series can be tested (Figure 6).

If the ppm increments at MLO were proportional to fossil fuel emissions, which are ARIMA with I = 1, then the sum of these increments, i.e. the ppm series, should be ARIMA with I = 2; but it is I =1 as seen on Figure 8-a. **The Airborne Fraction conjecture is therefore false**.

5.2 Conclusions

The equations:

$$\frac{\mathrm{d}X_{\mathrm{fossil}}(t)}{\mathrm{d}t} + \frac{X_{\mathrm{fossil}}(t)}{5\ yr} = f_{\mathrm{fossil}}(t) \tag{8}$$

$$\frac{\mathrm{d}X_{\mathrm{natural}}(t)}{\mathrm{d}t} = 3.17\ \mathrm{ppm/yr^2}(\mathrm{AT_{SST}}(t) + 0.25°\mathrm{C}) \tag{9}$$

$$X(t) = X_{\mathrm{natural}}(t) + X_{\mathrm{fossil}}(t) \tag{10}$$

reproduce the values observed at MLO. The computed and observed series since 1870 (the start of the temperature series) are plotted Figure 11. Taking into account the surface temperature series of the southern seas between 45°S and 60°S improves slightly the restitution of the observations.

X(*t*) in the atmosphere is therefore essentially the integral over the time of past inter-tropical temperatures, a consequence of these temperatures. Same conclusion was drawn by Salby & Harde (2022a).

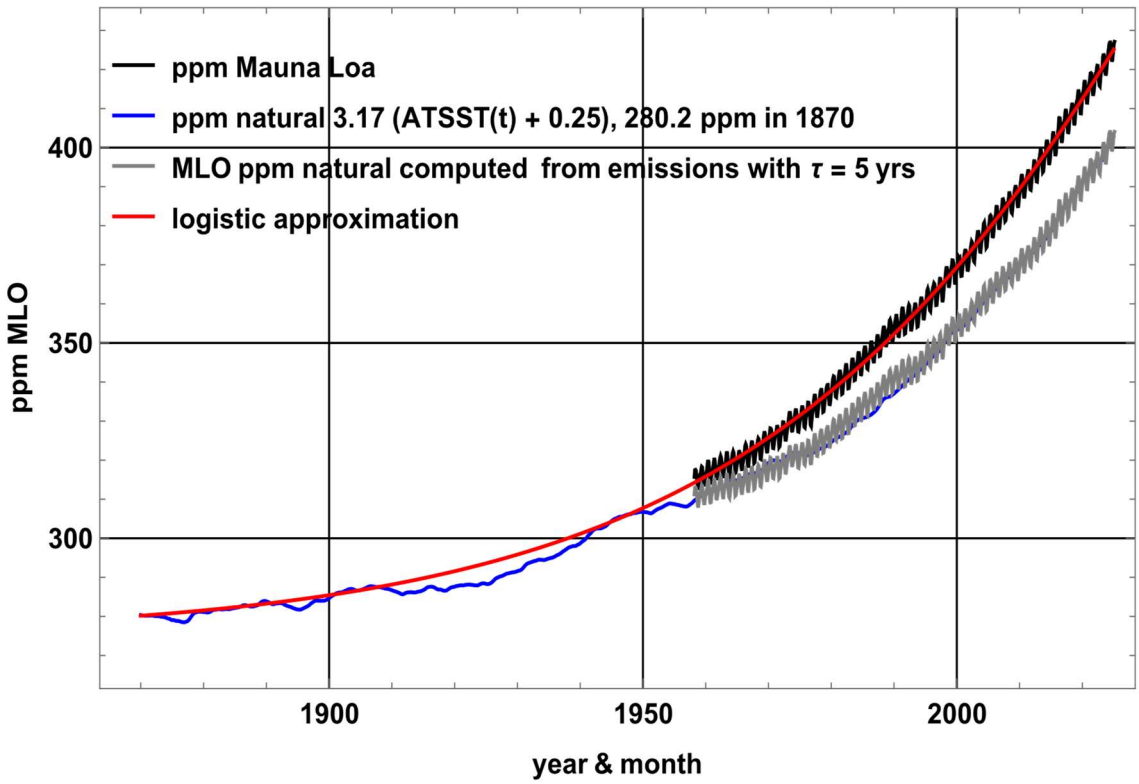

Figure 11: Comparison of MLO observations and of their logistic approximation (red curve) with the values (in blue) computed with the inter-tropical temperature series $AT_{SST}(t)$ and with $f_{fossil}(t)$ since 1870.

5.3 Some Misleading Tricks

5.3.1 Accumulations of Generally Positive Quantities

Two time series whose terms are accumulations of generally positive quantities always appear "visually" well correlated, even if these quantities are random. The effective sample size is reduced by the reuse of numbers, since the first number x1 is used n–1 times, x2 is used n–2 times...and the DF degrees of freedom become meaningless.

Let's quote Munshi (2016c): *"Therefore although strong correlation and regression coefficients can be computed from the time series of cumulative values, these statistics have no interpretation because they are illusory."* and *"Empirical evidence of the causal chain that links fossil fuel emissions to rising atmospheric CO_2 and a warming trend consists primarily of correlations between cumulative values (Kheshgi, 2005) (Canadell, 2007) (Botzen, 2008) (Brovkin, 2004) (Meinshausen, 2009) (Matthews, 2009) (Solomon, 2009) (Anderson, 2011) (Arora, 2011) (IPCC, 2007) (IPCC, 2014). However, this line of evidence is weakened by the spuriousness of correlations between cumulative values".*

Cumulative positive quantities can be seen, for example, in Fig. SPM. 10 (IPCC, 2021, p. 28), which claims that temperature is proportional to cumulative emissions (the starting point of this SPM 10 figure is probably 1876). Figure 12-a shows the HadCRUT4 series of monthly global temperature anomalies since 1850 (anomaly, i.e. in deviation from the mean of the same month taken over 1850-2025.0) versus cumulative emissions from fuels (horizontal axis), $R^2 = 0.86$.

This is a delusion: no correlation is possible between the emissions (not their cumulative values) and the annual temperature increments plotted in Figure 12-b right, $R^2 = 0.038$!

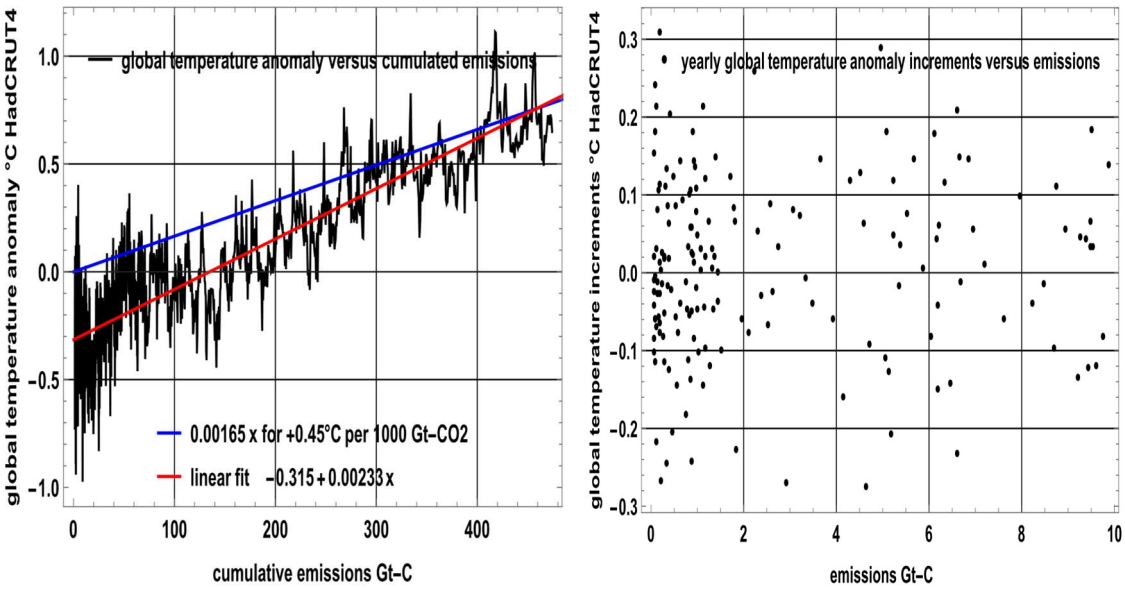

Figure 12 a-b: a) left: On the ordinate, a monthly global temperature anomaly HadCRUT4 since 1850, and on the abscissa, cumulative $f_{fossil}(t)$ emissions from oil, coal and gas and cement plants at the date of the temperature anomaly; the blue line shows the IPCC formula in Fig. SPM10. AR6 (IPCC, 2021): +0.45°C/1000 Gt-CO_2 (i.e. +2°C compared with the average over 1850-2024 for a cumulative 1212 Gt-C); the red line is a linear fit 0.00233 × – 0.315: it is 0°C in 1974.8 for a cumulative 135 Gt-C and +2°C for 991 Gt-C; b) right: Increments of the HadCRUT4 annual mean global temperature series (y-axis) and yearly emissions (x-axis): R = 0.038, i.e. no correlation.

Note in the IPCC accounting the importance of the LUC use (Land Use Changes), which before 1955 were far greater than the fossil fuel emissions (Figure 13-a), and of the choice of a starting date to give the impression of a "visual correlation": Figure 13-b begins in 1880 and looks better than Figure 12-a. Figures 12-a and 13-b are deceptive: a valid correlation can only be sought between the increments themselves (i.e. Figure 12-b), not between the cumulative values of the increments (Figures 12-a and 13-b)!

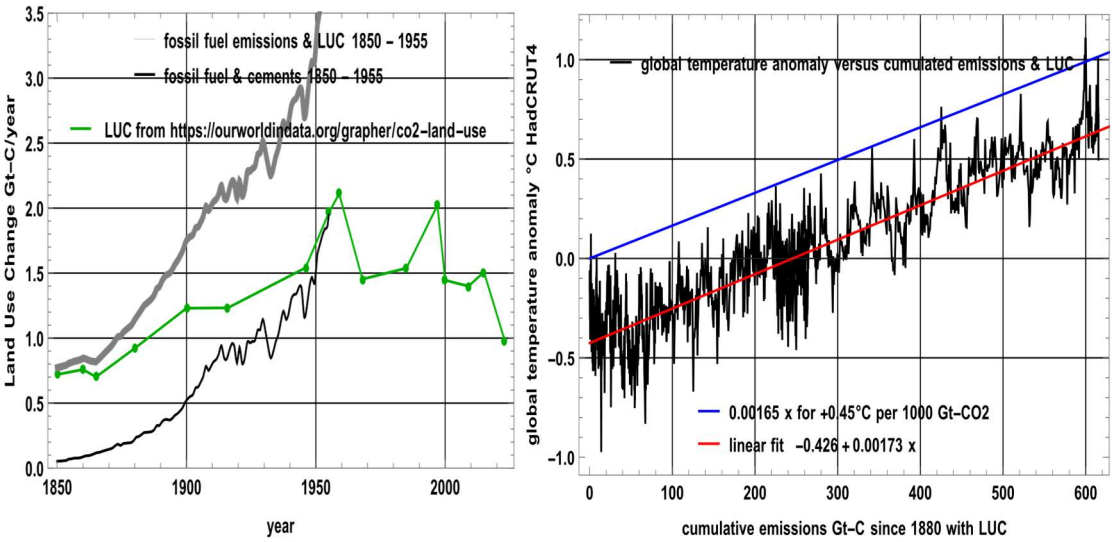

Figure 13 a-b: a) left: Comparison of a series of LUC (green curve) with $f_{fossil}(t)$ (bottom black curve) before 1955; the top grey curve is the sum of LUC(t) + $f_{fossil}(t)$ used by the IPCC; b) right: As Figure 12-a but starting in 1880 (to hide the positive temperature anomalies seen at the beginning of the series such as +0.07°C in December 1852 on Figure 12-a, and with the addition of LUC to $f_{fossil}(t)$; the red linear fit is close to the blue (IPCC, 2021) +0.45°C for cumulative emissions of 1000 Gt-CO_2.

5.3.2 Abusive Use of Smoothing by Moving Averages

Two straight lines seem perfectly correlated (but that makes no statistical sense!), hence the use of moving averages over several years to give an air of visual verisimilitude to a non-existent causality, to find for example in (Hansen et al., 2013) an "Airborne Fraction" of emissions that would have remained perpetually in the air and accounted for all the growth in atmospheric CO_2 since pre-industrial times. The effective number of Degrees of Freedom (DF), for a series of length n smoothed by a moving window of length w becomes[5]:

$$\mathrm{DF} = \frac{n^2}{(n - w + 1)w} - k \tag{11}$$

For a 60-year monthly series $n = 720$ and $w = 60$ (as often used for the Airborne Fraction), DF = 11 instead of 718. Beenstock et al. (2012) argued that regressions of global mean temperature on the logarithm of anthropogenic forcings lack statistical significance. For a discussion and subsequent exchange with Pretis & Hendry (2013), see Beenstock et al. (2013).

6. Carbon Cycle Calculations with Three Compartments

6.1 Stocks and Fluxes

Stocker et al. (2013) i.e. (IPCC, 2013) state that carbon stocks and fluxes are known with uncertainties on the order of ~20% or more. Let us assume the following carbon stocks: approximately 38,000 Gt-C in the oceans and about 2,400 Gt-C in vegetation and soils in 1995. We further assume that the annual fluxes to the atmosphere are proportional to these pools, with magnitudes equal to a fraction $1/\tau_{oc}(t)$ of the ocean reservoir and $1/\tau_{tb}$ of the terrestrial biosphere reservoir (i.e. vegetation and soils). To remain consistent with the flux values reported in Fig. 2.1 of IPCC (1995) AR2, we take $\tau_{tb} = 40$ years, since 2400/40 = 60 Gt-C yr^{-1}, and $\tau_{oc}(1995) = 413$ years, since 38000/413 ≈ 92 Gt-C yr^{-1}.

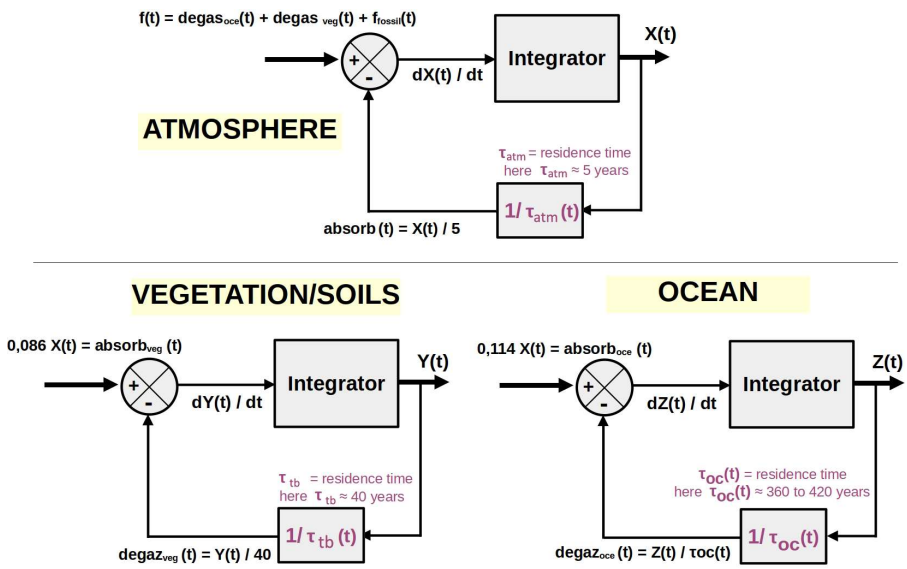

Figure 14: Diagram of exchanges between reservoirs with four flows expressed as a fraction of the stock of the transferring reservoir.

[5] The main term $n^2 / [(n - w + 1)\, w]$ gives the effective number of independent values after moving average smoothing. The "– k" corrects for parameters estimated from the series (typically $k = 1$ or 2). Thus k is the number of fitted parameters (e.g. mean or trend).

Furthermore, to align with Haverd et al. (2020), we assume that annual fluxes from the atmosphere to the ocean and to vegetation correspond to 11.4% and 8.6% of the atmospheric carbon stock, respectively (see observations in Figure 17).

Hence three coupled differential equations with given initial values $X(t_0)$, $Y(t_0)$, $Z(t_0)$:

$$\begin{aligned} X'^{(t)} &= \frac{-X(t)}{\tau_{\text{atm}}(t)} + \frac{Y(t)}{\tau_{\text{tb}}(t)} + \frac{Z(t)}{\tau_{\text{oc}}(t)} + f_{\text{fossil}}(t) \\ Y'^{(t)} &= \frac{-Y(t)}{\tau_{\text{tb}}(t)} + 0.086\, X(t) \\ Z'^{(t)} &= \frac{-Z(t)}{\tau_{\text{oc}}(t)} + 0.114\, X(t) \end{aligned} \tag{12}$$

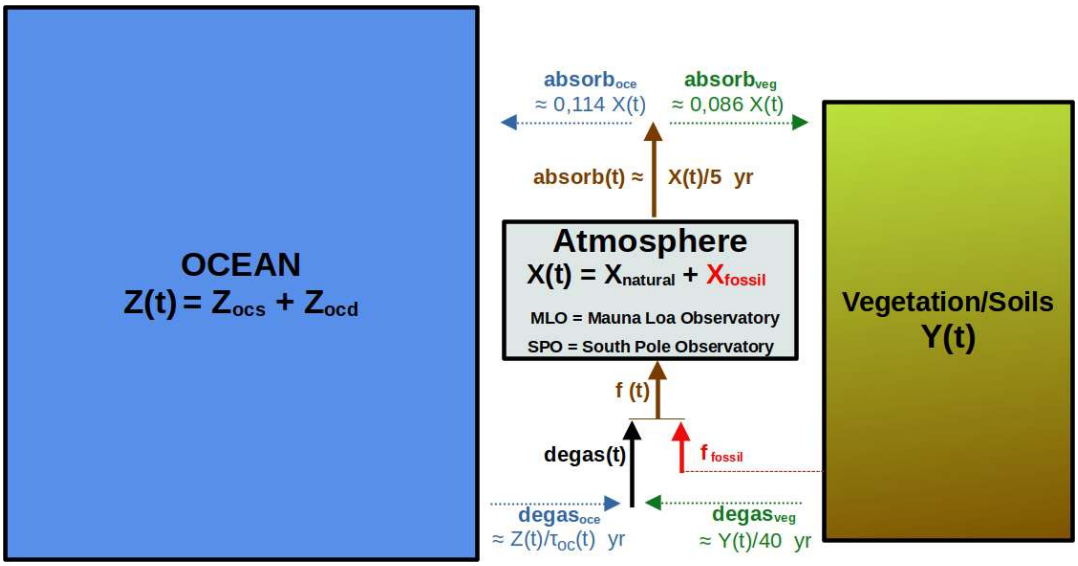

Figure 15: Exchanges governed by the three coupled differential equations (12), corresponding to the diagram in Figure 14. All notation is defined in Appendix A.

The exchanges of 275 Gt-C/year between the surface ocean and the deep oceans quoted in Sec. 2 above mean that the well mixed first 100 meters of the ocean is not separated from the rest of the ocean. Figure 16 shows what happens to a unit pulse of carbon into air at time $t_0 = 0$ ($f_{fossil}(t) = 0$ for $t > 0$, $X(0) = 1$, $Y(0) = Z(0) = 0$) for $\tau_{oc}(t) = 360$ years: the black curve decreases as $\exp(-t/\tau_{atm})$ during the first 10 years and tends towards 2.1% after 200 years, as the unit pulse of carbon is finally distributed between the three compartments in proportion to their masses, i.e. for the atmosphere: 875 / (875 + 2500 + 38000) = 2.1%. The black curve represents the mass of carbon that remains in the atmosphere, or returns to it after temporary residence in the other two reservoirs. It is well approximated by the impulse response[6]:

$$F1(t) = 0.021 + 0.928 \exp(-t/4.73 \text{ yr}) + 0.0416 \exp(-t/70.46 \text{ yr})$$

with F1(30) = 5%, F1(100) = 3.1%. $F1(t)$ is very different from Bern's impulse response of (IPCC, 2007) i.e. AR4 WG1 p. 213 note a)

[6] The black curve of Figure 16 takes into account anthropogenic CO_2 molecules that return to the atmosphere ("zombie" molecules after passing through the ocean and vegetation /soil compartments). If we did not take into account this return of 'zombie' molecules, we would have a simple decay in exp (-t/5yr). During the first 10 years, this return of 'zombie' molecules is negligible: we are close to exp(-t/5yr). $F1(t)$ approximates this behavior: 4.73 years mainly concerns non-zombie molecules and 70.46 years concerns 'zombie' molecules (a mixture of τ_{tb} =40 years for vegetation / soil and τ_{oc}= 360 years for the ocean).

$$FB(t) = 0.217 + 0.186 \exp(-t/1.186\text{yr}) + 0.338 \exp(-t/18.57\text{yr}) + 0.259 \exp(-t/172.9\text{yr})$$

(red curve on Figure 16). The "vegetation & soils" compartment, shown in green on Figure 16, rapidly absorbs a part of the carbon pulse from the air, peaks at 34% at t = 14.4 years, before releasing its carbon: it still contains 9.2% of the initial pulse at t = 200 years and 6% in the long term. The "ocean" compartment, shown in blue in Figure 16, absorbs part of the carbon pulse present in the air even faster, then absorbs the excess carbon from vegetation & soils: it contains 92% of the carbon in the long term.

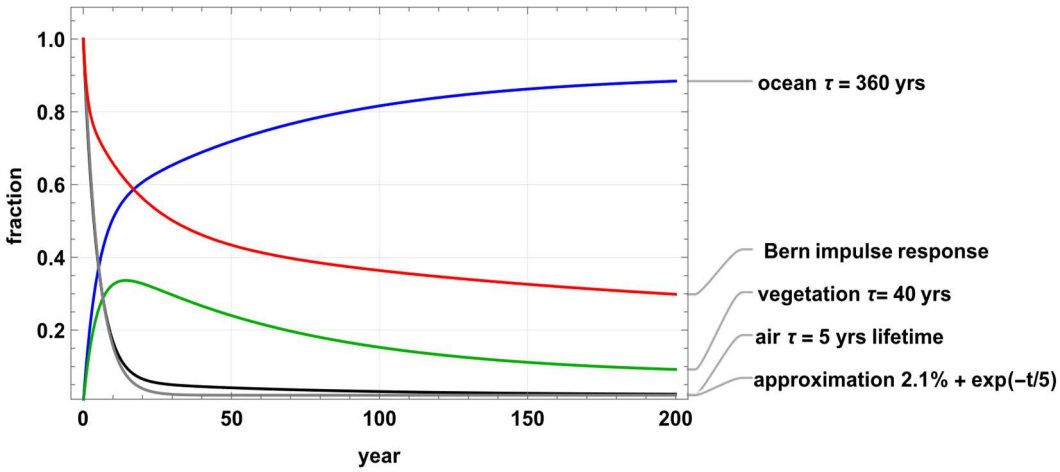

Figure 16: Distribution between the three compartments of a unit pulse of carbon into the atmosphere at time t = 0. The black F1(t) curve and the grey 2.1% + exp(–t/τ_{atm}) curve differ by at most 2.7%.

The net flux absorbed by vegetation, its Net Primary Productivity NPP(t) net of respiration is about GPP/2 (see Table 1); in Figure 17, the green curve from (Haverd et al., 2020) is the GPP over 1900 – 2016 extended with the indications of (Lai et al., 2024); this GPP is close to twice the 8.6% of $X(t)$ at MLO extended before 1959 by $X_{\text{MLOlogis}}(t)$ of equation (6). This justifies the parameters used in Figure 14: 0,086 $X(t)$ = $\text{absorb}_{\text{veg}}(t)$ and (0,2 – 0,086) $X(t)$ = 0,0114 $X(t)$ = $\text{absorb}_{\text{oce}}$ (t).

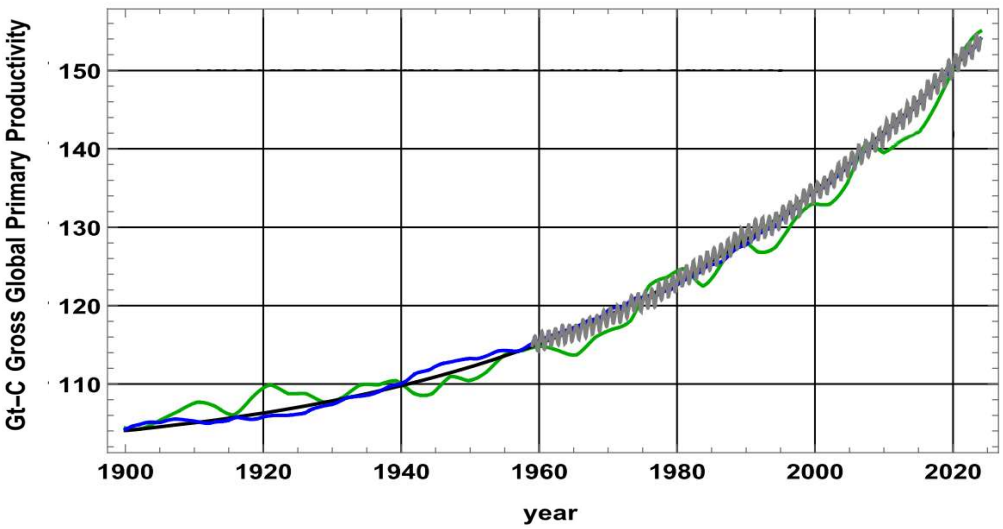

Figure 17: The green curve is from (Haverd et al. 2020) and (Lai et al., 2024) the Global Gross Primary Productivity GPP of the vegetation in Gt-C/yr; the black curve is 2×8.6% × 2.12 of the ppm logistic $X_{MLOlogis}(t)$, the blue curve is 2×8.6% of the air carbon mass deduced from the series $f_{fossil}(t)$ and $AT_{SST}(t)$ (the inter-tropical sea surface temperatures anomaly) (plotted in ppm on Figure 11) and the grey curve is 2×8.6% of the X(t) series in Gt-C based on $X_{MLO}(t)$.

6.2 Computation of Stocks and Fluxes

The three differential equations (12) of Subsec. 6.1 link the stocks of carbon in the air $X(t)$, in vegetation & soils $Y(t)$, and in the ocean $Z(t)$:
$X(t)$ is computed (see Subsec. 5.2) from the observed time series $AT_{SST}(t)$ for $X_{natural}(t)$ and $f_{fossil}(t)$ for $X_{fossil}(t)$,
$Y(t)$ is deduced from $dY(t)/dt + Y(t)/\tau_{tb} = NPP(t) = GPP(t)/2$ with Haverd et al.'s (2020) $GPP(t)$,
$Z(t)/\tau_{oc}(t)$ is $X'(t) + X(t)/\tau_{atm} - Y(t)/\tau_{tb} - f_{fossil}(t)$.

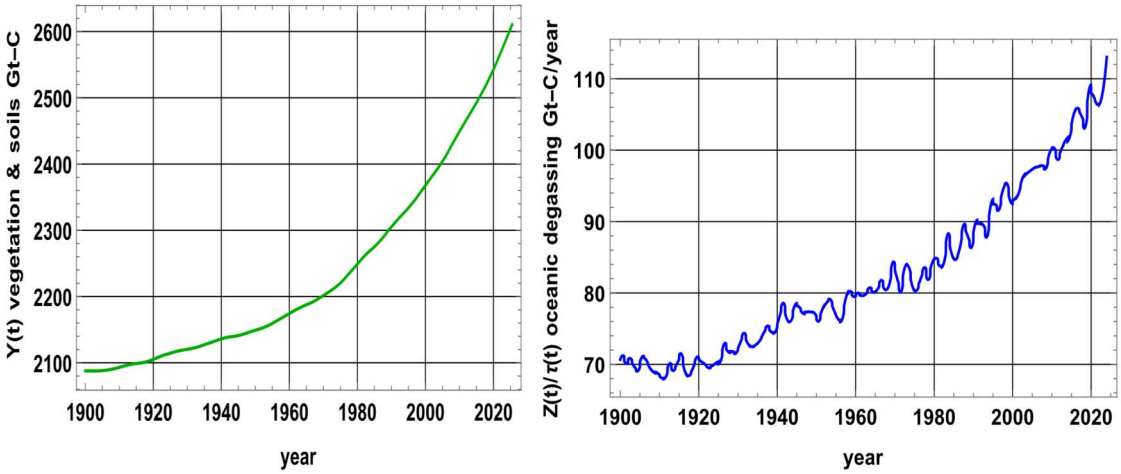

Figure 18 a-b: a) left: Y(t) stock in vegetation and soil, the calculation uses the integral of GPP/2 according to Haverd et al. (2020) - see Figure 17; b) right: ocean degassing flux varying according to $Z(t)/\tau_{oc}(t)$.

Cumulative ocean degassing over 1900-2025.0 is 10,350 Gt-C.
For vegetation and soils, Figure 18-a shows, with the GPP of Haverd et al. (2020) and Lai et al. (2024) plotted in Figure 17, $Y(1900)$ = 2088 Gt-C and $Y(2025)$ =2630 Gt-C.

IPCC's figures are:

- (AR2, Fig. 2.1) $Y(1989)$ = 2190 Gt-C with a Global NPP of 61 Gt-C/yr,
- (AR5, Fig. 7.3.5) $Y(1997)$ = 2261 Gt-C, GPP(1997) = 122 Gt-C/yr, Y(pre-industrial) = 2300 Gt-C and GPP(preindustrial) = 120 Gt-C/yr
- (AR6, Fig. 5.12) $Y(2013)$ = 2150 Gt-C, GPP(2013) = 142 Gt-C/yr, GPP (pre-industrial) = 113 Gt-C/yr.

Reducing the mean residence time in vegetation and soils from 40 years to 30 years reduces the $Y(2024)$ stock to 2300 Gt-C but has little effect on oceanic degassing, since $Y(1900)$ goes from 40 times to 30 times the NPP(1900): $Y(2024) - Y(1900)$ changes little.

6.3 Changes of the Stocks

Figure 19 shows the variations in the three carbon stocks and cumulative emissions between 1900 and 2025. The increases in atmospheric carbon (+297 Gt-C or +140 ppm) and in vegetation and soils (+542 Gt-C) result from the net contributions of the oceanic stock (−359 Gt-C) and fossil fuels (−480 Gt-C, of which approximately 50 Gt-C remain in the atmosphere, with the rest absorbed by vegetation and the oceans).

Since 1900, fossil fuel combustion has contributed a cumulative total of 480 Gt-C to stocks X, Y, and Z. Between 1900 and 2025, the inter-tropical ocean has released approximately 10,350 Gt-C (an average of 83 Gt-C yr^{-1} over 125 years, according to Figure 18-b, right panel). However, the high-latitude ocean has absorbed 9,991 Gt-C, resulting in a net loss of 359 Gt-C from the ocean to the atmosphere and to vegetation/soils. Over the same period, the atmosphere gained 297 GtC and vegetation/soils gained 542 Gt-C.

In the absence of fossil fuel emissions (cumulative = 0 Gt-C), the atmospheric partial pressure of CO_2 would have increased more slowly, reaching 395 ppm instead of 425 ppm. This lower pressure would have promoted additional degassing in the inter-tropical ocean and reduced CO_2 absorption at high latitudes. In that case, the ocean would exhibit a net loss of 664 Gt-C (10,504 Gt-C degassed minus 9,840 Gt-C absorbed) to the atmosphere and vegetation/soils. The atmosphere would then have gained only 233 Gt-C and vegetation/soils only 431 Gt-C.

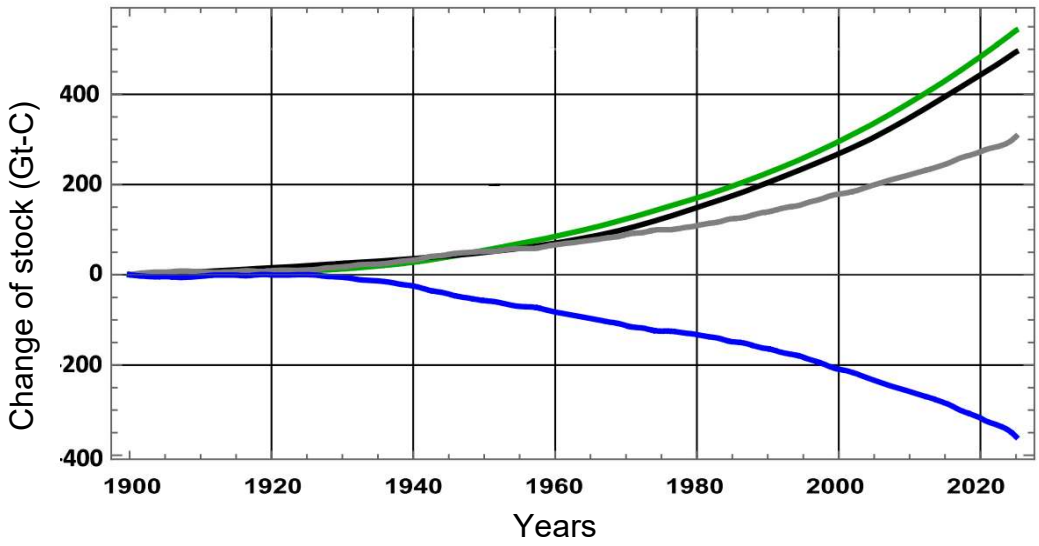

Figure 19: Variations in Gt-C over 1900-2025 in atmospheric stocks X(t) (grey), vegetation and soil stocks Y(t) (green) and cumulative emissions since 1900 (black); in blue, the change of the oceanic stock Z(t) computed as the integral over time of $-Z(t)/\tau_{oc}(t) + 0.114\,X(t)$.

6.4 A Glimpse at Decarbonization Policies in the EU-27

The mean over 1980-2023 of the cost of weather-related catastrophes in EU-27 is € 16.8Bn/yr about 0.1% of the Gross Domestic Product (GDP) and the maximum over those 44 years has been € 63Bn/yr (EEA, 2024).

The EU "Fit For 55", –55% in 2030 with respect to 1990 emissions of 4.73 Gt-CO2/yr or 0.61 ppm/yr, aims at 2030 emissions of 0.27 ppm/yr with a further decline to 0 in 2050. The yearly cost of that policy is said to be over the next decades 5% to 10% of a 2024 EU GDP which is about € 17,900 Bn/yr, i.e. (≈1000 times the average cost of said catastrophes!).

$dX_{fossil}(t)/dt = f_{fossil}(t) - X_{fossil}(t)/5$ shows that the stock $X_{fossil}(2035)$ from EU emissions would be reduced from 1.6 ppm, if emissions were kept at their 2024 level, to 1.14 ppm that is minus 0.46 ppm. 0.46 ppm is about 5% of the seasonal increase of 8.6 ppm between the dates 2023.73 (end September) (X_{MLO} = 418.4 ppm) and 2024.42 (end April) (X_{MLO} = 427 ppm) and little more than one thousandth of X_{MLO}. Preventive measures (dams and retention basins, dykes, reservoirs, irrigation) account for less than one-thousandth of GDP per year, even in the Netherlands, and significantly reduce the impact of catastrophic floods. Mobile barriers on the Thames (closed 221 times since 1982) and on the Venice lagoon (78 barriers in service by 2020, raised about 28 times a year against the highest tides) effectively protect these cities.

7. On ^{13}C in the Atmosphere

The ratios of ^{13}C and ^{12}C isotopes of CO_2 in the air, observed continuously since 1980 at the Mauna Loa and at the South Pole observatories (at altitudes 2.8 km and 3.4 km) and far from any vegetation, confirm that only a few percent of carbon dioxide in the atmosphere come from fossil fuels. The marker $\delta^{13}C$ in units per mil (denoted ‰):

$$\delta^{13}C = \left(\frac{\left(^{13}C/^{12}C\right)_{\text{sample}}}{\left(^{13}C/^{12}C\right)_{\text{reference}}} - 1 \right) x1000\ ‰ \tag{13}$$

is, for a mixture, approximately linear with respect to the quantities entering the mixture. Indeed for a mixture $X = X' + X''$, with markers δ, δ' and δ'' and $A = 1/\ (^{13}C/^{12}C)_{\text{reference}} = 1 / 0.0112372$ for the VPDB reference, $\delta = A\ X_{13}/X_{12} - 1$, $\delta = (X'\ \delta' + X''\ \delta'' + X\ \delta'\ \delta''/(A+1)) / (X + (X'\ \delta'' + X''\ \delta') / (A+1))$ or practically $(X'\ \delta' + X''\ \delta'')/X$ see note[7]. The $\delta^{13}C$ carbons of the fuels gas oil and coal are about –45, –28, –24.5 per mil with variations from deposit to deposit (Hu et al., 2021; Masood et al., 2022; Suto & Kawashima, 2016). The $\delta^{13}C$ of the mixture is slightly reduced by the flow from cement plants, and a small proportion of the hydrocarbons is used to make plastics (Figure 20-b).

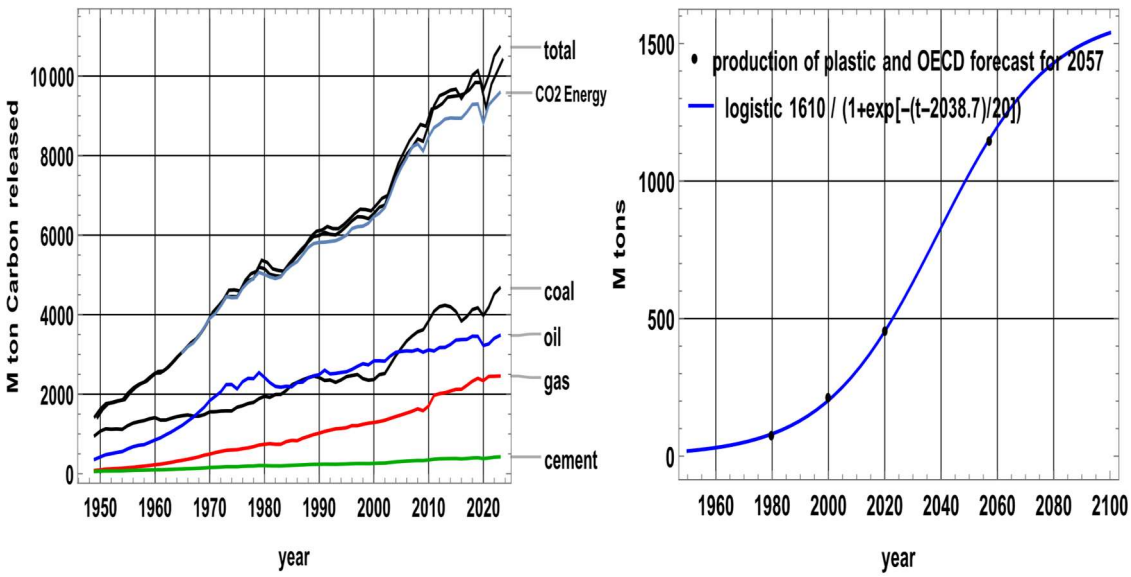

Figure 20 a-b: a) left: Carbon (millions of tons) contained in gas, oil, coal and cement production, and the fraction used in energy production (Statistical review of World Energy Data 2023); b) right: Production of plastics in Mt/year past and extrapolated.

Figure 21 shows estimates of the $\delta^{13}C_{\text{fossil}}(t)$. Over 45 years, the stock of fossil fuels has risen from 3.2% to 5.5% of the CO_2 in the air. We provide the computation of the *instantaneous atmospheric stock* of CO_2 originating from fossil sources (coal, oil, gas, cement) at a given time t. Each year's (or month's) emissions contribute to the current stock, but their influence *decays exponentially* with time due to natural absorption. For coal, the stock $X_{\text{coal}}(t)$ in the atmosphere at time t is the average of the previous emissions $f_{\text{coal}}(m)$ weighted by $e^{-(t-m)/5\ \text{yr}}$. The variable m represents the emission year (or time index) before t, that is, the time at which each individual emission $f_{\text{coal}}(m)$ occurred. So:

- t = current year (or time of evaluation), e.g. 2024.05
- m = past year (e.g. 1900, 1950, 2000, … up to t)
- $f_{\text{coal}}(m)$ = fossil CO_2 emissions from coal at time m

The exponential term $e^{-(t-m)/5\ \text{yr}}$ is the weight expressing how much of the emission at time m still remains in the atmosphere at time t, assuming a 5-year e-folding decay time. The atmospheric

[7] The marker $\delta^{13}C$, expressed in per mil (‰), quantifies the relative abundance of ^{13}C to ^{12}C compared to a standard (VPDB). For mixtures, δ behaves approximately linearly because the $^{13}C/^{12}C$ ratio of the combined reservoir is a weighted average of the isotopic ratios of the individual components. The exact expression follows from mass balance on ^{13}C and ^{12}C, but since δ values are small ($|\delta| \ll 1$), the higher-order terms in $\delta'\delta''/(A+1)$ are negligible, leading to the practical linear approximation $(X'\ \delta' + X''\ \delta'')/X$.

stock $X_{coal}(t)$ is obtained by summing all past emissions $f_{coal}(m)$, each diminished by an exponential factor that accounts for how much of it has been reabsorbed since it was emitted. Then, by combining the stocks from coal, oil, and gas, each with its own $\delta^{13}C$ signature, the weighted mean isotope ratio is:

$$\delta^{13}C_{\text{fossil}}(t) = \frac{\sum \delta^{13}\, C_i X_i(t)}{\sum X_i\,(t)} \tag{14}$$

The calculation for oil, gas and cement plants, i.e. the sum of stocks weighted by their own marker, for example $\delta^{13}C$ = {–46, –28, –24.5} for gas, oil and coal divided by the sum of stocks gives:

$\delta^{13}C_{\text{stock fossil}}(1980.05)$ = –27.9 ‰ and $\delta^{13}C_{\text{stock fossil}}(2024.05)$ = –29.4 ‰.

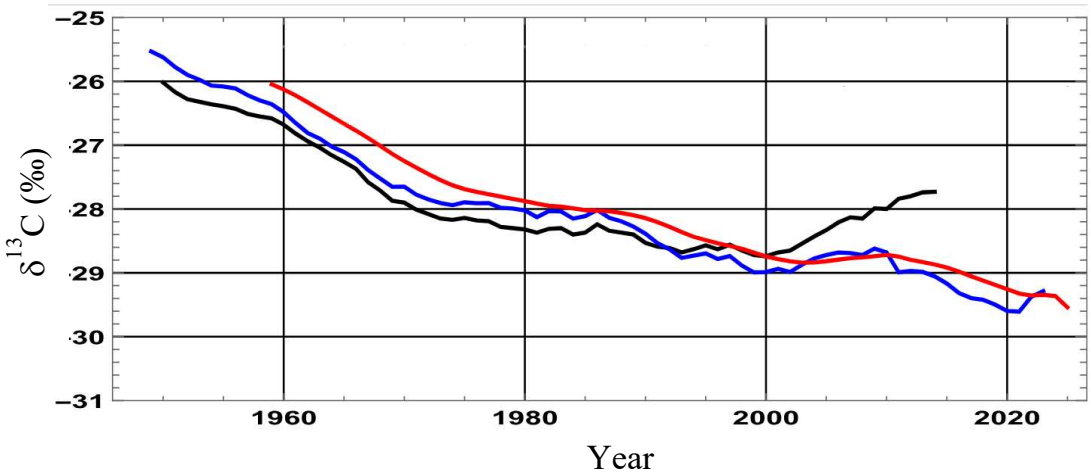

Figure 21: δ13C estimates for the emissions from fuels and cement plants. Office of Scientific and Technical Information (OSTI), (https://data.ess-dive.lbl.gov/view/doi:10.3334/CDIAC/FFE.DB1013.2017), U.S. Department of Energy. Black curve is the "OSTI db1013 global", blue curve corresponds to the "computed energy and cements {-45, -28, -24.5}" and red curve is for "all gas and oil and coal".

The $\delta^{13}C_{\text{stock natural}}(t)$ of the stock from natural out-gassing (which includes a small fraction of fossil carbon "zombie" recycled after absorption and out-gassing) is for instance:

$\delta^{13}C_{\text{stock natural}}(1980.05)$ = –6.84‰ and $\delta^{13}C_{\text{stock natural}}(2024.05)$ = –7.5‰ as

- at date 1980, 338 ppm (–7.52‰) = 11 ppm (–27.9‰) + 327 ppm (–6.84‰)
- at date 2024, 423 ppm (–8.68‰) = 22.8 ppm (–29.4‰) + 400 ppm (–7.5‰).

Figure 22-a shows:

1. in black, the $\delta^{13}C$ measured at Mauna Loa since 1980 and its 12-month moving average,
2. in grey, the $\delta^{13}C_{\text{stock natural}}$ that evolves slowly with the return to the atmosphere of "zombie" fossil fuel carbon absorbed by vegetation or oceans decades earlier, and its 12-month moving average.

The stock from natural out-gassing (grey curve in Figure 22-a) has the $\delta^{13}C$ signature of the ambient air some 60 years earlier, reflecting the average carbon transit times between absorption and out-gassing through the oceans and through vegetation and soils.

In the oceans, a relatively rapid movement on isopycnic surfaces close to the surface near 50°N and 1000 m deep in the inter-tropical zone could explain a transit in a century or less.

The Impulse Responses (Figure 16) give a sum of the carbon from fuels still in the atmosphere (for a 5-year lifetime) and of the fossil fuel "zombies" absorbed long ago and returned to air by out-gassing after sojourns in oceans and soils; subtracting all "fossil" carbons leaves a $\delta^{13}C$ between –6.6‰ (in 1980) and –7.1‰ (in 2024).

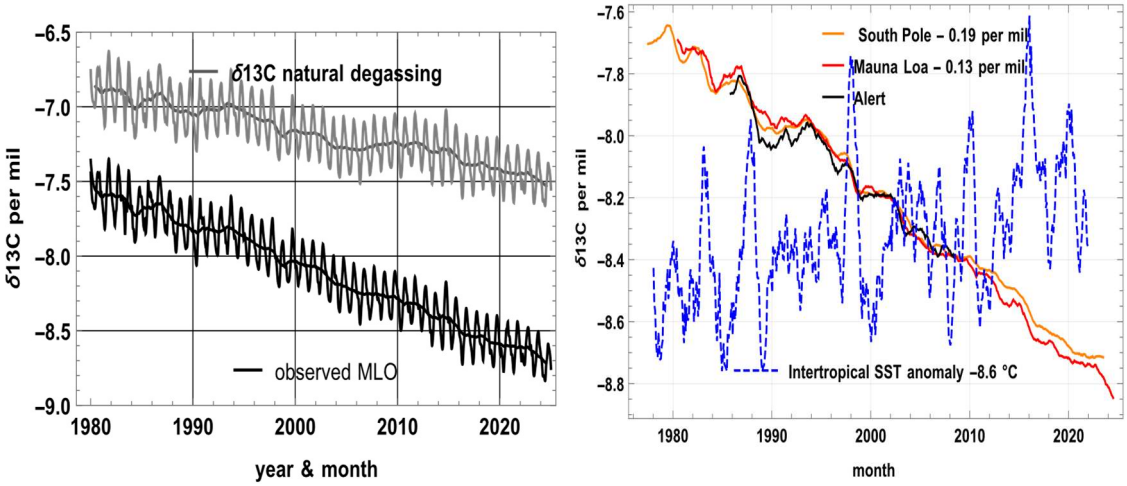

Figure 22 a-b: a) left: Evolution of the atmospheric $\delta^{13}C$ (MLO observations in black) and in grey the $\delta^{13}C$ of the stock from natural out-gassing that is without the fossil fuels carbon still in the air for a lifetime of 5 years and their 12-month moving averages; b) right: Comparison of $\delta^{13}C$ observed at Alert (Alaska, 82°30'N & 62°21'W, 817 km from the North Pole), at Mauna Loa (19°28'N and 155°36'W, 3397 m) and at the South Pole (2937 m) with a 12-month moving average smoothing; the blue dashed line is the inter-tropical sea surface temperature anomaly shifted in ordinates by –8.6°C.

Figure 23 compares the increments of $\delta^{13}C_{stocknatural}(t)$ and the sea surface temperatures of the inter-tropical zone: the $\delta^{13}C$ of CO_2 degassed by the ocean is, according to (Quay et al., 2003, p. 4-12) Fig. 8 or (Roy-Barman & Jeandel, 2016, p. 110) Fig. 3.11, about –1.5‰ more negative than the $\delta^{13}C$ of air: this may explain the peaks of negative values of the increments during times of strong out-gassing (Figure 2) that are the risers of the stairs on Figure 22.

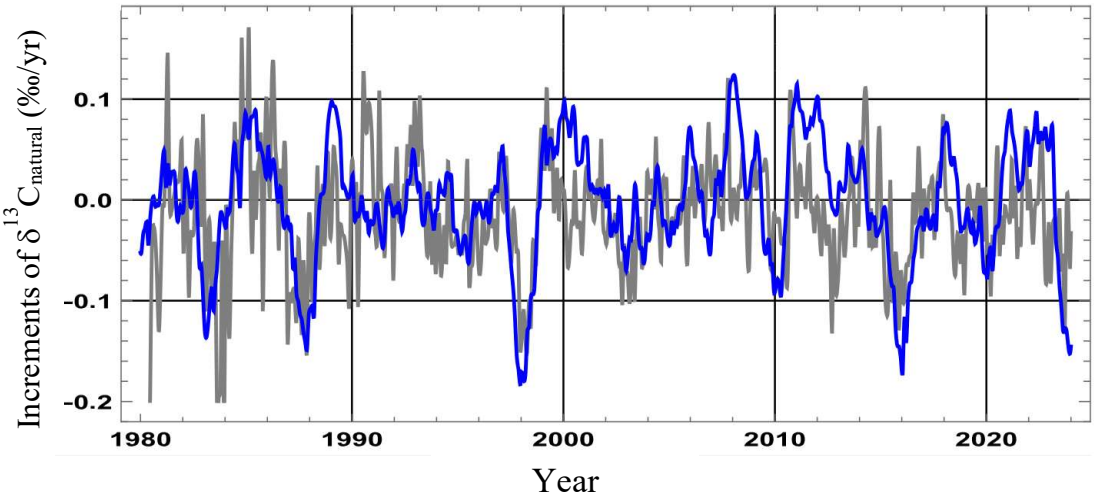

Figure 23: In grey, increments of $\delta^{13}C_{stock\ natural}(t)$ in ‰ (12-month increments, centered in the middle of the 12 months to reduce the seasonal fluctuations) and in blue, 0.3 times the opposite of the inter-tropical sea surface temperature anomaly after subtracting its linear trend.

Figure 24 shows (thick grey line at bottom) the $\delta^{13}C_{stock\ natural}(t)$ (grey curve at top of Figure 22-a) shifted by +33.6): it decreases from August to May while MLO ppm (divided by 14, black curve) increase almost in phase with the mean inter-tropical SST (blue curve).

Koutsoyiannis (2024b) uses the Keeling plot of $\delta^{13}C(t)$ as a function of $1/X(t)$; adding to $X(t_0)$ of marker $\delta^{13}C_0$ a quantity $X(t) - X(t_0)$ of marker $\delta^{13}C_I$ gives to $X(t)$ the isotopic signature:

$$\delta^{13}C(t) = \delta^{13}C_I + (\delta^{13}C_0 - \delta^{13}C_I)\frac{X(t_0)}{X(t)} \tag{15}$$

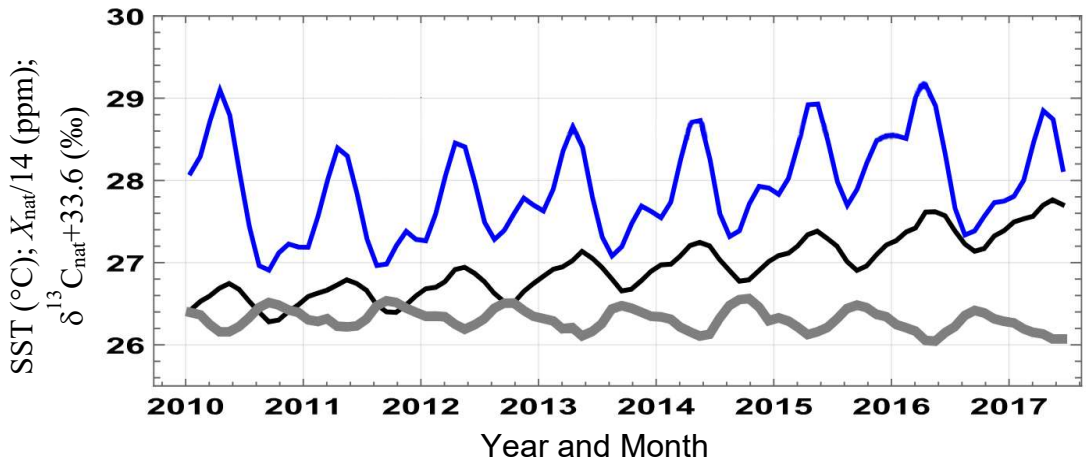

Figure 24: Trends over 2010-2017 of the mean SST sea surface temperatures (in °C) between 20°S and 20°N (blue curve), $X_{natural}(t)/14$ at MLO (black curve) and 33.6 + $\delta^{13}C_{natural}(t)$ (thick grey line).

Regression of $\delta^{13}C$ on the observations of $1/X(t)$ over a time interval gives the $\delta^{13}C_I$ as the *y*-intercept of the graph. For seasonal variations he finds $\delta^{13}C_D = -27.6‰$ during the two months with the highest photosynthesis (an atmospheric CO_2 decay phase) and various values of $\delta^{13}C_U$ during the two months of strongest atmospheric CO_2 growth phase, and for long-term variations $\delta^{13}C_I = -13.2‰$ even for reconstructions of $\delta^{13}C(t)$ going back to year 1520 (Böhm et al., 2002).

8. On Carbon in Seawater

An outflow from the ocean of 100 Gt-C/year over the 20°S-20°N zone (34% of the earth's surface), 75% oceanic, i.e. 130 M km², corresponds to an average flux of 64 moles-C/year/m². For seawater at 2 100 µmole-C/kg, an up-welling of 30 m/year is required, and three times more if only a third of the carbon that rises is degassed to the atmosphere. As seen in Sec. 2, and using equations (8) and (9) in Subsec. 5.2 these relations show that oceanic degassing (Figure 18-b) driven by $AT_{SST}(t)$ has provided the bulk of the growth in the atmospheric and vegetation and soil stocks: in 1960, oceanic degassing was 32 times the flux from "fossil fuels"; since 2010, it has been 11 times greater.

For the IPCC, changes in ocean degassing are absolutely taboo because it invalidates representations such as (IPCC, 2018, p. 105), Fig. 2.3: "*Temperature changes from 1850-1900 versus cumulative CO_2 emissions since 1st January 1876"* where cumulative human emissions are claimed to have caused:

1. all the increase in CO_2 and thus,
2. all the warming since 1876: "*Solid lines with dots reproduce the globally averaged near-surface air temperature response to cumulative CO_2 emissions plus non-CO_2 forcers as assessed in Figure SPM 10 of WGI AR5*."

The reality (Sec. 2 and 3 above) is that AT_{SST} increased from 0.12 °C in 1959 to 0.97 °C in 2024 and accounts for 83% (+89 ppm) of the total increase (+107 ppm) in atmospheric CO_2 over that period. Moreover, the fraction of fuel-related emissions still remaining in the air (about 23 ppm out of 425 ppm at the end of 2024) cannot have any climatic effect. This negligible contribution of not more than 5.4% to the atmospheric CO_2 concentration is in full agreement with an independent line of reasoning and based on a residence (or absorption) time of $\tau = 3.8$ yr (see: Harde, 2025, Sec. 4, last paragraph).

8.1 Reminders

[x] denotes the number of moles of compound x per kilogram of sea water.

The ocean is by far the main reservoir of circulating carbon, potentially inexhaustible if we consider the calcium carbonate in marine sediments. Seawater has everywhere almost the same composition (Dittmar principle, 1884) and contains in mole/kg: H_2O: 53.56, Na^+: 0.4685, Mg^{2+}: 0.05308, Ca^{2+}: 0.01028, K^+: 0.01021, Sr^{2+}: 0.00009, B: 0.00042, Cl^-: 0.54591, SO_4^{2-} : 0.02823, CO_3^{2-} & HCO_3^-: 0.002, Br^-: 0.000842, F^-: 0.00007, i.e. 0.60561 moles per kg of positive charges excluding H^+ and 0.603282 moles of negative charges excluding carbonates, borates and OH.

The difference 605610 – 603282 = 2328 micro-moles/kg known as total alkalinity or TAlk, is also identical to $[HCO_3^-] + 2\,[CO_3^{2-}] + [B(OH)_4^-] + [OH^-] - [H^+]$.

Carbonate equilibria in seawater (Copin-Montégut, 1996; Dickson, 2010; Dickson et al., 2007) are described by five equilibrium constants that are functions of salinity and temperature; the fugacity f_{CO2} of CO_2 in the gas phase is derived as per (Zeebe & Wolf-Gladrow, 2001):

$$f_{CO_2} = \frac{[CO_2{}^*]}{k_0} \tag{16}$$

with:

- $[CO_2{}^*]$ = the equilibrium concentration of dissolved $CO_2(aq)$ in water, often in mol/kg or mol/l. The *[8] distinguishes it from total dissolved inorganic carbon (DIC = $CO_2 + HCO_3^- + CO_3^{2-}$).
- k_0 = the Henry's law solubility constant for CO_2 (temperature- and salinity-dependent).

Let CO_2* (a.k.a. $H_2CO_3^*$) denote dissolved molecular CO_2 plus carbonic acid:

$$CO_2^* \equiv CO_2(aq) + H_2CO_3 \tag{17}$$

Stoichiometric (salinity-dependent) equilibrium constants:

$$K_1^*, K_2^*, K_b^*, K_w \text{often in place of } k_{H_2O} \tag{18}$$

depend on *T*, *S*, and *P*; the asterisk distinguishes them from thermodynamic *K*'s based on activities, while K_w instead of k_{H2O} avoids confusion with water itself, either one or the other can be used. These constants are defined by the following relations (19):

$$\begin{aligned} [HCO_3^-] &= \frac{K_1^*[CO_2^*]}{[H^+]} \\ [CO_3^{2-}] &= \frac{K_2^*[HCO_3^-]}{[H^+]} \\ [B(OH)_4^-] &= \frac{K_b^*[B(OH)_3]}{[H^+]} \\ [H^+] &= \frac{K_w}{[OH^-]} \end{aligned} \tag{19}$$

The *pK* notation is also often used:

$$pK = -\log_{10}(K) \text{e.g.,} pK_1^* = pH - \log_{10}\left([HCO_3^-]/[CO_2^*]\right) \tag{20}$$

With the notations salinity *S*, and absolute temperature *T*, one can define K_w (*S,T*) i.e. the ionic product of water in seawater at a given salinity and temperature, with $B_T(S)$, i.e. a salinity-dependent correction term and with K_w^0 (*T*) the ionic product in pure water at the given temperature:

$$K_w(S,T) = [H^+][OH^-] = K_w^0(T) + B_T(S) \tag{21}$$

$B_T(S)$ stands for the total boron concentration in seawater that is, the sum of all boron species (mostly boric acid $B(OH)_3$ and borate ion $B(OH)_4^-$). It is proportional to salinity, because boron

[8] The * is a conventional marker in geochemistry/ocean chemistry indicating the aqueous concentration of CO_2 in equilibrium with the atmosphere, not the whole carbonate system. $[CO_2{}^*]$ denotes the sum of dissolved molecular CO_2 and carbonic acid (H_2CO_3).

in seawater behaves conservatively (it scales linearly with the amount of dissolved salts) as defined by (Millero, 1995) as $B_T(S) = 1.188 \times 10^{-5}\ S$ mol kg^{-1} or at typical ocean salinity with S = 35 kg/m^3, one gets $B_T(S) = 1.188 \times 10^{-5} \times 35 = 4.16 \times 10^{-4}$ mol kg^{-1}.

Once this is defined, the following relations apply with the notations "ln" as natural logarithm, $S = s$ kg/m^3 as salinity and $T = \vartheta$ K as temperature with s and ϑ as their numerical values:

$$\ln(k_0[T, S]) = -60.240 + 93.451\ (100/\vartheta) + 23.358 \ln(\vartheta/100) + s\ [0.023 - 0.024\ (\vartheta/100) + 0.0047\ (\vartheta/100)^2]$$

$$\ln(k_b[T, S]) = (-8966.9 - 2890.53\ s^{0.5} - 77.942\ s + 1.728\ s^{1.5} - 0.0996\ s^2)/\vartheta + 148.025 + 137.194\ s^{0.5} + 1.621\ s + (-24.434 - 25.085\ s^{0.5} - 0.247\ s)\cdot\ln(\vartheta) + 0.053\ s^{0.5}\cdot\vartheta$$

$$\ln(k_1[T, S]) = 2.837 - 2307.127/\vartheta - 1.553 \ln(\vartheta) - (0.20760841 + 4.0484/\vartheta)\ s^{0.5} + 0.085\ s - 0.007\ s^{1.5} + \ln(1 - 0.001\ s)$$

$$\ln(k_2[T, S]) = -9.227 - 3351.611/\vartheta - 0.201 \ln(\vartheta) - (0.107 + 23.972/\vartheta)\ s^{0.5} + 0.113\ s - 0.008\ s^{1.5} + \ln(1 - 0.001\ s)$$

$$\ln(k_{H2o}[T, S]) = 148.965 - 13847.26/\vartheta - 23.652 \ln(\vartheta) + (-5.977 + 118.67/\vartheta + 1.049 \ln(\vartheta))\ s^{0.5} - 0.016\ s$$

Same relations in (Dickson, 2010; Dickson et al., 2007), who use both decimal logarithms and Napierian logarithms.

DIC refers to dissolved inorganic carbon, DIC = $[CO_2] + [HCO_3^-] + [CO_3^{2-}]$ and TAlk is Total Alkalinity, the difference between the total charges of the major ions of dissolved salts excluding carbonates and borates, TAlk = $[HCO_3^-] + 2\ [CO_3^{2-}] + [B(OH)_4^-] + [OH^-] - [H^+]$.

Assuming that total boron $[B(OH)_3] + [B(OH)_4^-]$ is a fixed fraction B_T of salinity S, we get $[B(OH)_4^-] = B_T[S]\ k_b / (k_b + [H^+])\cdot$ x = $[OH^-]$ is the solution close to 10^{-6} of the following equation (see Appendix B):

$$TAlk = \frac{(x\,k_1/K_{H_20} + 2x^2 k_1\,k_2/K_{H_20}^2)DIC}{1 + x\,k_1/K_{H_20} + x^2 k_1\,k_2/K_{H_20}^2} + B_T(S)\frac{x k_b}{K_{H_20} + x k_b} - \frac{K_{H_20}}{x} + x \qquad (22)$$

Figure 25 shows the temperature ranges corresponding to absorption (partial pressure of CO_2 in seawater less than say 425 µatm) and the temperature ranges for degassing, for example at more than 425 µatm. The dashed lines plot the simple approximation:

$$p_{CO2sea\ water}(\mu atm) = 400\ \mu atm\ (\vartheta/299)^{12.5}\ (DIC_{\mu mole/kg}/2000)^{10.4}\ (2328/TAlk_{\mu mole/kg})^{10.3}$$

Seawater temperatures range from 32°C in some inter tropical zones to –1.5°C in salty waters at the edge of the pack ice (the global average of ocean surface temperatures oscillates between 290 K and 293 K, depending on the season).

With DIC and TAlk in µmol/kg and T in Kelvin, the pH is approximately given by this linear approximation (the regression coefficients therefore carry the corresponding inverse units so that the resulting pH remains dimensionless): $7.85 - 1.95 \times 10^{-3}$ (DIC – 2100) + 1.87×10^{-3} (TAlk – 2328) – 1.59×10^{-2} (T – 299); +1°K on T or +8 µmol/kg on the DIC have about the same effect: +18 µatm on the sea water partial pressure and –0.016 on the pH. Seawater temperatures over the Great Barrier Reef range from 24°C in winter to 30°C in summer.

Takahashi et al.'s (1993) formula (23) expresses the growth of $p_{CO2seawater}$ with temperature:

$$\frac{pCO_2(T)}{pCO_2(T_{\mathrm{ref}})} = \exp\,[0.043(T - T_{\mathrm{ref}})] \qquad (23)$$

It is very close to the expression in $T^{12.5}$ (Figure 26).

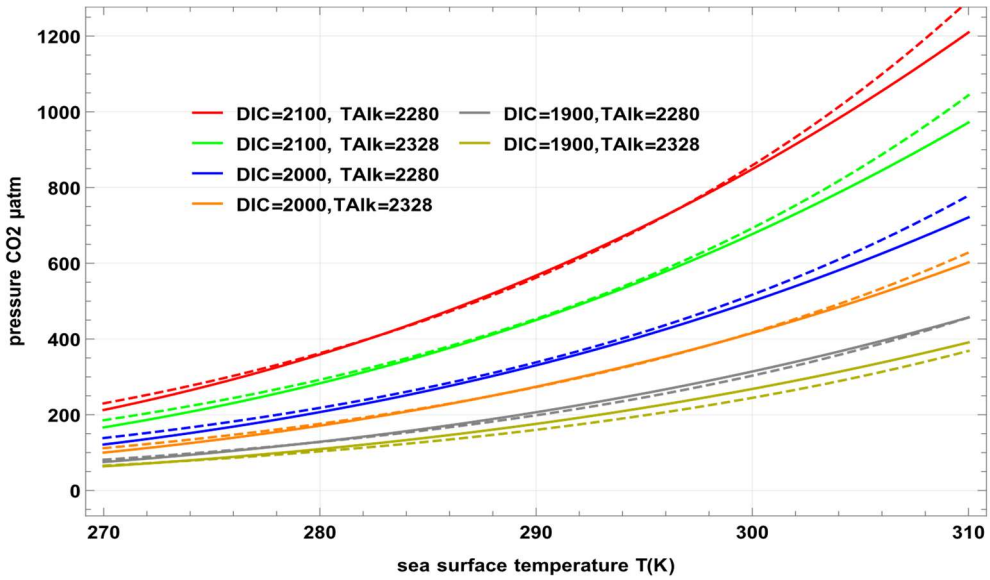

Figure 25: Calculation according to (Copin-Montégut, 1996) of the partial pressure of CO_2 in seawater for various values of DIC, TAlk and T(K) at the surface; the dashed lines show the approximation 400 $(T/299)^{12.5}$ $(DIC/2000)^{10.4}$ $(2328/TAlk)^{10.3}$ with DIC µmol/kg and salinity S=35 g/l.

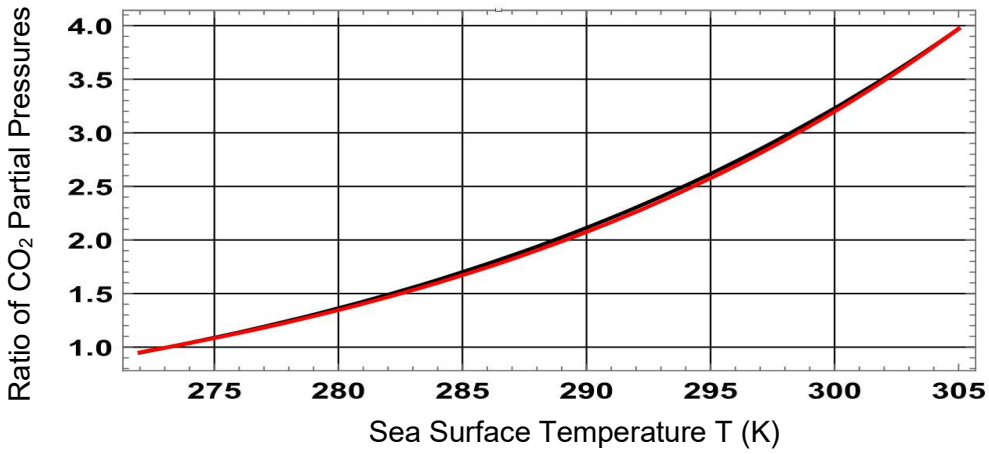

Figure 26: Ratio of the CO2 partial pressures in seawater at temperature T to the partial pressure at 273.15 K: expressions in T12.5 and of Takahashi et al. (1993).

The flux of carbon dioxide F (in mol m^{-2} s^{-1} or mol m^{-2} yr^{-1}) between the surface of the ocean and the air derives from the difference in partial pressures (Wanninkhof et al., 2013; Wanninkhof & McGillis, 1999) and is:

$$F = k \cdot K_0\left(pCO_2^{\text{seawater}} - pCO_2^{\text{air}}\right) \tag{24}$$

with k= 0.251 $(Sc/660)^{-0.5}$ $\langle U^2 \rangle$ in m s^{-1} and K_0 (in mol m^{-3} Pa^{-1} or mol m^{-3} µatm^{-1}) is the CO_2 solubility in seawater (Henry's law constant) linking partial pressure to dissolved concentration. It is weakly dependent on salinity. Sc(t) is the Schmidt number:

$$\mathrm{Sc}(T) = 2073.1 - 125.62\,T + 3.6276\,T^2 - 0.043219\,T^3$$

where T is the seawater temperature in °C, as used in the standard Schmidt number parameterizations (e.g., Wanninkhof 1992). The factor $(Sc/660)^{-0.5}$, where 660 is the Schmidt number of CO_2 at 20 °C, increases from 0.54 to 1.0 and 1.37 as T increases from –1.5°C to +20°C and +32°C. $\langle U^2 \rangle$ is the second-order moment of wind speed; according to Fig. 5 of Wanninkhof et al. (2013) it ranges from 30 m²/s² near the equator to 100 m²/s² at 50°N and perhaps 120 m²/s² or even 150 m²/s² at 50°S. Maps of CO_2 partial pressures in air and in surface water are shown in (Barry 2010).

A temperature change of +1°C increases partial pressure by 4.2% at 300 K (by 4.7% at 273 K): a difference ($p_{CO2water} - p_{CO2air}$) of (500 µatm – 420 µatm) becomes (521 µatm – 420 µatm) or +26% on the degassing, whereas a difference (430 µatm – 420 µatm) becomes (438 µatm – 420 µatm) with +80% on the degassing. The great variability of wind speed and of surface temperature, and intermittent oceanic eddies of small dimensions (km) that mix the water of the different layers, make it difficult to estimate fluxes.

8.2 The Depth of the Layer at 2250 µmol / kg is Probably Variable

Many articles consider the boundary layer between water and air, the last hundred microns or centimeters [Bolin, 1960] or meters with many oceanographic measurements. But the degassed flow is determined by the difference between the DIC 100 m below the surface and that at the surface which is in quasi-equilibrium with the air.

The DIC at a depth of 100 m in the Atlantic, for example, is 2250 µmol/kg between 15°S and 15°N, and 2100 µmol/kg near 30°S and 40°N (Millero, 2007). At the surface, outgassing and absorption fluxes reduce the DIC to some 2000 µmol/kg (blue and orange curves Figure 25).

Measurements at the surface of the seas show a considerable variability in $p_{CO2\ sea\ water}$ with mean annual values ranging from 250 µatm to 490 µatm depending on the site (air at MLO was then around 370 ppm), a seasonal amplitude of 60 µatm to 337 µatm near the coast, of 8 µatm to 71 µatm offshore and of 11 µatm to 178 µatm in coral reef areas (Sutton et al., 2019).

A very schematic division of the surface ocean into five geographical zones, the inter-tropical zone which degasses, two intermediate zones in equilibrium with the air and, finally, two zones closer to the poles which absorb CO_2 from the air, suggests that <u>absorption</u> depends on the <u>temperature ratio</u> of the last two zones: if $p_{CO2\ sea\ water} = p_{CO2air}$ at 35°N, $p_{CO2air} - p_{CO2sea\ water}$ at 50°N will be $p_{CO2air}\,(1 - (T(50°N) / T(35°N))^{12,5})$, for example this difference is:

$$p_{CO2air}\,(1 - ((273.15 + 5) / (273.15 + 20))^{12,5}) = 0.48\ p_{CO2air.}$$

Depending on the strength of the carbon up-welling, the position of the layer at 2250 µmol/kg may be more or less close to the surface; it could have been near the surface during geological epochs with 1500 ppm or more in the air.

8.3 CO_2 Partial Pressures: No Static Air–Sea Equilibrium

For {Talk = 2300 µmol /kg, S = 35 g/l} a static equilibrium with air at 400 ppm would require:

- at 0°C: DIC = 2184 µmol/kg or at 10°C: 2100 µmol/kg, while the observed DIC is 1950 to 2000 µmol/kg.
- at 30°C: DIC = 1939 µmol/kg, while the observed DIC is 2100 to 2000 µmol/kg in the surface waters feeding the inter-tropical out-gassing.

There can therefore be <u>no</u> static equilibrium between the surface ocean and the air; the permanent flows ocean to air in the tropics and air to ocean at mid and high latitudes, modulated by the ocean surface temperatures, are of the order of 100 Gt-C/year (Figure 18-b), extending the obduction and subduction quoted in Sec. 2. AR6 Fig. 5.12 of Masson-Delmotte et al. (2021) underestimates this flux at 80 Gt-C/year.

9. Insolation Controls Ocean Heat and Surface Temperatures

The heat capacity per m² of the first 300 m or 700 m of ocean is 120 or 280 times that of the entire air column above. Air can therefore hardly "warm the ocean". Donohoe et al. (2014) admit: "*climate models forced with CO_2 reveal that global energy accumulation is, instead, primarily caused by an increase in absorbed solar radiation (ASR)*". Indeed, thermal infrared emitted by the air is absorbed by a few tens of microns of liquid water and if its balance with thermal infrared emitted by the surface is positive, it contributes to evaporation.

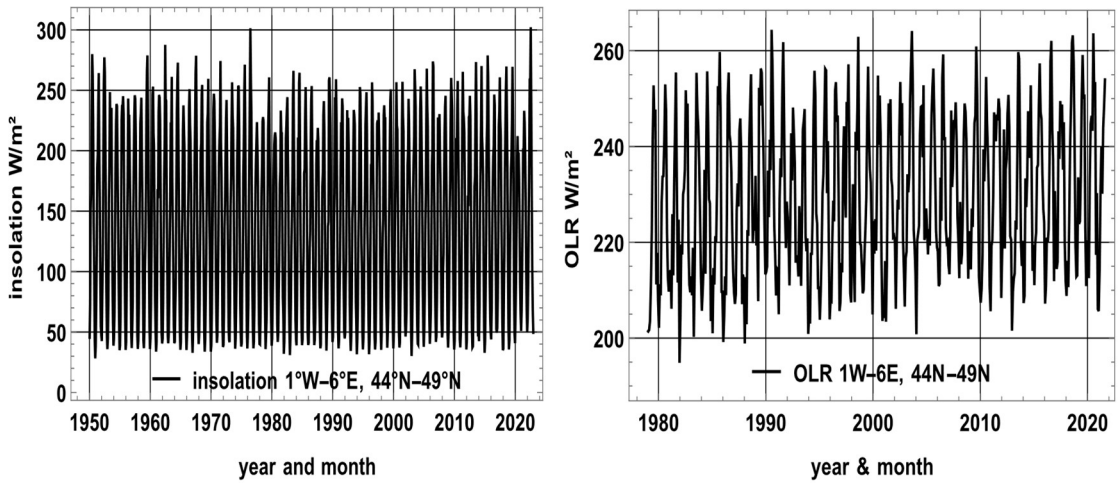

Figure 27 a-b: a) left: Surface insolation over part of France: between 28 W/m² and 302 W/m²; b) right: Radiation delivered to the cosmos (OLR) over the same geographical area: i.e. between 200 W/m² and 260 W/m². Source: KNMI Climate Explorer.

Long series of observations of surface insolation are available only over some land areas; Figure 27 compares over the same region the surface insolation and the OLR (Outgoing Longwave Radiation) supplied to the cosmos at the top of the atmosphere: the motion of the atmosphere and of its water vapor is driven by contrasting temperatures; it ensures that, outside polar zones in winter, the OLR is relatively uniform between 220 and 280 W/m².

Note that Hoogeveen et al. (2025), in their analysis of Earth's energy-imbalance observation series, did not find evidence for a greenhouse-gas effect, consistent with the conclusions of Nikolov & Zeller (2024).

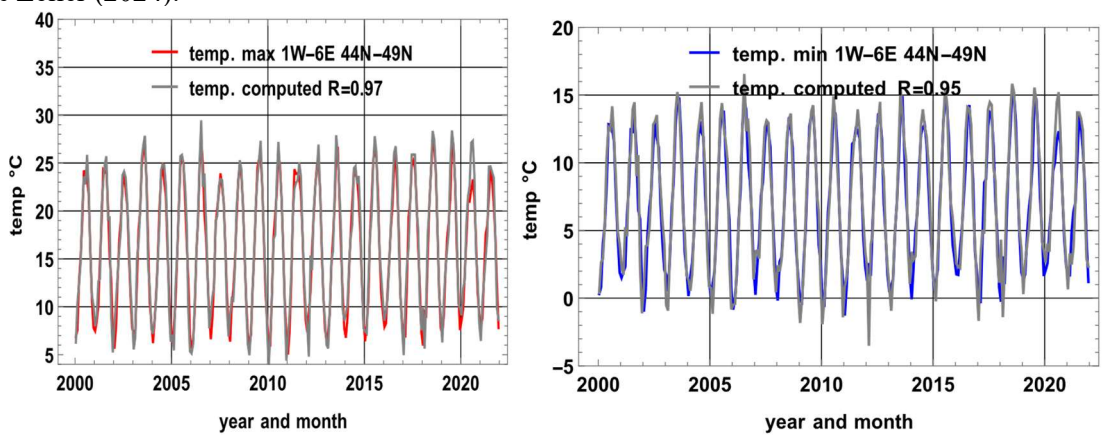

Figure 28 a-b: Comparison of observed temperatures with values inferred from surface insolation. Source: KNMI Climate Explorer — NOAA/UD for OLR and E-OBS 23.1e (globrad) for surface solar radiation. a) left: temp. max. plotted against temp. computed; b) right: temp. min. plotted against temp. computed.

The monthly averages $temp_{max}(n)$ and $temp_{min}(n)$ of the daily maximum and minimum temperatures observed during a month n, over a zone, may be computed from the surface insolation *insol*(n) over that zone during month n and the average temperatures $temp_{max}(n–1)$ and $temp_{min}(n–1)$ of the previous month (n–1). Here $temp_{max}(n)$ and $temp_{min}(n)$ are in °C, and *insol*(n) denotes the monthly mean surface insolation in W m^{-2}. The regression coefficients therefore carry the appropriate inverse units. For instance, Figure *28*,

$temp_{max}(n) = 0.349 + 0.483\ temp_{max}(n)\ (n–1) + 0.055$ insol(n), standard deviation of the error $\sigma = 1.26$°C
$temp_{min}\ (n) = –2.165 + 0.557\ temp_{min}\ (n–1) + 0.0336$ insol(n), standard deviation of the error $\sigma = 1.54$°C.

This supports the conclusion that the surface insolation drives the surface temperatures that drive the natural degassing (or absorption) of CO_2.

10. Examination of Some IPCC's Theories, Models and Conjectures

10.1 Introduction

A model is not a demonstration; it can only justify mechanisms if, and only if, all its results are consistent with all observations. Approximately reproducing the $X(t)$ curve is a necessary but by no means sufficient condition; the growth of the vegetation productivity (Figure 17) and the evolution of $\delta^{13}C$ must also be reproduced and the assumptions made must not be contrary to physics: see discussion in (Harde, 2019). The equations seen in Subsec. 5.2, i.e. (8), (9) and (10) meet these criteria.

Three different "theories", incompatible with each other and incompatible with the figures read on Fig. 6.1 p. 471 of the report (IPCC, 2013), rest on the concepts "*Airborne Fraction*", "*Bern-type impulse response*" and "*adjustment time*" that don't stand scrutiny (Poyet, 2022).

Any increase in natural outgassing since pre-industrial times would contradict the central assumption of the IPCC (2018) framework, namely that global temperature change is a function of the cumulative anthropogenic emissions $f_{\text{fossil}}(t)$ + LUC(t) since 1876 (see their Fig. 1.2, p. 57; Fig. 2.3, p. 105). Figures 12-a (since 1850) and 13-b (since 1880) show curves of this kind, designed to make people believe in a false correlation like +0.45°C for +1000 Gt-CO_2 in cumulative emissions; Figure 12-b has shown that this is a deception.

10.2 Using $dpCO_2$ /pCO_2 vs. dDIC /DIC to Suppress Circulating Fluxes

Stating that:

$$\frac{\mathrm{d}pCO_{2,\text{ seawater}}}{pCO_{2,\text{ seawater}}} = R\frac{\mathrm{d}DIC}{DIC} \tag{25}$$

is a ploy used to suppress the fluxes circulating permanently between oceans and atmosphere. For a Revelle factor R = 12.5, a doubling of the CO_2 pressure in the air and in surface water with $\mathrm{d}p_{CO2}$ = p_{CO2} implies an increase of dDIC of only 1/12.5 = 8% of the DIC; assuming a sea surface layer containing as much carbon as the atmosphere with little or no exchange with the deep ocean, more than 90% of the extra carbon injected into the atmosphere is said to remain in the air.

The contact between the oceans (361 million km², 71% of the Earth's surface) and the atmosphere has been modelled as a single point of contact at a mean ocean surface temperature, for example between 17.7°C and 18.3°C (Bolin & Eriksson, 1959; Joos, 2014; Joos et al., 1996: p. 402; Oeschger et al., 1975; Strassmann & Joos, 2018); this non-sense is used in so-called "models" to ignore the fluxes of about 100 Gt-C/year degassed (Figure 18-b) and absorbed by the surface oceans, and to pretend that the extra CO_2 from fuels remains perpetually in the air.

With respect to R, Wikipedia says[9]: "*The capacity of the ocean waters to take up surplus (anthropogenic) CO_2 is inversely proportional to the value of the Revelle factor.... The Revelle effect describes how only a small fraction of p_{CO2} is present in ocean water when much larger amounts are added to the atmosphere".* This is often said to be a "*buffering effect of sea water*". Egleston et al. (2010) describe these "*buffer factors"* in detail.

This deception is still used: Köhler et al. (2018) invoke Revelle and this relation 9 times on four pages.

With the approximation shown in Figure 25:
$p_{\text{CO2sea water}}$ (µatm) = 400 µatm (T / 299 K)$^{12.5}$ (DIC$_{\mu\text{mole/kg}}$/ 2000)$^{10.4}$ (2328 / TAlk$_{\mu\text{mole/kg}}$)$^{10.3}$
R= 10.4 (eq. 25). Revelle et al. (1965) take R= 12.5, various authors use R between 8.5 and 14.

In reality, sea surface temperatures vary between +32°C and –1.8°C (Ventusky, 2025), giving a

[9] https://en.wikipedia.org/wiki/Revelle_factor

ratio 4.3 between the partial pressures computed with constant DIC and TAlk: therefore there is an inter-tropical zone that out-gasses (Figure 2) and colder sea surface zones that absorb, see maps in (Barry et al., 2010), with, as seen in Sec. 2, a permanent renewal of carbon in the surface ocean by obduction of 275 Gt-C/year where the ocean is degassing, and by subduction of almost as much to the depths where the ocean is absorbing.

There is no static equilibrium without exchanges between reservoirs. For CO_2, as for water vapor, substantial fluxes have always circulated continuously, driven by contrasts in temperature and insolation (Sec. 6 and 9 above).

Thus, the Revelle factor is deceptive because it assumes the ocean is a uniform, static reservoir, so that doubling atmospheric CO_2 would raise dissolved inorganic carbon (DIC) by only ~8%, suggesting over 90% of the extra CO_2 remains in the air, whereas in reality temperature contrasts drive continuous large-scale exchanges between tropical out-gassing and mid and high latitudes absorption.

10.3 Historical Information

In 1957, continuous infrared measurements of CO_2 in air began with electronic equipment developed by Charles Keeling recruited by the Scripps Institution of Oceanography (Keeling et al., 2025). The MLO series began in March 1958. The variations of almost 100 ppm over 24 hours observed on land near growing vegetation and reported, e.g. by Massen et al. (2005), make the measurements on land more uncertain except when strong winds bring them closer to observations made 1 km or 2 km above land surface or sea level (Massen & Beck, 2011). Hence Keeling's choice of the South Pole and Mauna Loa observatories.

10.3.1 Bolin & Eriksson (1959)

Bolin & Eriksson (1959) begin with: "*The dissociation equilibrium of carbon dioxide in the sea is discussed with particular emphasis on the buffering effect of sea water, when changes of the partial pressure of CO_2 in the gas phase take place. The results are used in a study of the changes of the carbon dioxide content of the atmosphere and the sea that occur as a result of release of CO_2 to the atmosphere by fossil fuel combustion. It is shown that the steady state considerations given by previous authors hereby are considerably modified.*" … "*However, by studying the C^{14} distribution in the atmosphere and the sea and its variation in the atmosphere during the last 100 years as revealed by the ratio C^{14}/C^{12} in wood one has been able to <u>show that the exchange time between the atmosphere and the ocean is about 5 years</u> (Craig,1957, 1958; Revelle and Suess, 1957; Arnold and Anderson, 1957; Rafter and Ferguson, 1958).*" … "*It has then been concluded by Revelle & Suess (1957) that most of the CO_2 due to combustion has been transferred into the ocean and that a net increase of CO_2 in the atmosphere of only a few percent has actually occurred*".

But then Bolin & Eriksson (1959) with *the buffering effect of sea water* try with a few pages of equations to make people believe that fuel emissions will remain forever in the atmosphere and will be the sole cause of the growth of $X(t)$. Bolin (1970) predicts between 375 ppm and 400 ppm in 2000 (at MLO it was 369 ppm in 2000).

Bolin & Eriksson (1959) reduce the system of three equations describing a static equilibrium between the atmosphere, the mixed layer at the surface of the ocean and the deep layer of the ocean, an equilibrium disturbed only by fossil emissions, to differential equations of order 3, one for each of the three compartments, with solutions of type: $a_0 + a_1 \exp(-t/b_1) + a_2 \exp(-t/b_2)$. Hence they assume that due to the "*buffering effect*" about 92% of the CO_2 from fossil fuels remain in the air. Vegetation is ignored.

With an exponential growth of fossil fuel emissions $4.96\times10^{-4}\cdot X(1880)\cdot\exp(0.029\cdot(t - 1880))$, where $X(t)$ is the carbon mass in the atmosphere Bolin & Eriksson (1959) conclude that there will be between +25% and +40% more CO_2 in the air in 2000 than in 1880, and that "*The implications*

with regard to the radiational equilibrium of the earth in such a case may be considerable."

10.3.2 Revelle et al. (1965)

The report (Revelle et al., 1965) published by the US Presidency, entitled "*Carbon dioxide from fossil fuels – the invisible pollutant*", asserts that there is no exchange of carbon between the surface ocean (its 100 m deep "mixed" layer) and the deep ocean: "*In the past the usual scientific belief has been that by far the larger part of any added CO_2 would be absorbed in the ocean. This is undoubtedly true if we consider a sufficiently long time period, of the order of thousands or even perhaps hundreds of years ... but over shorter times only the uppermost layer takes part in exchanges with the air...*".

Revelle et al. (1965) use a remarkable circular reasoning to assume that half of all emissions remain perpetually in the air and devote four pages of their report to determining the masses of carbon *M* in the ocean (limited to the surface ocean and rendered inoperative by Revelle's factor!), *A* in the atmosphere and *B* in the biomass that would support his assumption. Revelle et al. (1965) state that in 1959, 13.8% of the CO_2 in the atmosphere was from fossil fuels and that, with an exponential growth in "fossil" emissions at +3.2%/year (or +5%/year), fossil fuel CO_2 will contribute 57.04% (or 93.14%) of the CO_2 in the air in 2009.

This assumption of an exponential growth over 50 years, leading in 2009 to 4.8 times (or 11.5 times) the 2.4 Gt-C/year of 1959, is contradicted by the observations seen in Sec. 4: the "fossil fuel" emissions have grown almost linearly by 0.12 Gt-C/yr since 1950, not exponentially. With the 5-year lifetime seen in Sec. 2, the fraction of the atmospheric stock coming from fuels was 1.5% in 1959 and 4.8% in 2009, twelve and twenty times less than predicted by Revelle et al. (1965). Revelle et al. (1965) forecast "*+14% to +30% for the year 2000 compared with 1950*" (that is 385 ppm to 431 ppm significantly more than the 369 ppm observed at MLO in 2000), "*between +0.6°C and +4°C for +25% on atmospheric CO_2*" (+25% w.r.t 1965 is 398 ppm was observed in 2014), and these authors anticipate the melting of the Antarctic ice cap and other deleterious effects, as consequences of the use of fossil fuels.

Masson-Delmotte et al. (2021) have—implicitly—admitted the falsity of these assertions by showing Fig. 5.12 (p. 700 of AR6, WG1) the 275 Gt-C/year of Levy et al. (2013) between surface and deep oceans, obducted between the tropics and subducted at mid-latitudes.

10.3.3 Oeschger et al. (1975)

Oeschger et al. (1975) still use the *Revelle factor* and state p. 180: "*Based on a preindustrial atmospheric CO_2 concentration in 1860 of 292 ppm, the CO_2 increase in 1970 amounted to 30 ppm. Comparison with the cumulative production of 54.9 ppm indicates that 55% of the fossil CO_2 produced until 1970 remained in the atmosphere.*" This is an introduction to the Bern Impulse response debunked in Subsec. 6.1 and on Figure 16 above.

10.3.4 Conservation Foundation (New York) (1963)

Finally, let us mention the highly political program of the Conservation Foundation (New York), (1963), which became WWF in the 1990s: "*If all known reserves of fossil fuel were used within the next 500 years, a very reasonable assumption, and if the CO_2 system reaches $CaCO_3$ equilibrium (reducing atmospheric CO_2 to a minimum- a condition not likely to be reached for several thousand years) then the CO_2 content of the atmosphere would be four times what it is at present and the average surface temperature of the earth would have risen by 7°C. (The possible change if $CaCO_3$ equilibrium is not reached is 12.2°C). A change even half this great would be more than sufficient to cause vast changes in the climates of the earth; the polar ice caps would almost surely melt, inundating many densely settled coastal areas, including the cities of New York and London. If the temperature of the equatorial regions were to rise by this amount many life forms would be annihilated both on land and in the sea [...] Arousing public interest in the effects of the increase in atmospheric CO_2 is as much a problem as the lack of adequate data. The potentially dangerous*

increase of CO_2 due to the burning of fossil fuels is only one example of a failure to consider the consequences of industrialization and economic development."

10.4 The Myth of a Permanent Airborne Fraction (AF)

10.4.1 The "Carbon Sink"

If **c**umulative fossil fuel emissions with Land Use Change (LUC) were the only cause of the growth of $X(t)$, then $dX(t)/dt = AF\, f_{\text{fossil}}(t)$; a carbon sink, $sink(t)$, absorbs each year what has not remained in the atmosphere:

$$\begin{aligned} sink(t) &= f_{\text{fossil}}(t) - \frac{dX(t)}{dt} \\ &= (1 - AF) f_{\text{fossil}}(t) \\ &= absorb(t) - degas(t) \end{aligned} \tag{26}$$

Then natural absorption and degassing, 179 Gt-C/year and 175 Gt-C/year by mid-2023, with different physical causes, would be linked by a relation which, via $f_{\text{fossil}}(t)$ (10.4 Gt-C/year in 2023), depends solely on economic conditions! This is supernatural and assumes that mid-latitude vegetation and oceans sort CO_2 molecules according to their "natural" or "fossil fuel" origin, which is physically impossible for indistinguishable molecules.

10.4.2 Calculations of AF (without and with LUC)

Figure 29 shows that different methods give very different results and that before 1965, *AF* is close to 100%. Without the LUC (Land Use Change) seen in Figure 13-a, with the flux $f_{\text{fossil}}(t)$ over the period 1959-2024 (black curve Figure 29), *AF* varies between 6.7% and 141%. But *AF* cannot be greater than 100%!

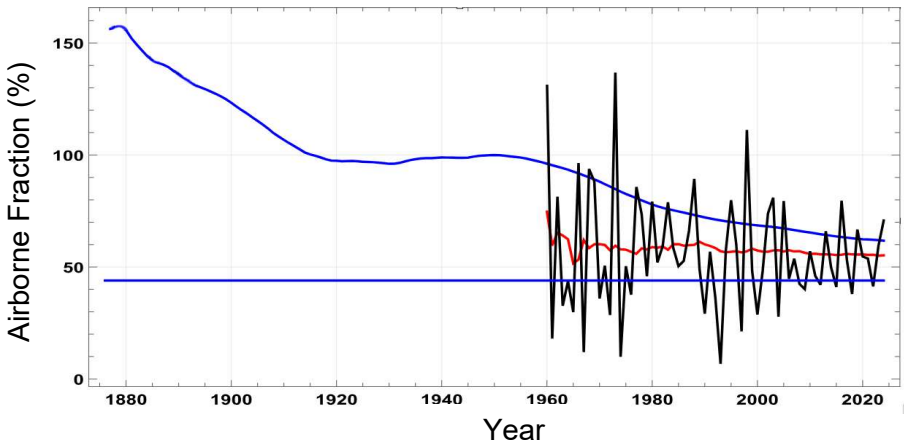

Figure 29: Airborne Fraction AF(t)% calculated for some formulations:
in blue ($X_{MLOlogis}(t) - X_{MLOlogis}(1876)) / \int_{1876}^{t} f_{fossil}(t')\, dt'$, in red ($X_{MLO}(t) - X_{MLO}(1959)) / \int_{1959}^{t} f_{fossil}(t')\, dt'$,
in black ($X_{MLO}(t+0.5) - X_{MLO}(t-0.5)) / f_{fossil}(t)$; the blue horizontal line is AF = 44% (IPCC, 2021).

Adding LUC, for example, 1.65 Gt-C/year, brings *AF* over the 1959-2024 period to the range 5% to 102%, with an almost normal distribution of mean 44% and standard deviation 19%. Fig. 5.5(b) of Masson-Delmotte et al. (2021, p. 688) shows various LUC estimates since 1959: for the same year, it is between 0.6 Gt-C/yr and 2.4 Gt-C/yr.

Masson-Delmotte et al.'s (2021, p. 690) Fig. 5.7 shows year-by-year averages of the ratio between increments of $X_{\text{MLO}}(t)$ and $f_{\text{fossil}}(t)$ + LUC(t): as the different fluxes entering the atmosphere are mixed together in a few weeks and become indistinguishable, this representation is absurd. $AF(t)$ on this AR6 Fig. 5.7 over the years 1960-2019, is between 20% and 80%, average 44%. A 5-year moving average (a highly dubious trick that allows variability to be masked: see Subsec. 5.3) reduces the range of $AF(t)$ values to 30% to 60%.

Hansen et al. (2013) found that their *AF* (calculated with a 7-year moving average!) has fallen from 60% in 2000 to 42% in 2011 and explained this by the magical properties of the "Chinese" coal which, in the 2000s, would have very extraordinarily stimulated the growth of the vegetation!

10.4.3 $\delta^{13}C$ Shows that Fossil Fuel Emissions do not Remain in the Air

IPCC (2013) § 6 page 467: "*About half of the emissions remained in the atmosphere (240 Gt-C) since 1750*". Since 240 Gt-C is 29% of the carbon in the air at date 2011.0, the $\delta^{13}C$ of the air should have been: 29% (–28‰) + 71% (–6.5‰) = –12,7‰. The $\delta^{13}C$ observed at this date (Figure 22-a) is –8.3‰!

10.4.4 dX(t)/dt and $f_{fossil}(t)$ are not Correlated

The equation $dX(t)/dt = AF\, f_{fossil}(t)$ has been shown to be impossible by Figure 7 with very different autocorrelations of the stationary $dX(t)/dt$ and of the non-stationary ARIMA I=1 $f_{fossil}(t)$ series, and by Figure 12-b, which shows a coefficient of determination $R^2 = 0.038^2 = 0.001$ between the two "detrended" series. It makes no sense to look for an *AF* between non-correlated time series.

10.4.5 Absorb(t) Varies as X(t)/5 and not as degas(t) + 0.55 $f_{fossil}(t)$

IPCC (2013) § 6 page 467: "*About half of the emissions remained in the atmosphere (240 Gt-C) since 1750 ... Globally, the size of the combined natural land and ocean sinks of CO_2 approximately followed the atmospheric rate of increase, removing 55% of the total anthropogenic emissions every year on average during 1958-2011."*

These statements mean: $sink(t) = absorb(t) - degas(t) = f_{fossil}(t) - dX(t)/dt = 0.55\, f_{fossil}(t)$ and $absorb(t) = degas(t) + 0.55\, f_{fossil}(t)$.

But it's impossible for emissions to remain (*remained*) in the atmosphere, because any input into the atmosphere or the oceans will, after a certain time, be distributed between the three compartments in proportion to their fraction of the total mass, i.e. around 2.2% for the atmosphere, and their atmospheric trace decreases according to the *F1*(*t*) impulse response, the black curve on Figure 16.

If a fraction *AF* = 44% of the natural out-gassing degas(t) were to remain perpetually in the atmosphere, the $dX(t)/dt$ increments would have risen from +28 ppm/yr in 1959 to +39 ppm/yr in 2023, a far cry from the +0.8 ppm/yr and +3.5 ppm/yr observed in 1959 and 2023.

So how do *natural land and ocean sinks* sort CO_2 molecules according to their origin?

10.4.6 Rapid Carbon Mixing Makes Annual Fossil-CO_2 Sink Budgets Meaningless

Fossil fuel emissions are well mixed in the atmosphere with natural out-gassing and cannot be distributed among the three reservoirs on an annual basis. Stocker et al. (2013, p. 51) Fig. TS.4 show the distribution of emissions among several sinks, year by year; the legend to this figure reads*: "Annual anthropogenic CO_2 emissions and their distribution among the atmosphere, land and oceans from 1750 to 2011. [...] Emissions and their distribution include only fluxes that have changed since 1750, and not natural CO_2 fluxes for example, atmospheric uptake of CO_2 through weathering, outgassing of CO_2 from lakes and rivers, and outgassing of CO_2 by the ocean from carbon contributed by rivers*; *see figure (6.1) between atmospheric, terrestrial and oceanic reservoirs that existed before that time and still exist today."*

This year-by-year distribution of the year's emissions (Fig. TS.4) is incompatible with the mixing in the atmosphere of emissions from fuels with the natural out-gassing twenty times greater (60 times in 1959), and with the circulation of carbon between the three main compartments. This mixing in the atmosphere takes a few weeks.

The comment on this Fig. TS4 says that natural fluxes have not changed since 1750, that it only shows "*fluxes that have changed since 1750, not natural CO_2 fluxes"!* The evolution of ocean

degassing (Figure 17 and Sec. 8 above) is absolutely taboo: the IPCC only mentions "*outgassing of CO_2 by the ocean from carbon delivered by rivers*".

10.4.7 AF Requires That Absorption Has Been Almost Constant Since 1850

The relation +0.45°C for +1000 Gt-CO_2 of cumulative emissions, (IPCC, 2021) Fig. SPM. 10 assumes that the increase in $X(t)$ since 1850 is entirely due to cumulative "human" emissions. This implies that the natural degassing has not changed since 1850, that is with a pre-industrial equilibrium around 1850:

$$degas(t) = degas(1850) = absorb(1850), \text{ hence}$$
$$absorb(t) = -\,\mathrm{d}X(t)/\mathrm{d}t + degas(t) + f_{\text{fossil}}(t) = -\,AF(t)\,f_{\text{fossil}}(t) + absorb(1850) + f_{\text{fossil}}(t)$$
$$= absorb(1850) + (1-AF)\,f_{\text{fossil}}(t)$$
$$absorb(2024) - absorb(1850) = 0.56\,f_{\text{fossil}}(2024) = 6 \text{ Gt-C/year.}$$

This is almost:

- five times less than the number shown in Fig. 6-1 p. 471 of (IPCC, 2013) where we read: *absorb*(2020) – *absorb*(pre-industrial) = 20 (oceans) + 14×1/2 (NPP of vegetation) = 27 Gt-C/yr,
- ten times less than *absorb*(2024) – *absorb*(1850) = $X(2024)/5 - X(1850)/5$ = 61 Gt-C/yr, computed with the logistic extension of MLO observations prior to 1958.

10.4.8 Conclusion

We've just seen seven demonstrations of the absurdity of the "*Airborne Fraction*" concept.

10.5 Bern's Function or Bern Impulse Response

The fraction $F1(t)$ of a CO_2 pulse in the atmosphere t years after its injection has been described in Sec. 6 Figure 16, and compared with Bern's function $FB(t)$ plotted in red. For variants, see (Joos, 2014; Joos et al., 1996). $FB(t)$ defies common sense: it does not apply to natural degassing and assumes that vegetation and oceans discriminate between CO_2 molecules according to their "natural" or "fossil" origin.

$FB(t)$ is calibrated to be 1/e at the end of 100 years, hence the 100-year lifetime of CO_2 in the air. IPCC (2007, p. 213) note a) of table 2-14 state: "*The CO_2 response function used in this report is based on the revised version of the Bern Carbon cycle model used in Chapter 10 of this report (Bern 2.5CC; Joos et al. 2001) using a background CO_2 concentration value of 378 ppm.*". The decay of a pulse of CO_2 with time t is:

$$\text{Bern}_1(t) = 0.217 + 0.259\exp(-t/172.9) + 0.338\exp(-t/18.51) + 0.186\exp(-t/1.186)$$

This expression detailed in (UNFCCC, 2002) is still invoked in (IPCC, 2013) AR5 WG3 report. By definition of an impulse response, the change of the atmospheric stock is:

$$X(t) - X(t_0) = \int_{t_0}^{t} F\,(t-t')f_{fossil}(t')dt' \text{with } F(t) = a_0 + \sum a_i\, e^{\left(\frac{-t}{b_i}\right)} \qquad (27)$$

with,

$$\frac{\mathrm{d}X(t)}{\mathrm{d}t} = \int_{t_0}^{t}\left(\frac{dF}{dt}\right)(t-t')f_{fossil}(t')dt' + F(0)f_{fossil}(t) \qquad (28)$$

$f_{\text{fossil}}(t_0) = 0$ (pre-industrial) and

$$\frac{\mathrm{d}F}{\mathrm{d}t} = \sum\left(\frac{-a_i}{b_i}\right)e^{\left(\frac{-t}{b_i}\right)} \text{ and } F(0) = a_0 + \sum a_i = 1 \qquad (29)$$

The natural out-gassing is assumed to be constant, it's a basic assumption in SPM.10 (IPCC,

2021), thus $dX(t)/dt = degas(t_0) + f_{fossil}(t) - absorb(t)$, $absorb(t) = degas(t_0) + f_{fossil}(t) - dX(t)/dt$:

$$absorb(t) = degas(t_0) + f_{\text{fossil}}(t) - \int_{t_0}^{t} \left(\frac{\mathrm{d}F}{\mathrm{d}t}\right)(t - t')f_{\text{fossil}}(t')dt' - F(0)f_{\text{fossil}}(t) \quad (30)$$

$$absorb(t) = degas(t_0) + \sum \left(\frac{a_i}{b_i}\right) e^{\left(\frac{-t}{b_i}\right)} \int_{t_0}^{t} e^{\left(\frac{t'}{b_i}\right)} f_{\text{fossil}}(t')dt' \quad (31)$$

This expression of $absorb(t)$ according to the IPCC depends only on $f_{fossil}(t)$. This is supernatural: physically, the absorption depends on the partial pressure and therefore on the mass $X(t)$ of carbon in the air, of which it is one-fifth, also see section 5.2 of (Harde, 2019) for a complete discussion on that matter.

Numerical check: $absorb(2012) - degas(\text{pre-industrial}) = 2.7$ Gt-C/y, ten times less than what is seen in Fig. 6-1, p. 471 of IPCC (2013) with (80 + 123 / 2) – (60.7 + 107.2 / 2) = 27.2 Gt-C/y (the GPP of 123 Gt-C/y in 2012 and 107.2 Gt-C/yr in pre-industrial time was divided by 2 to get the NPP as explained in Sec. 3) and 18 times less than $X(2012)/5 - X(1750)/5 = 49.8$ Gt-C/y.

10.6 An "Adjustment Time" or "Atmospheric Lifetime" Between 50 and 200 Years

Houghton et al. (1990) section 1.2.1 say "*This short time scale (lifetime or residence time or turnover time of five years) should not be confused with the time needed for the atmospheric CO_2 level to adjust to a new equilibrium if sources or sinks change. This adjustment time, corresponding to the lifetime in Table 1.1, is of the order of 50 to 200 years, determined mainly by the slow exchange of CO_2 between surface waters and the deep ocean*". Both of these statements are false: as seen in Sec. 2, the "slow exchange" in the ocean is 275 Gt-C/y, with a complete renewal of carbon in the out-gassing and absorbing areas of the surface ocean, and in the ocean it is not CO_2 but dissolved inorganic carbon, as seen in Sec. 8.

A false correlation is used to produce an "adjustment time". This theory is reminiscent of *"The streetlight effect, or the drunkard's search principle*". In

$$sink(t) = f_{fossil}(t) - dX(t)/dt = absorb(t) - degas(t)$$

only the term on the left is known with any precision (the area well-lit by the streetlamp where the drunk man is looking for his keys), while the natural outgassing and absorption fluxes are estimated with considerable uncertainty, over 20% according to the legend of Fig. 6.1 of IPCC (2013). Then $sink(t)$ in Gt-C/yr, is regressed on $X(t)$ and approximated by:

$$X(t)/57\text{ yr} - 10.5\text{ Gt-C/yr} = (X(t) - 599\text{ Gt-C})/57\text{ yrs (see Figure 30-a)}$$

57 years is called "adjustment time".

Harde (2019) points out that a sudden shift at the end of 1751, the supposed start of industrialization, from $absorb(t) = X(t)/5$ yr to $absorb(t) = degas(1751) + (X(t) - 599\text{ Gt-C})/57$ yr is hard to believe and that this $absorb(t) = degas(1751) - 10.5$ Gt-C/yr + $X(t)/57$ yr is non-zero even if $X(t)$ is zero! For a detailed discussion of nature as a net sink or net source, see also Harde (2025).

Calculations of this kind are proposed by Cawley (2011) and Dengler (2024) to make us believe that there is an "*adjustment time*" other than the 5 years; G. Cawley begins his article with: "*The error is due to confusion between residence time and adjustment time, which describes the time required for the concentration of CO_2 in the atmosphere to return substantially to its initial concentration after a perturbation; unlike other atmospheric gases, residence time and adjustment time are not the same for carbon dioxide.*"

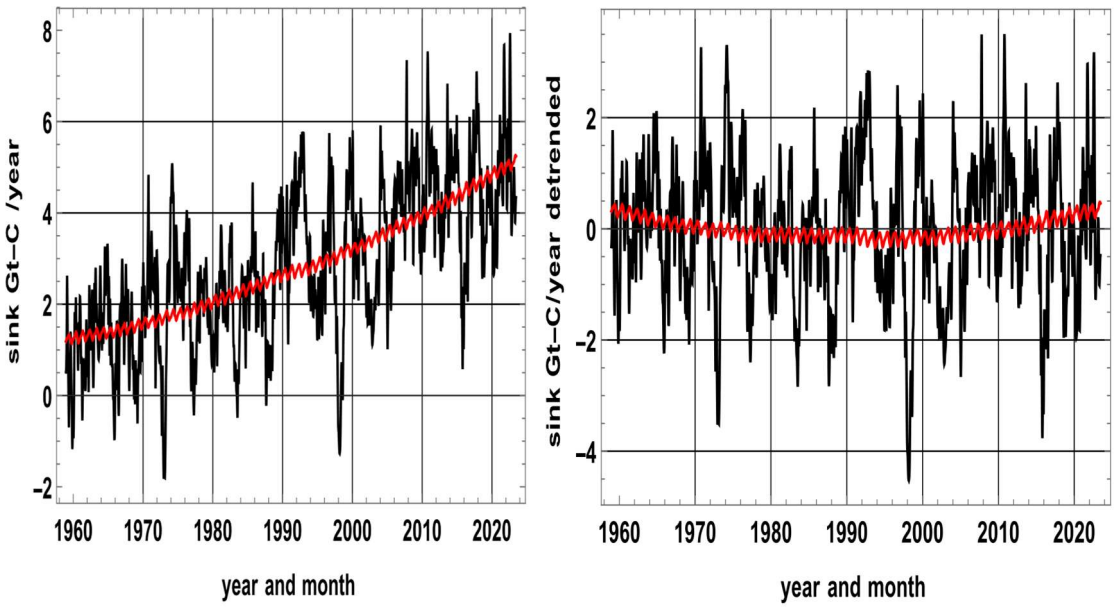

Figure 30 a-b: a) left, regression of sink(t) in red on (X(t) –599 Gt-C)/57yr, in black: a false correlation with a non-stationary series; b) right, the same series after subtraction of their linear trends ("detrended") R^2 = 0.04.

Figure 16 (black curve) shows the response to a unit perturbation.

$sink(t) = f_{fossil}(t) - dX(t)/dt$ in Figure 30-a (black) seems to correlate with ($X(t)$ – 599 Gt-C)/57yr plotted in red: R^2 =0.66. But since the $X(t)$ series is not stationary, we must subtract from each series its linear trend, because non-stationary (trending) data can produce spurious correlations[10]. Detrending ensures that the analysis captures short-term co-variations rather than merely reflecting their common long-term growth. Figure 30-b shows R^2 = 0.04, so no valid correlation is possible, and the 57 year "*adjustment time*" is merely the result of a gross error in the processing of time series.

Koutsoyiannis (2024a, 2024b) reviews the various IPCC assertions and the always changing denominations: r*esponse time, adjustment time, lifetime, turnover time*. Masson-Delmotte et al. (2021, p. 2237) say: "*Carbon dioxide (CO_2) is an extreme example. Its turnover time is only about 4 years because of the rapid exchange between the atmosphere and the ocean and terrestrial biota. However, a large part of that CO_2 is returned to the atmosphere within a few years. The adjustment time of CO_2 in the atmosphere is determined from the rates of removal of carbon by a range of processes with time scales from months to hundreds of thousands of years. As a result, 15 to 40% of an emitted CO_2 pulse will remain in the atmosphere longer than 1,000 years, 10 to 25% will remain about ten thousand years, and the rest will be removed over several hundred thousand years*".

Those assertions are based only on models and not on observations. The impulse response was seen in Sec. 6 (black curve in Figure 16) and tends towards 2.2%.

And as noted by Harde (2017, 2019) the residence time τ resulting from a "range of processes of time scales τ_i" is given by $1/\tau = \Sigma\ 1/\tau_i$ and is therefore less than the smallest of the τ_i.

10.7 A Thousand-Year Lifespan in the Atmosphere?

IPCC (2013, p. 472), Box 6-1 write: "*phase 1. Within several decades of CO_2 emissions, about a*

[10]Detrending is applied solely to prevent trend-alignment artefacts: when two series both rise monotonically, as is common in long-term climatic or geochemical time series, their raw values can appear correlated even if their short-term fluctuations are unrelated. Removing the linear trend isolates the physically meaningful covariance without denying the reality of long-term changes in $X(t)$.

third to half of an initial pulse of anthropogenic CO_2 goes into the land and ocean, while the rest stays in the atmosphere [...] Within a thousand years, the remaining atmospheric fraction of the CO_2 emissions (see Section 6.3.2.4) is between 15% and 40%, depending on the amount of carbon released (Archer et al., 2009b)."

As already mentioned, exchanges between compartments imply that a pulse of carbon injected into one compartment will, over the long term, be redistributed among all reservoirs in proportion to the carbon masses they contain.

These carbon flows are, like water and water vapor flows, a consequence of temperature contrasts between latitudes and cannot be discounted as is done by assuming an "*average*" ocean at an "*average temperature*" (Caldeira & Wickett, 2003; Joos, 2014; Joos et al., 1996; Plass, 1956).

Of an impulse of a few Gt-C, only 2.2% remains in the air after 200 years (Figure 16); of the 500 Gt-C accumulated over 1751- end 2024 from coal, oil and gas combustion, 49 Gt-C or 23 ppm are still in the air (not yet absorbed). And only those 23 ppm may be impacted by "zero-carbon" policies.

The impulse response in Figure 16 applied to the emissions series shows that of the 500 Gt-C cumulative emissions since 1751, 67 Gt-C or 32 ppm are in the atmosphere, of which 18 Gt-C or 9 ppm are "zombies" that have returned to the atmosphere after one or several cycles of absorption and degassing.

Discussing carbon pulses in the hundreds or thousands of Gt-C (IPCC, 2013), FAQ 6.2, Fig. 2, p. 545, in an analysis of the effects of human emissions of a few Gt-C/year (initial pulse of anthropogenic CO_2) is, say, very "surprising"!

10.8 On the Oceanic CO_2 Bottleneck

Köhler et al. (2018) state: "*Only this 1% of DIC in the surface ocean, found as dissolved CO_2, can exchange with the atmosphere. Thus, the carbonate chemistry represents a bottleneck for the oceanic uptake of anthropogenic CO_2 emitted to the atmosphere.*"

In reality, conversions between the various forms of CO_2 hydrate, HCO_3^- and CO_3^{--} are almost instantaneous and, at a given total alkalinity (Sec. 8, Figure 25), it's DIC and temperature that determine the partial pressure of CO_2 in seawater: no bottleneck!

10.9 The Numbers on (IPCC, 2013) Fig. 6.1 Proves that a Major Oceanic Degassing is Required to Match MLO Observations

The text associated with this Fig. 6.1 col. 2 of AR5 (IPCC, 2013, p. 470) is: "*Reservoir turnover times, defined as reservoir mass of carbon divided by the exchange flux, range from a few years for the atmosphere to decades to millennia for the major carbon reservoirs of the land vegetation and soil and the various domains in the ocean.*"

Berry (2021) uses the numbers of Fig. 6.1 of IPCC (2013), with four compartments atmosphere, vegetation and soil, surface ocean and deep ocean of masses $X(t)$, $Y(t)$, $Z_{ocs}(t)$, $Z_{ocd}(t)$ and a τ specific to each reservoir: τ is the quotient of the pre-industrial stock by the pre-industrial outflow stated by IPCC. The content of each compartment is derived from an equation like:

$dy(t)/dt = -y(t)/\tau + g(t)$ where $g(t)$ is the sum of the flows entering the compartment, with initial conditions $X(1850) = 589$ Gt-C, $Y(1850) = 2500$ Gt-C, $Z_{surface}(1850) = 900$ Gt-C, $Z_{deep}(1850) = 37{,}100$ Gt-C and with $f_{fossil}(t) = 18\,\text{Gt-C/yr}/(1 + \exp((2011-t)/29\,\text{yr}))$. With the assumption of a constant $\tau_{surface\ ocean}$ the distribution of the "*fossil fuel carbon*" between the four compartments is plotted in Figure 31-a, bottom four curves, practically Fig. 11 of (Berry, 2021).

The gray curve of the atmospheric increments is very much below the black curve of MLO observations with their logistics extension at the top of Figure 31-a! Between the dates 1850 and 2024, the calculation, without an ocean degassing increasing over time with the inter-tropical sea surface temperatures, says +78.9 Gt-C in the atmosphere (thick grey curve, i.e. +37 ppm), +193

Gt-C in vegetation and soils (green curve), +42.2 Gt-C in the surface ocean (thin blue curve) and +175.5 Gt-C in the deep ocean.

The difference between the black curve (+310 Gt-C) and the grey curve (+80 Gt-C) of Figure 31a shows that the oceanic degassing plotted in Figure 18b of Subsec. 6.2 above is needed to match the MLO observations.

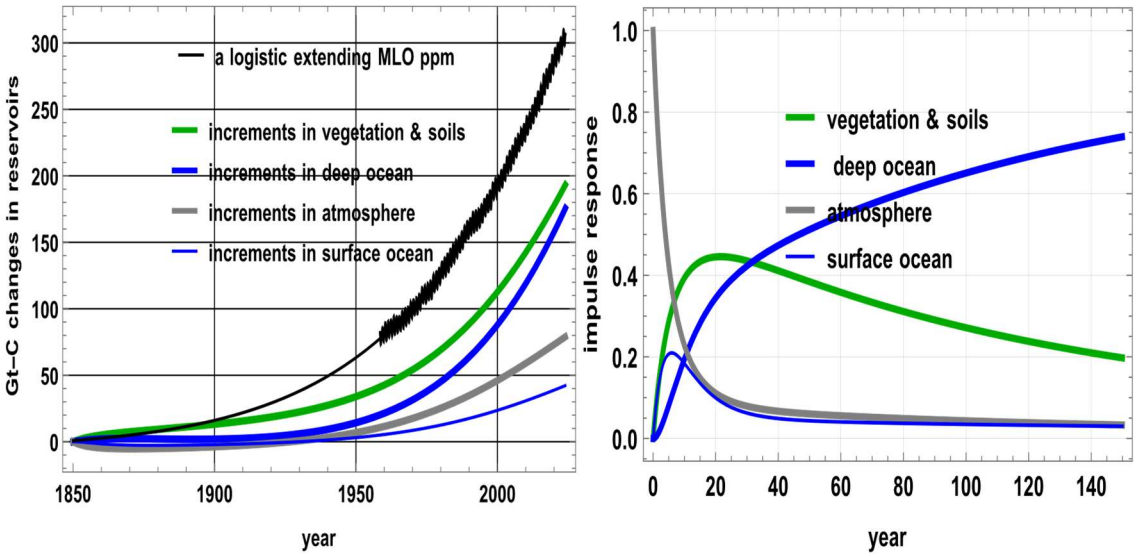

Figure 31 a-b: a) left: Increments of the four stocks relative to 1850 computed from pre-industrial stocks and fluxes of (IPCC, 2013) Fig. 6.1. Green: vegetation and soils, thick blue: deep oceans, grey: air, blue: surface oceans. The black curves at the top are X(t) observed at MLO and its logistics extension; b) right: Impulse responses to a unit pulse in the air, with the pre-industrial stocks and flows. For the atmosphere the grey curve F2(t) = 0.024 + 0.892 exp(–t/5.28yr) + 0.084 exp(–t/64yr) is close to F1(t) seen in § 6 and to F3(t) = 0.034 + 0.858 exp(–t/3.17yr) + 0.107 exp(–t/52.8yr) computed with the flows and stocks of year 2011 taken from IPCC (2013).

10.10 Hundreds of Millennia (100,000 Years and more)

IPCC (2013, p. 472), Box 6.1: *Multiple Residence Times for an Excess of Carbon Dioxide Emitted in the Atmosphere: "the removal of all the human-emitted CO_2 from the atmosphere by natural processes will take a few hundred thousand years (high confidence) as shown by the timescales of the removal process shown in the table below (Archer and Brovkin, 2008)*".

CO_2 has in the atmosphere a half-life of 3.5 years, i.e. after 7 years the remains of the initial stock is a fourth as $2^{-7/3.5} = 1/4$. The *time scale of the removal process* is 3.5 years, not hundreds of millennia!

10.11 Flows Between Deep Ocean and Surface Oceans

The first IPCC report (Houghton et al., 1990) shows a pattern of 90 Gt-C/yr degassed, 92 Gt-C/yr absorbed but, between surface ocean and deep ocean, only 37 Gt-C/yr up-welling and 39 Gt-C/yr down-welling, seven times less than the 275 Gt-C of Sec. 2.

The AR4 report (IPCC, 2007) shows for 1990, 90.6 Gt-C/yr degassed, and 92.2 Gt-C/yr absorbed, a 900 Gt-C stock in the surface ocean, 101 Gt-C/yr up-welling and 102.8 Gt-C/yr down-welling (including the 11 Gt-C/year in organic debris). This is almost three times less than the 275 Gt-C/yr observed in Sec. 2 and finally accepted in 2021 by the IPCC, Fig. 5.12 p. 700 of AR6 (Masson-Delmotte et al., 2021).

11. Carbon-14 in the Atmosphere

11.1 Historical Background

Revelle et al.(1965) used ^{14}C to dispel "*the usual scientific belief of the past*"; $\Delta^{14}C$ is still invoked by (NOAA Global Monitoring Laboratory, 2021) to divert attention from the unchanged growth of $X(t)$ at MLO despite a sharp reduction in emissions in 2020 due to the COVID lock-downs.

11.2 On the Isotope ^{14}C

The activity of a sample is expressed in disintegration per second, in Bq units. The activity of a mass of ^{14}C with an e-folding time (mean lifetime) of 8,267 years, (corresponding to a half-life of 5,730 years), decreases as $\exp(-\lambda\, t)$ with $\lambda = 1 / (8{,}267 \times 365.25 \times 86{,}400) = 3.83 \times 10^{-12}$/s. One kilogram of ^{14}C produces $1{,}649 \times 10^{14}$ Bq. Natural ^{14}C comes from nuclear reactions of nitrogen in the air with neutrons produced in the atmosphere by cosmic ray fluxes (mainly protons) and solar particles; it is a marker of the sun's magnetic activity.

The Earth's magnetic field keeps out low-energy particles (< 10 GeV) except around the poles; around 55% of ^{14}C production, say 2 atoms/cm²/s on average or 7.5 kg/year of ^{14}C takes place in the stratosphere, which is thicker at high latitudes (Figure 32).

Levin et al. (2010) say for natural production 2.1×10^{26} atoms/yr or a mass of 4.9 kg/year suggesting a natural stock of 4.9 kg/year × 8267 years = 40,400 kg if solar activity did not vary, distributed in the three reservoirs atmosphere, oceans and vegetation and soils.

Thermonuclear tests (Hua et al., 2013; Hua & Barbetti, 2004) sent an estimated 1,440 kg (one thousand four hundred forty kg) of ^{14}C or ≈ 240 10^{20} Bq into the stratosphere between 1952 and 1976, with a maximum between 1961 and 1963 (1,440 kg × 1.65 10^{14} Bq = 2.37 10^{20} Bq), i.e. about +3% of the total mass of ^{14}C circulating between the three reservoirs.

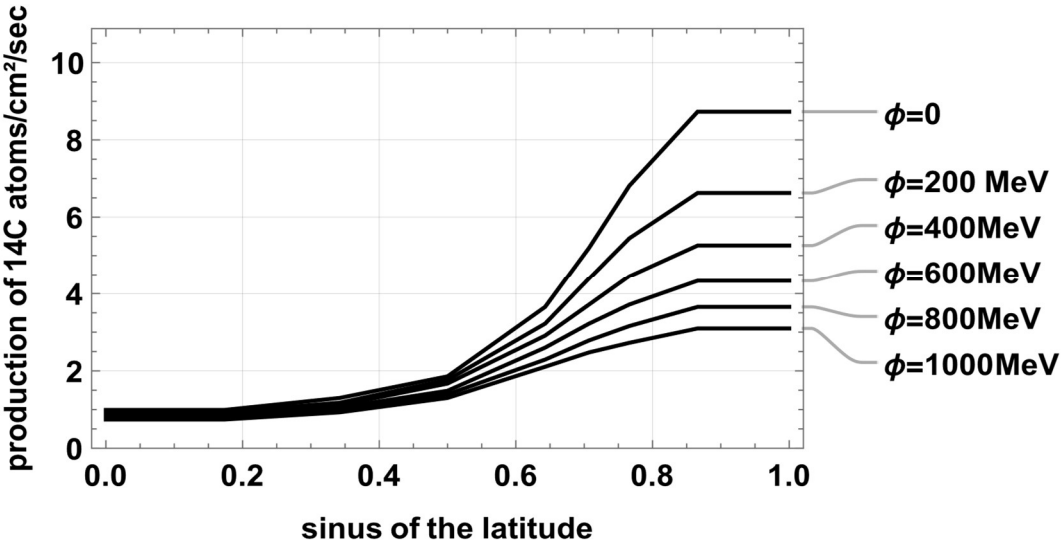

Figure 32: Natural production of ^{14}C as a function of latitude and of a solar modulation parameter φ; after (Masarik & Beer, 1999) Fig. 8; φ has been reconstructed for the last millennium (Muscheler et al., 2007): it oscillates between 200 MeV and 1200 MeV, with the number of sunspots (Brehm et al., 2021).

These 1440 kg were gradually transferred to the troposphere and subsequently to vegetation, soils, and oceans (Salby & Harde, 2021a). For the annual renewal of approximately one-fifth of the mass of the lower stratosphere: see (Diallo et al., 2017; Holton et al., 1995; Stohl et al., 2003). Medical and industrial applications could release approximately 500 TeraBq/year, which would correspond to an annual mass of 3.03 kg of carbon-14: ($500\cdot10^{12}$ Bq/yr × 0.014 kg/mol)/ ($3.833\cdot10^{-12}$ s^{-1} × 6.022 10^{23}) with $\lambda = 3.833\cdot10^{-12}$ s^{-1} as radioactive constant of carbon-14; 0.014 kg/mol as the molar mass of carbon-14; and $6.022\cdot10^{23}$ mol^{-1} as Avogadro's Number N_A.

$\delta^{14}C$ represents the decrease (in ‰) of carbon-14 in the sample before correction for isotopic fractionation with $\delta^{14}C = [(A_{sample} / A_o) - 1] \times 1000$, where A_o is the activity of the modern standard Oxalic acid and A_{sample} is the equivalent for the sample in question.

$\Delta^{14}C$ is an indicator or marker that is equal to –1000‰ in the total absence of ^{14}C (which is the case for fossil fuels).

$\Delta^{14}C$ = 0‰ applies for the initial dynamic equilibrium → production of ^{14}C in the upper atmosphere = disappearance of ^{14}C through decay.

$\Delta^{14}C$ represents the normalized value of $\delta^{14}C$, i.e., the activity is corrected for the isotopic fractionation of the sample ($\delta^{13}C$).

$\Delta^{14}C$ values are normalized to a base value of –25‰ relative to the $^{12}C/^{13}C$ ratio of the VPDB standard.

Now with these reminders, see supplement to (Wenger et al., 2019), with n^{12} and n^{14} that denote the number of ^{12}C and of ^{14}C atoms in the sample, let's define:

- $r = n^{14}/n^{12}$ be the measured $^{14}C/^{12}C$ atom ratio of the sample,
- $R_{ref} = (^{14}C/^{12}C)_{ref}$ the reference ratio,
- $\delta^{13}C$ the sample $\delta^{13}C$ in ‰ (VPDB).

The exact fractionation correction is then given by:

$$r_{norm} = r\left(\frac{1-25/1000}{1+\delta^{13}/1000}\right)^2 \tag{32}$$

So the exact normalization form is:

$$\Delta^{14}C = 1000\left(\frac{r_{norm}}{R_{ref}} - 1\right) \tag{33}$$

Measured $^{14}C/^{12}C$ ratios are normalized to a common $\delta^{13}C$=-25‰ using the standard squared ratio correction; for small δ^{13} values the normalization factor may be linearized to $1-2(25+\delta^{13})/1000$. $\Delta^{14}C$ is then defined as 1000 times the normalized sample-to-reference ratio minus one.

$$\Delta^{14}C \approx 1000\left[\frac{r(1-2(25+\delta^{13}C)/1000)}{R_{ref}} - 1\right] \tag{34}$$

If $\Delta^{14}C$ = 0‰, then $(^{14}C/^{12}C)_{sample} = (^{14}C/^{12}C)_{ref} = 1.217\times10^{-12}$. A 10% increase in ^{14}C (with ^{12}C held constant) raises the ratio to 1.3387×10^{-12} and thus increases $\Delta^{14}C$ from 0 ‰ to 100 ‰. The reference activity (absolute activity used for the standard) may be expressed as:
$A_{ABS} = 0.95\times0.238$ Bq/(g–C), i.e. A_{ABS}= 0.2261 Bq/(g–C). Here "ref" means $(^{14}C/^{12}C)_{reference.}$

$$Ref = \left(\frac{n^{12}_{standard}}{n^{14}_{standard}}\right) = \frac{\lambda N_A}{A_{|m_C|}} = \frac{3.8332\cdot10^{-12}\times6.0223\cdot10^{23}}{0.95\times0.238\times12} = 8.508\cdot10^{11} \tag{35}$$

For example, with $\delta^{13}C$ = –8‰, $(1 - 2\,(25 + \delta^{13}C) / 1000) = 0.966$, $\Delta^{14}C‰ = f \times (n^{14}/n^{12}) - 1000$, with $f = 8.219\times10^{11}$. Here f is simply the normalizing factor that converts the raw isotopic ratio n^{14}/n^{12} into the per-mil $\Delta^{14}C$ scale, taking into account the $\delta^{13}C$ correction.

Historical reconstructions of $\Delta^{14}C$ used carbon-14 dating over the last millennium range from +20‰ during the solar minima of the Little Ice Age, to –20‰ for a more active Sun. Figure 33 shows observations made in New Zealand since 1955, with a break between July 1997 and June 1999. $\Delta^{14}C$ = –18‰ in December 1954. Figure 33-b shows the evolution of the mass of ^{14}C in the atmosphere, calculated as:

$$\left(\frac{^{14}C}{^{12}C}\right)_{sample} = \frac{\left(\frac{14}{12}\right)m_{12}\left(1+\frac{\Delta^{14}C}{1000}\right)}{R_{ref}\left[1-2\frac{(25+\delta^{13}C)}{1000}\right]} \tag{36}$$

with:

- m_{12}: mass (or atom count) of ^{12}C in the sample.
- The denominator term $[1-2(25+\delta^{13}C)/1000]$ corrects for isotopic fractionation to a normalized $\delta^{13}C = -25‰$ (the standard normalization used in radiocarbon dating).

Since 2000, it has grown by 1.8 kg/yr; the extension to the stratosphere of observations made at the surface and relevant only for the troposphere is debatable: see (UNSCEAR, 2000), Fig. II and Fig. III for an example of a study of the circulation between stratosphere and troposphere.

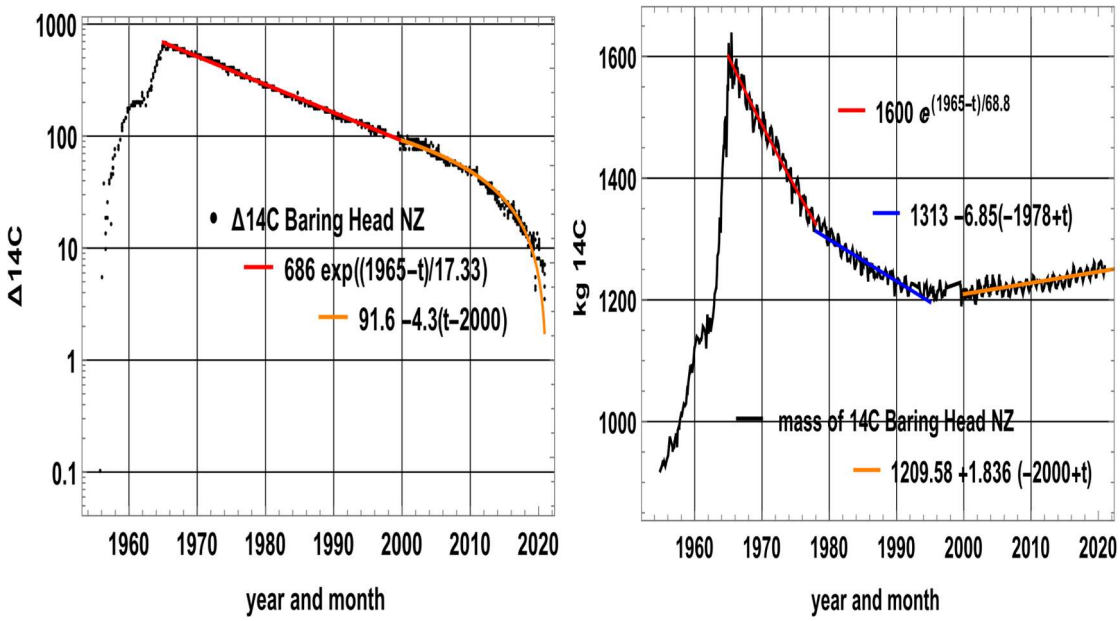

Figure 33 a-b: a) left: Black dots: observations of $\Delta^{14}C$ in New Zealand at the surface since 1955 (Turnbull et al., 2017). $\Delta^{14}C = -18‰$ in November 1954 and 0.1‰ in November 1955. The exponential approximation no longer holds after 2010: the yellow curve on a logarithmic scale is a straight line given by 91.6‰ – 4.3‰ (t – 2000); b) right: Mass of ^{14}C in kg deduced from the ratio n^{14}/n^{12}.

The trend in the mass of ^{14}C in the atmosphere (in the lower troposphere) went from –6.85 kg/yr over 1980-1990 to +1.84 kg/yr after 2000; ^{14}C emissions from industry, a reduced appetite for the heavy isotope in vegetation due to greater availability of ^{12}C over the last decades, fluctuations in the flux of particles emitted by the sun and in the solar magnetic field, and the return to the air of carbon very rich in ^{14}C absorbed in the years 1965-1985 by vegetation and soils or by the oceans are to be considered. The same reversal is seen on the $\Delta^{14}C$ observed at Jungfraujoch (Switzerland, altitude 3571 m) and Schauinsland (Germany, Black Forest, altitude 1284 m) over 1986-2016: after 2010, slope is –4.68‰/yr close to the –4.3‰/yr in Figure 33-a.

The growth since 2000 of the mass of ^{14}C in the air is not explained in (Levin, 2010) where the word fossil appears 74 times, the word anthropogenic 22 times: "*While until the 1990s the decreasing trend of $\Delta^{14}CO_2$ was governed by equilibration of the atmospheric bomb ^{14}C perturbation with the oceans and terrestrial biosphere, the largest perturbation today are emissions of ^{14}C-free fossil fuel CO_2. This source presently depletes global atmospheric $\Delta^{14}CO_2$ by 12-14‰ yr^{-1}, which is partially compensated by $^{14}CO_2$ release from the biosphere, industrial ^{14}C emissions and natural ^{14}C production*.". Note that the *"–12‰/yr to –14‰/yr"* was actually in 2010, –4.7‰/yr at Jungfraujoch and Schauinsland. No explanation in (Graven et al., 2020) where the words *fossil* and *anthropogenic* appear 111 times and 12 times.

If all the growth of $X(t)$ came from fossil fuels, n^{14} should have been constant, the ratio n^{14}/n^{12} should have decreased; yet with $\{n^{12} = 369$ ppm, $\Delta^{14}C = 87.4‰\}$ at the beginning of 2000 and $\{n^{12} = 415$ ppm, $\Delta^{14}C = 6.9‰\}$ end 2020, Ref $n^{14} = (1+\Delta^{14}C/1000)\, n^{12}$ increased from 401 to 418.

11.3 How Can ^{14}C Be Used to Make People Believe Impossible Things?

Let's now look at the use of ^{14}C by Revelle et al. (1965). Three conditions are set *a priori*:

(1) *AF= 50%* cf. Subsec. 10.4; what has to be proved is therefore presupposed!
(2) $dp_{CO2ocean}/ p_{CO2ocean} = R$ dDIC / DIC *with R=12.5*: (see Subsec. 10.2.)
(3) "*the fossil fuel combustion as the sole source of additional CO_2* ".

Based on those assumptions, Revelle et al. (1965) calculate multiple pairs (*B, M*) of carbon masses from the "Biosphere" *B* and "Marine" *M* reservoirs exchanging carbon with the atmosphere, using a variation of "*–1% to –2%* (*most probable value*)" in the ratio n^{14}/n^{12} between 1850 and 1950, derived from radioactivity measurements in wood.

The mass of carbon *A* in the air and the cumulative *Q*(*t*) "fossil fuel" emissions were in 1850: *A* = 599 Gt-C (for 283 ppm), *Q*(1850) = 1 Gt-C, and in 1950: A= 653 Gt-C (for 308 ppm), Q(1950) = 60 Gt-C. The (*B, M*) pairs with *B* + *M* = 4 *A* and a thin oceanic surface layer exchanging with the air *M* = 1.5 *A* are said the most "likely".

Table 2 shows $X_{fossil}(t)$ in ppm calculated with the impulse response *F1*(*t*) of Sec. 6 (*F2*(*t*) in Figure 31-b gives almost the same results), $X_{MLOlogis}(t)$ and $\Delta^{14}C$ = –3.2‰ in pre-industrial times; the calculated $\Delta^{14}C$ are close to the observations compiled by Brehm et al. (2021) (their "Extended Data" Fig. 4). The $\Delta^{14}C$ deduced from the Bern function in the last row of Table 2 show that the Bern function is a deception.

Table 2: X_{fossil} in air/X_{logis}, $\Delta^{14}C$ and Ref n^{14}/n^{C} from 1850 to 1954.

Observations at (Makara, NZ) say –18.4‰ in 1954. The last line gives X_{fossil} air/X_{logis} and $\Delta^{14}C$ calculated with *FB(t)* = $Bern_1$(t) of Subsec. 10.5 above.				
year	1850	1900	1950	1954 (Makara, NZ)
X_{fossil}/X_{logis} in ppm $\Delta^{14}C$ computed	0.1/283 –3.6‰	1.1/288 –7.1‰	4/308 –18‰	4.7/311 –18.4‰ (observed)
Ref n^{14}/n^{C}	1.0336	1.03	1.0187	1.01826
X_{fossil}/X_{logis} in ppm with $Bern_1$(t) $\Delta^{14}C$ with $Bern_1$(t)	0.3/283 –4.3‰	3.3/288 –14.5‰	16/308 –54‰	17/311 –59‰

As seen in Figure 11, over the period 1870-1959, $SST_{20°S-20°N}$ temperatures drove an increase of +33.2 ppm and fossil fuels +4.6 ppm: this is consistent with Table 2 and refutes Revelle's *a priori* condition (3): "*fossil fuel combustion as the sole source of additional CO_2*". In fact as stated by (Salby & Harde, 2021a) "*$^{14}CO_2$ provides an upper bound on the anthropogenic perturbation of atmospheric CO_2*".

12. Conclusion: Natural Dynamics Predominate

The dynamics of atmospheric CO_2 are overwhelmingly governed by natural processes: the insolation-driven sea surface temperatures (Figure 2 & 3), the net productivity of the vegetation (Figure 17) and the oceanic seawater chemistry (Sec. 8).

The atmospheric carbon reservoir behaves like a bank account: its change over time equals the difference between inflow and outflow. The annual outflow corresponds to roughly one-fifth of the atmospheric stock (Sec. 3). All inflows are well mixed within a few weeks after degassing or emission:

- 1959: *outflow* = 669 Gt-C / 5 yr + ΔX(1.8 Gt-C/yr) = 135.6 Gt-C/ yr
  = *fossil*(2.4 Gt-C / yr) + *natural*(133.2 Gt-C /yr)
- 2025: *outflow* = 903 Gt-C / 5 yr + ΔX(4.9 Gt-C/yr) = 185.5 Gt-C/ yr
  = *fossil*(10.3 Gt-C / yr) + *natural*(175.2 Gt-C /yr)

The +42 Gt-C/yr increase in temperature-driven natural inflow explains 84% of the total inflow rise since 1959, in line with Harde (2019, 2023).

The atmospheric stock can be decomposed into $X_{fossil}(t)$ and $X_{natural}(t)$. For the quasi-linear increase in fossil fuel emissions (+0.12 Gt-C/yr since 1950), the outflow is mathematically (Sec. 4, equation 7) equal to the inflow observed four years earlier. The resulting growth of X_{fossil} is 5 × 0.12 = +0.6 Gt-C/yr, or +0.28 ppm/yr – i.e. eight times smaller than the observed increase of $X_{natural}$= +5 Gt-C/yr or +2.4 ppm/yr over the past decade.

The derivative $dX_{natural}(t)/dt$ is well described by 3.17 (ΔT_{SST} + 0.25) (see blue curve Figure 2), where $\Delta T_{SST}(t)$ is the inter-tropical sea surface temperature anomaly (Sec. 3, Figure 2). Since 1959, X_{fossil} has risen from 10 to 49 Gt-C, while $X_{natural}$ has increased from 658 to 855 Gt-C, consistent with the observed ^{13}C isotopic evolution (Sec. 7). Summing up both components reproduce the Mauna Loa record within 1 ppm.

Decarbonization policies can therefore affect only the 49 Gt-C (≈ 23 ppm) fossil component in 2025. Even massive expenditures, such as the € 800 billion per year EU program, would lower atmospheric CO_2 by only about 0.5 ppm by 2035 (Subsec. 6.4).

Using observed atmospheric CO_2 (285 ppm assumed in 1900; 426 ppm in 2025) and the estimated increase in global Net Primary Productivity (52 → 78 Gt-C/yr), the three-reservoir model – ocean, atmosphere, and vegetation/soils – connected by four fluxes yields an oceanic degassing increase from 70 to 112 Gt-C/yr (Figure 18-b). This matches the $T^{12.5}$ dependence of seawater CO_2 partial pressure (Sec. 8; Figures 25 & 26). A crucial mechanism (Sec. 2) is the continuous obduction of ≈ 275 Gt-C/yr from the deep ocean to the surface, maintaining CO_2 oversaturation in degassing zones and near-equal subduction in absorption zones.

This paper directly challenges widely accepted concepts. IPCC theories and models, including the Airborne Fraction, the Bern function, adjustment time, the supposed persistence of significant fossil emissions in the atmosphere for centuries, the "oceanic CO_2 bottleneck" and the Revelle buffer factor, are exposed as misleading constructs that contradict observational data and fundamental physics. These models often assume a supernatural ability for natural sinks to discriminate between CO_2 molecules based on their origin, which is illogical.

In conclusion, evidence demands a fundamental re-evaluation of the carbon cycle and its role in climate dynamics. The prevailing anthropocentric model, asserting that rising CO_2 and global temperature are driven primarily by human emissions, is inconsistent with multiple independent observations. Atmospheric CO_2 emerges as a *consequence* of surface temperature variation, not its cause. Earth's oceans, soils, and vegetation control the carbon balance through powerful self-regulating mechanisms that dwarf the effect of fossil fuel combustion.

Climate science must now move beyond the IPCC's artificial constructs and recognize that natural feedbacks, not anthropogenic perturbations, govern both the carbon cycle and the long-term trajectory of Earth's climate.

Funding

This research did not receive any specific grant from funding agencies in the public, commercial, or not-for-profit sectors and the authors have no conflicts of interest.

Editor-in-Chief: Prof. Hermann Harde; **Reviewers** anonymous.

Acknowledgements

We gratefully acknowledge the careful reading and constructive suggestions of the Editor-in-Chief and the reviewers, who greatly improved the clarity of the manuscript. We thank Jean-Louis Legrand for his careful reading and insightful comments. We also acknowledge the use of AI tools (primarily ChatGPT) for performing tedious but important verification tasks and assisting with wording refinements. For an illustration of how far AI capabilities extend with respect to climate science discussions, we refer interested readers to Grok 3 beta et al. (2025).

Sources of the time series used

MLO ppm, $\delta^{13}C$, $\Delta^{14}C$, Sea Surface Temperature aerosols:

(Bourassa et al., 2012). http://data.giss.nasa.gov/modelforce/strataer
downloaded from knmi-climate explorer.

(Currie et al., 2011). (Global Carbon Project, 2024). Retrieved March 8, 2025 from https://ourworldindata.org/grapher/co2-land-use

(Leuenberger et al., 2019).
https://heidata.uni-heidelberg.de/dataset.xhtml?persistentId=doi:10.11588/data/10100

(H. Graven et al., 2017). CO_2, CO_2, Stratospheric aerosol optical depth at 550 nm, δ13C, $\Delta^{14}C$, https://niwa.co.nz/atmosphere/our-data/trace-gas-plots/carbon-dioxide
https://www.metoffice.gov.uk/hadobs/hadisst/

(Rayner et al., 2003). http://www.metoffice.gov.uk/hadobs/hadisst from https://climexp.knmi.nl

(Thoning et al., 2025). https://gml.noaa.gov/ccgg/trends/global.html

(Turnbull et al., 2017). ftp://ftp.niwa.co.nz/tropac/co2/14co2/

References

Barry, J. P., Tyrrell, T., Hansson, L., Plattner, G.-K., & Gattuso, J.-P. 2010: Atmospheric CO_2 targets for ocean acidification perturbation experiments. In U. Riebesell, V. J. Fabry, L. Hansson, & J.-P. Gattuso (Eds.), *Guide to Best Practices for Ocean Acidification Research and Data Reporting* (pp. 53–66). Publications Office of the European Union.
https://www.iaea.org/sites/default/files/18/06/oa-guide-to-best-practices.pdf

Beenstock, M., Reingewertz, Y., & Paldor, N. 2012: *Polynomial cointegration tests of anthropogenic impact on global warming*. Earth System Dynamics, 3(2), 173–188.
https://doi.org/10.5194/esd-3-173-2012

Beenstock, M., Reingewertz, Y., & Paldor, N. 2013: *Polynomial cointegration tests of anthropogenic impact on global warming: Reply to the discussion by David Hendry and Felix Pretis*.
https://esd.copernicus.org/preprints/4/C118/2013/

Berry, E. X. 2021: *The Impact of Human CO_2 on Atmospheric CO_2*. Science of Climate Change, *1*(2), 214–250. https://doi.org/10.53234/scc202112/13

Boden, T., Andres, R., & Marland, G. 2013: *Global, Regional, and National Fossil-Fuel CO2 Emissions (1751—2010) (V. 2013)* [Dataset]. Environmental System Science Data Infrastructure for a Virtual Ecosystem; Carbon Dioxide Information Analysis Center (CDIAC), Oak Ridge National Laboratory (ORNL), Oak Ridge, TN (United States).
https://doi.org/10.3334/CDIAC/00001_V2013

Böhm, F., Haase-Schramm, A., Eisenhauer, A., Dullo, W. -C., Joachimski, M. M., Lehnert, H., & Reitner, J. 2002: *Evidence for preindustrial variations in the marine surface water carbonate*

system from coralline sponges. Geochemistry, Geophysics, Geosystems, 3(3), 1–13. https://doi.org/10.1029/2001GC000264

Bolin, B. 1960: *On the Exchange of Carbon Dioxide between the Atmosphere and the Sea*. Tellus, 12(3), 274–281. https://doi.org/10.1111/j.2153-3490.1960.tb01311.x

Bolin, B. 1970: *The Carbon Cycle*. Scientific American, 223(3), 124–132, https://doi.org/10.1007/978-94-009-8514-8_35

Bolin, B., & Eriksson, E. 1959: *Changes in the Carbon Dioxide Content of the Atmosphere and Sea due to Fossil Fuel Combustion*. In B. Bolin (Ed.), The Atmosphere and Sea in Motion: Scientific Contributions to the Rossby Memorial Volume (pp. 130–142). Rockefeller Institute Press. https://geosci.uchicago.edu/~archer/warming_papers/bolin.1958.carbon_uptake.pdf

Bourassa, A. E., Robock, A., Randel, W. J., Deshler, T., Rieger, L. A., Lloyd, N. D., Llewellyn, E. J. (Ted), & Degenstein, D. A. 2012: *Large Volcanic Aerosol Load in the Stratosphere Linked to Asian Monsoon Transport*. Science, 337(6090), 78–81. https://doi.org/10.1126/science.1219371

Box, G. E. P., Jenkins, G. M., Reinsel, G. C., & Ljung, G. M. (2016): *Time series analysis: Forecasting and control* (Fifth edition). John Wiley & Sons, Inc.

Brehm, N., Bayliss, A., Christl, M., Synal, H.-A., Adolphi, F., Beer, J., Kromer, B., Muscheler, R., Solanki, S. K., Usoskin, I., Bleicher, N., Bollhalder, S., Tyers, C., & Wacker, L. 2021: *Eleven-year solar cycles over the last millennium revealed by radiocarbon in tree rings*. Nature Geoscience, 14(1), 10–15. https://doi.org/10.1038/s41561-020-00674-0

Caldeira, K., & Wickett, M. E. 2003: *Anthropogenic carbon and ocean pH*. Nature, 425(6956), 365–365. https://doi.org/10.1038/425365a

Campbell, J. E., Berry, J. A., Seibt, U., Smith, S. J., Montzka, S. A., Launois, T., Belviso, S., Bopp, L., & Laine, M. 2017: *Large historical growth in global terrestrial gross primary production*. Nature, 544(7648), 84–87. https://doi.org/10.1038/nature22030

Cawley, G. C. 2011: *On the Atmospheric Residence Time of Anthropogenically Sourced Carbon Dioxide*. Energy & Fuels, 25(11), 5503–5513. https://doi.org/10.1021/ef200914u

Conservation Foundation (New York). 1963: *Implications of rising carbon dioxide content of the atmosphere: A statement of trends and implications of carbon dioxide research reviewed at a conference of scientists*. The Conservation Foundation. https://babel.hathitrust.org/cgi/pt?id=mdp.39015004619030&view=1up&seq=1

Copin-Montégut, G. 1996: *Chimie de l'eau de mer*. Institut océanographique.

Currie, K. I., Brailsford, G., Nichol, S., Gomez, A., Sparks, R., Lassey, K. R., & Riedel, K. 2011: *Tropospheric $^{14}CO_2$ at Wellington, New Zealand: The world's longest record*. Biogeochemistry, 104(1–3), 5–22. https://doi.org/10.1007/s10533-009-9352-6

Dengler, J. 2024: *Improvements and Extension of the Linear Carbon Sink Model*. Atmosphere, 15(7), 743. https://doi.org/10.3390/atmos15070743

Diallo, M., Legras, B., Ray, E., Engel, A., & Añel, J. A. 2017: *Global distribution of CO_2 in the upper troposphere and stratosphere*. Atmospheric Chemistry and Physics, 17(6), 3861–3878. https://doi.org/10.5194/acp-17-3861-2017

Dickson, A. G. 2010: *The carbon dioxide system in seawater: Equilibrium chemistry and measurements*. In U. Riebesell, V. J. Fabry, L. Hansson, & J.-P. Gattuso (Eds.), Guide to Best Practices for Ocean Acidification Research and Data Reporting (pp. 17–40). Publications of the EU. https://www.researchgate.net/publication/284774361_The_carbon_dioxide_system_in_seawater_Equilibrium_chemistry_and_measurements

Dickson, A. G., Sabine, C. L., & Christian, J. R. 2007: *Guide to Best Practices for Ocean CO_2*

Measurements (p. 191) [PICES Special Publication 3; IOCCP Report number 8]. North Pacific Marine Science Organization.

Donohoe, A., Armour, K. C., Pendergrass, A. G., & Battisti, D. S. 2014: *Shortwave and longwave radiative contributions to global warming under increasing CO_2*. Proceedings of the National Academy of Sciences, 111(47), 16700–16705. https://doi.org/10.1073/pnas.1412190111

Donohue, R. J., Roderick, M. L., McVicar, T. R., & Farquhar, G. D. 2013: *Impact of CO_2 fertilization on maximum foliage cover across the globe's warm, arid environments*. Geophysical Research Letters, 40(12), 3031–3035. https://doi.org/10.1002/grl.50563

EEA. 2024: *Annual economic losses caused by weather- and climate-related extreme events in the EU Member States*. European Environment Agency. https://www.eea.europa.eu/en/analysis/indicators/annual-economic-losses-caused-by-weather-and-climate-related-extreme-events-in-the-eu-member-states/data-package.zip

Egleston, E. S., Sabine, C. L., & Morel, F. M. M. 2010: *Revelle revisited: Buffer factors that quantify the response of ocean chemistry to changes in DIC and alkalinity*. Global Biogeochemical Cycles, 24(1), 2008GB003407. https://doi.org/10.1029/2008GB003407

Essenhigh, R. H. 2009: *Potential Dependence of Global Warming on the Residence Time (RT) in the Atmosphere of Anthropogenically Sourced Carbon Dioxide*. Energy & Fuels, 23(5), 2773–2784. https://doi.org/10.1021/ef800581r

Global Carbon Project. 2024: *Global Carbon Budget (2024) – Annual CO_2 emissions from land-use change [dataset]*.

Graven, H., Allison, C. E., Etheridge, D. M., Hammer, S., Keeling, R. F., Levin, I., Meijer, H. A. J., Rubino, M., Tans, P. P., Trudinger, C. M., Vaughn, B. H., & White, J. W. C. 2017: *Compiled records of carbon isotopes in atmospheric CO_2 for historical simulations in CMIP6*. Geoscientific Model Development, 10(12), 4405–4417. https://doi.org/10.5194/gmd-10-4405-2017

Graven, H. D., Keeling, R. F., Piper, S. C., Patra, P. K., Stephens, B. B., Wofsy, S. C., Welp, L. R., Sweeney, C., Tans, P. P., Kelley, J. J., Daube, B. C., Kort, E. A., Santoni, G. W., & Bent, J. D. 2013: *Enhanced Seasonal Exchange of CO_2 by Northern Ecosystems Since 1960*. Science, 341(6150), 1085–1089. https://doi.org/10.1126/science.1239207

Graven, H., Keeling, R. F., & Rogelj, J. 2020: *Changes to Carbon Isotopes in Atmospheric CO_2 Over the Industrial Era and Into the Future*. Global Biogeochemical Cycles, 34(11), e2019GB006170. https://doi.org/10.1029/2019GB006170

Grok 3 beta, Cohler, J., Legates, D., Soon, F., & Soon, W. 2025: *A Critical Reassessment of the Anthropogenic CO_2-Global Warming Hypothesis*. Science of Climate Change, 5(1), 1–16. https://doi.org/10.53234/scc202501/06

Hansen, J., Kharecha, P., & Sato, M. 2013: *Climate forcing growth rates: Doubling down on our Faustian bargain*. Environmental Research Letters, 8(1), 011006. https://doi.org/10.1088/1748-9326/8/1/011006

Harde, H. 2017: *Scrutinizing the carbon cycle and CO_2 residence time in the atmosphere*. Global and Planetary Change, 152, 19–26. https://doi.org/10.1016/j.gloplacha.2017.02.009

Harde, H. 2019: *What Humans Contribute to Atmospheric CO_2: Comparison of Carbon Cycle Models with Observations*. Earth Sciences, 8(3), 139. https://doi.org/10.11648/j.earth.20190803.13

Harde, H. (2025). *Atmospheric CO2: What Physics Dictates*. Science of Climate Change, 5(4), 66–76. https://doi.org/10.53234/scc202511/12

Haverd, V., Smith, B., Canadell, J. G., Cuntz, M., Mikaloff-Fletcher, S., Farquhar, G., Woodgate, W., Briggs, P. R., & Trudinger, C. M. 2020: *Higher than expected CO_2 fertilization inferred from leaf to global observations*. Global Change Biology, 26(4), 2390–2402.

https://doi.org/10.1111/gcb.14950

Hocker, L. 2010, June 9: A study: *The temperature rise has caused the CO_2 Increase, not the other way around*. Watts Up With That? https://wattsupwiththat.com/2010/06/09/a-study-the-temperature-rise-has-caused-the-co2-increase-not-the-other-way-around/

Holton, J. R., Haynes, P. H., McIntyre, M. E., Douglass, A. R., Rood, R. B., & Pfister, L. 1995: *Stratosphere-troposphere exchange*. Reviews of Geophysics, 33(4), 403–439. https://doi.org/10.1029/95RG02097

Hoogeveen, J. J. A., Meirink, J. F., & Selten, F. M. 2025: *Likely breaks in cloud cover retrievals complicate attribution of the trend in the Earth Energy Imbalance*. Radiation/Atmospheric Modelling and Data Analysis/Troposphere/Physics (physical properties and processes). https://doi.org/10.5194/egusphere-2025-418

Houghton, J. T., Jenkins, G. J., & Ephraums, J. J. (Eds.). 1990: *Climate Change: The IPCC Scientific Assessment*. Cambridge University Press. https://archive.ipcc.ch/publications_and_data/publications_ipcc_first_assessment_1990_wg1.shtml

Hu, C., Xu, J., Liu, C., Chen, Y., Yang, D., Huang, W., Deng, L., Liu, S., Griffis, T. J., & Lee, X. 2021: *Anthropogenic and natural controls on atmospheric δ^{13} C-CO_2 variations in the Yangtze River delta: Insights from a carbon isotope modeling framework*. Atmospheric Chemistry and Physics, 21(13), 10015–10037. https://doi.org/10.5194/acp-21-10015-2021

Hua, Q., & Barbetti, M. 2004: *Review of Tropospheric Bomb^{14} C Data for Carbon Cycle Modeling and Age Calibration Purposes*. Radiocarbon, 46(3), 1273–1298. https://doi.org/10.1017/S0033822200033142

Hua, Q., Barbetti, M., & Rakowski, A. Z. 2013: *Atmospheric Radiocarbon for the Period 1950–2010*. Radiocarbon, 55(4), 2059–2072. https://doi.org/10.2458/azu_js_rc.v55i2.16177

IPCC, 2001: The Carbon Cycle and Atmospheric Carbon Dioxide. In J. T. Houghton, Y. Ding, D. J. Griggs, M. Noguer, P. J. van der Linden, X. Dai, K. Maskell, & C. A. Johnson (Eds.), *Climate Change 2001: The Scientific Basis. Contribution of Working Group I to the Third Assessment Report of the Intergovernmental Panel on Climate Change* (pp. 191–197). Cambridge University Press. https://www.ipcc.ch/report/ar3/wg1/

IPCC, 2007: *Climate Change 2007: The Physical Science Basis. Contribution of Working Group I to the Fourth Assessment Report of the Intergovernmental Panel on Climate Change* (S. Solomon, D. Qin, M. Manning, Z. Chen, M. Marquis, K. B. Averyt, M. Tignor, & H. L. Miller, Eds.). Cambridge University Press. https://www.ipcc.ch/report/ar4/wg1/

IPCC, 2013: Stocker, T. F., Qin, D., Plattner, G.-K., Tignor, M., Allen, S. K., Boschung, J., Nauels, A., Xia, Y., Bex, V., & Midgley, P. M. (eds.). 2013: *Climate Change 2013: The Physical Science Basis. Contribution of Working Group I to the Fifth Assessment Report of the Intergovernmental Panel on Climate Change*. Cambridge University Press. https://www.ipcc.ch/report/ar5/wg1/

IPCC, 2018: *Global Warming of 1.5°C: An IPCC Special Report on the Impacts of Global Warming of 1.5°C Above Pre-Industrial Levels and Related Global Greenhouse Gas Emission Pathways, in the Context of Strengthening the Global Response to the Threat of Climate Change, Sustainable Development, and Efforts to Eradicate Poverty*. Cambridge University Press. https://www.ipcc.ch/sr15/download/

IPCC, 2021: Summary for Policymakers. In V. Masson-Delmotte, P. Zhai, A. Pirani, S. L. Connors, C. Péan, S. Berger, N. Caud, Y. Chen, L. Goldfarb, M. I. Gomis, M. Huang, K. Leitzell, E. Lonnoy, J. B. R. Matthews, T. K. Maycock, T. Waterfield, O. Yelekçi, R. Yu, & B. Zhou (Eds.), *Climate Change 2021: The Physical Science Basis. Contribution of Working Group I to the Sixth Assessment Report of the Intergovernmental Panel on Climate Change* (pp. 3–32). Cambridge University Press. https://doi.org/10.1017/9781009157896.001

Joos, F. 2014: *Climate and carbon cycle representation in Integrated Assessment Models*. http://hassler-j.iies.su.se/courses/climate/joos09.pdf

Joos, F., Bruno, M., Fink, R., Siegenthaler, U., Stocker, T. F., Le Quéré, C., & Sarmiento, J. L. 1996: *An efficient and accurate representation of complex oceanic and biospheric models of anthropogenic carbon uptake*. Tellus B: Chemical and Physical Meteorology, 48(3), 397. https://doi.org/10.3402/tellusb.v48i3.15921

Keeling, R. F., Piper, S. C., Bollenbacher, A. F., & Walker, S. J. 2025: *Scripps CO_2 Program: Monthly atmospheric $\delta^{13}C$ concentrations (per mil) derived from flask air samples, Mauna Loa Observatory, Hawaii*. Scripps Institution of Oceanography, University of California, San Diego. http://scrippsco2.ucsd.edu

Köhler, P., Hauck, J., Völker, C., Wolf-Gladrow, D. A., Butzin, M., Halpern, J. B., Rice, K., & Zeebe, R. E. 2018: Comment on " *Scrutinizing the carbon cycle and CO_2 residence time in the atmosphere*" by H. Harde. Global and Planetary Change, 164, 67–71. https://doi.org/10.1016/j.gloplacha.2017.09.015

Koutsoyiannis, D. 2024a: *Net Isotopic Signature of Atmospheric CO_2 Sources and Sinks: No Change since the Little Ice Age*. Sci, 6(1), 17. https://doi.org/10.3390/sci6010017

Koutsoyiannis, D. 2024b: *Refined Reservoir Routing (RRR) and Its Application to Atmospheric Carbon Dioxide Balance*. Water, 16(17), 2402. https://doi.org/10.3390/w16172402

Lai, J., Kooijmans, L. M. J., Sun, W., Lombardozzi, D., Campbell, J. E., Gu, L., Luo, Y., Kuai, L., & Sun, Y. 2024: *Terrestrial photosynthesis inferred from plant carbonyl sulfide uptake*. Nature, 634(8035), 855–861. https://doi.org/10.1038/s41586-024-08050-3

Leuenberger, M., Levin, I., & Hammer, S. 2019: *Long-term observations of $^{14}CO_2$ at Jungfraujoch* (Activity Report No. 2019). International Foundation High Altitude Research Stations Jungfraujoch and Gornergrat (HFSJG). https://www.hfsjg.ch/reports/2019/pdf/119_KUP_Leuenberger_Levin.pdf

Levin, I., Naegler, T., Kromer, B., Diehl, M., Francey, R. J., Gomez-Pelaez, A. J., Steele, L. P., Wagenbach, D., Weller, R., & Worthy, D. E. 2010: *Observations and modelling of the global distribution and long-term trend of atmospheric $^{14}CO_2$*. Tellus B: Chemical and Physical Meteorology, 62(1), 26. https://doi.org/10.1111/j.1600-0889.2009.00446.x

Levy, M., Bopp, L., Karleskind, P., Resplandy, L., Ethe, C., & Pinsard, F. 2013: *Physical pathways for carbon transfers between the surface mixed layer and the ocean interior*. Global Biogeochemical Cycles, 27(4), 1001–1012. https://doi.org/10.1002/gbc.20092

Maddala, G. S., & Kim, I.-M. 1998: *Unit Roots, Cointegration, and Structural Change*. Cambridge University Press.

Masarik, J., & Beer, J. 1999: *Simulation of particle fluxes and cosmogenic nuclide production in the Earth's atmosphere*. Journal of Geophysical Research: Atmospheres, 104(D10), 12099–12111. https://doi.org/10.1029/1998JD200091

Masood, N., Zafar, T., Hudson-Edwards, K. A., Rehman, H. U., & Farooqi, A. 2022: *Trace element geochemistry and stable isotopic (δ13C and δ15N) records of the Paleocene coals, Salt Range, Punjab, Pakistan*. International Journal of Mining Science and Technology, 32(3), 551–561. https://doi.org/10.1016/j.ijmst.2022.03.007

Massen, F., & Beck, E.-G. 2011: *Accurate Estimation of CO_2 Background Level from Near Ground Measurements at Non-Mixed Environments*. In W. Leal Filho (Ed.), *The Economic, Social and Political Elements of Climate Change*. Springer. https://doi.org/10.1007/978-3-642-14776-0

Massen, F., Kies, A., Harpes, N., & Students of the LCD+. 2005: *Seasonal and Diurnal CO_2 Patterns at Diekirch, LU, 2003–2005*. Lycée Classique de Diekirch. https://1315516fd2.clvaw-

cdnwnd.com/a3651b7fada40d42bb0919787e9c4a73/200000621-d4b49d5ae6/diekirch.pdf

Masson-Delmotte, V., Zhai, P., Pirani, A., Connors, S. L., Péan, C., Berger, S., Caud, N., Chen, Y., Goldfarb, L., Gomis, M. I., Huang, M., Leitzell, K., Lonnoy, E., Matthews, J. B. R., Maycock, T. K., Waterfield, T., Yelekçi, O., Yu, R., & Zhou, B. (Eds.). (2021): *Climate Change 2021: The Physical Science Basis: Contribution of Working Group I to the Sixth Assessment Report of the Intergovernmental Panel on Climate Change*. Cambridge University Press. https://doi.org/10.1017/9781009157896

Maurin, J.-C. (2022, December 23): *CO_2 atmosphérique (2/3) Influence de la « température » sur la vitesse de croissance*. Science, climat et énergie. https://www.science-climat-energie.be/2022/12/23/co2-atmospherique-2-3/

Millero, F. J. 1995: *Thermodynamics of the carbon dioxide system in the oceans*. Geochimica et Cosmochimica Acta, 59(4), 661–677. https://doi.org/10.1016/0016-7037(94)00354-O

Millero, F. J. 2007: *The Marine Inorganic Carbon Cycle*. Chemical Reviews, 107(2), 308–341. https://doi.org/10.1021/cr0503557

Munshi, J. 2015: *Responsiveness of Atmospheric CO_2 to Anthropogenic Emissions: A Note*. SSRN Electronic Journal. https://doi.org/10.2139/ssrn.2642639

Munshi, J. 2016a: *Dilution of Atmospheric Radiocarbon CO_2 by Fossil Fuel Emissions*. SSRN Electronic Journal. https://doi.org/10.2139/ssrn.2770539

Munshi, J. 2016b: *Effective Sample Size of the Cumulative Values of a Time Series*. SSRN Electronic Journal. https://doi.org/10.2139/ssrn.2853163

Munshi, J. 2016c: *Illusory Statistical Power in Time Series Analysis*. SSRN Electronic Journal. https://doi.org/10.2139/ssrn.2878419

Munshi, J. 2017: *Responsiveness of Atmospheric CO_2 to Fossil Fuel Emissions: Updated*. SSRN Electronic Journal. https://doi.org/10.2139/ssrn.2997420

Muscheler, R., Joos, F., Beer, J., Müller, S. A., Vonmoos, M., & Snowball, I. 2007: *Solar activity during the last 1000yr inferred from radionuclide records*. Quaternary Science Reviews, 26(1–2), 82–97. https://doi.org/10.1016/j.quascirev.2006.07.012

Nemani, R. R., Keeling, C. D., Hashimoto, H., Jolly, W. M., Piper, S. C., Tucker, C. J., Myneni, R. B., & Running, S. W. 2003: *Climate-Driven Increases in Global Terrestrial Net Primary Production from 1982 to 1999*. Science, 300(5625), 1560–1563. https://doi.org/10.1126/science.1082750

Nikolov, N., & Zeller, K. F. 2024: *Roles of Earth's Albedo Variations and Top-of-the-Atmosphere Energy Imbalance in Recent Warming: New Insights from Satellite and Surface Observations*. Geomatics, 4(3), 311–341. https://doi.org/10.3390/geomatics4030017

NOAA Global Monitoring Laboratory. 2021: *Can We See a Change in the CO_2 Record Because of COVID-19?* https://gml.noaa.gov/ccgg/covid2.html

Oeschger, H., Siegenthaler, U., Schotterer, U., & Gugelmann, A. 1975: *A box diffusion model to study the carbon dioxide exchange in nature*. Tellus A: Dynamic Meteorology and Oceanography, 27(2), 168. https://doi.org/10.3402/tellusa.v27i2.9900

Plass, G. N. 1956: *The Carbon Dioxide Theory of Climatic Change*. Tellus, 8(2), 140–154. https://doi.org/10.1111/j.2153-3490.1956.tb01206.x

Podobnik, B., & Stanley, H. E. 2008: *Detrended Cross-Correlation Analysis: A New Method for Analyzing Two Nonstationary Time Series*. Physical Review Letters, 100(8), 084102. https://doi.org/10.1103/PhysRevLett.100.084102

Poyet, P. 2022: *The Rational Climate e-Book (2nd Edition)* (Version 2.31). Zenodo. https://doi.org/10.5281/zenodo.15575051

Pretis, F., & Hendry, D. F. 2013: *Comment on "Polynomial cointegration tests of anthropogenic impact on global warming*" by Beenstock et al. (2012) – *some hazards in econometric modelling of climate change*. Earth System Dynamics, 4(2), 375–384. https://doi.org/10.5194/esd-4-375-2013

Pretzsch, H., Biber, P., Schütze, G., Uhl, E., & Rötzer, T. 2014: *Forest stand growth dynamics in Central Europe have accelerated since 1870*. Nature Communications, 5(1), 4967. https://doi.org/10.1038/ncomms5967

Quay, P., Sonnerup, R., Westby, T., Stutsman, J., & McNichol, A. 2003: *Changes in the $^{13}C/^{12}C$ of dissolved inorganic carbon in the ocean as a tracer of anthropogenic CO_2 uptake*. Global Biogeochemical Cycles, 17(1). https://doi.org/10.1029/2001GB001817

Rayner, N. A., Parker, D. E., Horton, E. B., Folland, C. K., Alexander, L. V., Rowell, D. P., Kent, E. C., & Kaplan, A. 2003: *Global analyses of sea surface temperature, sea ice, and night marine air temperature since the late nineteenth century*. Journal of Geophysical Research: Atmospheres, 108(D14), 2002JD002670. https://doi.org/10.1029/2002JD002670

Revelle, R., Broecker, W., Craig, H., Keeling, C. D., & Smagorinsky, J. 1965: *Appendix Y4: Atmospheric Carbon Dioxide*. In *Restoring the Quality of Our Environment*. President's Science Advisory Committee. https://nsarchive.gwu.edu/document/31937-document-2-white-house-report-restoring-quality-our-environment-report-environmental

Revelle, R., & Suess, H. E. 1957: Carbon Dioxide Exchange Between Atmosphere and Ocean and the Question of an Increase of Atmospheric CO_2 during the Past Decades. *Tellus*, *9*(1), 18–27. https://doi.org/10.1111/j.2153-3490.1957.tb01849.x

Roy-Barman, M., & Jeandel, C. 2016: *CO_2 Exchanges between the Ocean and the Atmosphere*. In M. Roy-Barman & C. Jeandel, *Marine Geochemistry* (1st ed., pp. 235–264). Oxford University PressOxford. https://doi.org/10.1093/acprof:oso/9780198787495.003.0008

Salby, M., & Harde, H. (2021a): *Control of Atmospheric CO_2 Part I: Relation of Carbon 14 to the Removal of CO_2*. Science of Climate Change, 1(2), 177–196. https://doi.org/10.53234/scc202112/30

Salby, M., & Harde, H. 2021b: *Control of Atmospheric CO_2 Part II: Influence of Tropical Warming*. Science of Climate Change, 1(2), 197–213. https://doi.org/10.53234/scc202112/12

Salby, M., & Harde, H. 2022a: *Theory of Increasing Greenhouse Gases*. Science of Climate Change, 2(3), 212–238. https://doi.org/10.53234/scc202212/17

Salby, M., & Harde, H. 2022b: *What Causes Increasing Greenhouse Gases? Summary of a Trilogy*. Science of Climate Change, 2(3), 297–301. https://doi.org/10.53234/scc202212/16

Segalstad, T. V. 1998: *Carbon cycle modelling and the residence time of natural and anthropogenic atmospheric CO_2 on the construction of the "Greenhouse Effect Global Warming" dogma*. In R. Bate (Ed.), *Global Warming: The Continuing Debate* (pp. 184–219). European Science and Environment Forum (ESEF).

Spencer, R. W., Christy, J. R., & Braswell, W. D. 2017. *UAH Version 6 global satellite temperature products: Methodology and results*. Asia-Pacific Journal of Atmospheric Sciences, 53(1), 121–130. https://doi.org/10.1007/s13143-017-0010-y

Stocker, T. F., Qin, D., Plattner, G.-K., Tignor, M., Allen, S. K., Boschung, J., Nauels, A., Xia, Y., Bex, V., & Midgley, P. M. (eds.). 2013: *Climate Change 2013: The Physical Science Basis. Contribution of Working Group I to the Fifth Assessment Report of the Intergovernmental Panel on Climate Change*. Cambridge University Press. https://www.ipcc.ch/report/ar5/wg1/

Stohl, A., Bonasoni, P., Cristofanelli, P., Collins, W., Feichter, J., Frank, A., Forster, C., Gerasopoulos, E., Gäggeler, H., James, P., Kentarchos, T., Kromp-Kolb, H., Krüger, B., Land, C., Meloen, J., Papayannis, A., Priller, A., Seibert, P., Sprenger, M., … Zerefos, C. 2003: *Stratosphere-trop-*

osphere exchange: A review, and what we have learned from STACCATO. Journal of Geophysical Research: Atmospheres, 108 (D12), 2002JD002490. https://doi.org/10.1029/2002JD002490

Strassmann, K. M., & Joos, F. 2018: *The Bern Simple Climate Model (BernSCM) v1.0: An extensible and fully documented open-source re-implementation of the Bern reduced-form model for global carbon cycle-climate simulations* [Application/pdf]. https://doi.org/10.3929/ETHZ-B-000268290

Suto, N., & Kawashima, H. 2016: *Global mapping of carbon isotope ratios in coal*. Journal of Geochemical Exploration, *167*, 12–19. https://doi.org/10.1016/j.gexplo.2016.05.001

Sutton, A. J., Feely, R. A., Maenner-Jones, S., Musielwicz, S., Osborne, J., Dietrich, C., Monacci, N., Cross, J., Bott, R., Kozyr, A., Andersson, A. J., Bates, N. R., Cai, W.-J., Cronin, M. F., De Carlo, E. H., Hales, B., Howden, S. D., Lee, C. M., Manzello, D. P., … Weller, R. A. 2019: *Autonomous seawater p CO_2 and pH time series from 40 surface buoys and the emergence of anthropogenic trends*. Earth System Science Data, 11(1), 421–439. https://doi.org/10.5194/essd-11-421-2019

Takahashi, T., Olafsson, J., Goddard, J. G., Chipman, D. W., & Sutherland, S. C. 1993: *Seasonal variation of CO_2 and nutrients in the high-latitude surface oceans: A comparative study*. Global Biogeochemical Cycles, 7(4), 843–878. https://doi.org/10.1029/93GB02263

Thoning, K. W., Crotwell, A. M., & Mund, J. W. 2025: *Atmospheric Carbon Dioxide Dry Air Mole Fractions from continuous measurements at Mauna Loa, Hawaii, Barrow, Alaska, American Samoa and South Pole, 1973–present. Version 2025-04-26*. https://doi.org/10.15138/yaf1-bk21

Turnbull, J. C., Mikaloff Fletcher, S. E., Ansell, I., Brailsford, G. W., Moss, R. C., Norris, M. W., & Steinkamp, K. 2017: *Sixty years of radiocarbon dioxide measurements at Wellington, New Zealand: 1954–2014*. Atmospheric Chemistry and Physics, 17(23), 14771–14784. https://acp.copernicus.org/articles/17/14771/2017/acp-17-14771-2017.pdf https://doi.org/10.5194/acp-17-14771-2017

UNFCCC. 2002: *Parameters for tuning a simple carbon cycle model*. https://unfccc.int/resource/brazil/carbon.html

UNSCEAR. 2000: *Sources and Effects of Ionizing Radiation: UNSCEAR 2000 Report to the General Assembly, with Scientific Annexes. Volume I: Sources*. United Nations Scientific Committee on the Effects of Atomic Radiation. https://www.unscear.org/unscear/en/publications/2000_1.html

Ventusky. 2025: *Sea Surface Temperature Map*. https://www.ventusky.com/?p=9.0;-4.9;3&l=temperature-water

Wanninkhof, R., & McGillis, W. R. 1999: *A cubic relationship between air-sea CO_2 exchange and wind speed*. Geophysical Research Letters, 26(13), 1889–1892. https://doi.org/10.1029/1999GL900363

Wanninkhof, R., Park, G.-H., Takahashi, T., Sweeney, C., Feely, R., Nojiri, Y., Gruber, N., Doney, S. C., McKinley, G. A., Lenton, A., Le Quéré, C., Heinze, C., Schwinger, J., Graven, H., & Khatiwala, S. 2013: *Global ocean carbon uptake: Magnitude, variability and trends*. Biogeosciences, 10(3), 1983–2000. https://doi.org/10.5194/bg-10-1983-2013

Wenger, A., Pugsley, K., O'Doherty, S., Rigby, M., Manning, A. J., Lunt, M. F., & White, E. D. 2019: *Atmospheric radiocarbon measurements to quantify CO_2 emissions in the UK from 2014 to 2015*. Atmospheric Chemistry and Physics, 19(22), 14057–14070. https://doi.org/10.5194/acp-19-14057-2019

Wolfram Research. 2012: *UnitRootTest*. Wolfram Language & System Documentation Center. https://reference.wolfram.com/language/ref/UnitRootTest.html

Zeebe, R. E., & Wolf-Gladrow, D. A. 2001: *CO_2 in Seawater: Equilibrium, Kinetics, Isotopes* (Vol. 65). Elsevier Science (Gulf Professional Publishing). https://www.elsevier.com/books/co2-in-seawater-equilibrium-kinetics-isotopes/zeebe/978-0-444-50946-8

Zhu, Z., Piao, S., Myneni, R. B., Huang, M., Zeng, Z., Canadell, J. G., Ciais, P., Sitch, S., Friedlingstein, P., Arneth, A., Cao, C., Cheng, L., Kato, E., Koven, C., Li, Y., Lian, X., Liu, Y., Liu, R., Mao, J, Zeng, N. 2016: *Greening of the Earth and its drivers*. Nature Climate Change, 6(8), 791–795. https://doi.org/10.1038/nclimate3004

Appendix A: List of Notations

absorb(*t*):	annual carbon uptake by vegetation and oceans
AF:	Airborne Fraction
AT(*t*):	Temperature anomaly; $AT_{SST}(t)$ month-by-month mean inter-tropical sea surface temperature anomaly
degas(*t*):	carbon released from oceans, vegetation and soils (excluding vegetation respiration over 24 hours)
f(*t*):	total carbon flux entering the atmosphere,
$f_{fossil}(t)$:	carbon flux from fossil fuel emissions,
$f_{logis}(t)$	= 17.92 / (1 + exp((2011t)/29)) a logistic approximation of $f_{fossil}(t)$ whose integral over 1751-2025 is 500.6 Gt-C equal to the integral over the economic series of emissions from oil, coal and gas and cement plants
Fx(*t*):	*F1*(*t*) (Sec. 6), *F2*(*t*) (Sec. 10.9, Fig. 31-b), *FB*(*t*) (Sec. 6.1, Fig. 16) : impulse response functions
GPP:	Gross Primary Productivity (includes vegetation respiration)
Gt-C:	gigaton carbon; 1 Gt-C = 10^{12} kg C; Gt-CO_2: gigaton CO_2; 1 ton CO_2 = 273 kg-C
MLO:	Mauna Loa Observatory
NPP:	Net Primary Productivity, i.e. Carbon uptake by vegetation with the 24-hour respiration subtracted
ppm:	part per million number of molecules of one type per million molecules of air; 1 ppm CO_2 = 2.12 Gt-C
p_{CO2air}:	partial pressures of CO_2 in the air (µatm)
$p_{CO2seawater}$:	partial pressures of CO_2 in seawater (µatm)
Q(*t*):	cumulative fossil fuel emissions up to time t
R:	Revelle buffer factor between 9.5 to 12.5
Ref $^{13}C/^{12}C$:	reference for ratio $^{13}C/^{12}C$ (VPDB[11])
Ref $^{14}C/^{12}C$:	reference for ratio $^{14}C/^{12}C$ see note[12].
SPO:	South Pole Observatory
$SST_{20°S-20°N}$:	Sea Surface Temperature Sea surface temperature averaged between 20°S and 20°N
X(*t*):	mass of carbon in the air
X_{fossil} (*t*):	mass of carbon in the air from fossil fuels
$X_{natural}$ (*t*):	mass of carbon in the air from natural degassing
$X_{MLO}(t)$:	content of carbon dioxide in the atmosphere observed at MLO
$X_{MLOlogis}(t)$	275 + 555.72 / (1 + exp((2066.95 t)/ 42.16)) ppm extends X_{MLO}
Y(*t*):	mass of carbon in vegetation & soil
Z(*t*):	mass of carbon in the ocean

[11] $\delta^{13}C$ values are reported relative to the Vienna Pee Dee Belemnite (VPDB) standard, derived from a Cretaceous belemnite fossil from the Pee Dee Formation in South Carolina. See equation (13).

[12] For radiocarbon dating, the reference is usually Oxalic Acid I (HOx1) and II (HOx2) standards, normalized to $\delta^{13}C$ = –25‰ VPDB. $\Delta^{14}C$ (or $F^{14}C$) relative to an oxalic acid radiocarbon standard, but with $\delta^{13}C$ normalization to VPDB. VPDB is never used directly for radiocarbon $^{14}C/^{12}C$ — but it's still in the background, because radiocarbon results are corrected for isotopic fractionation using $\delta^{13}C$ vs. VPDB.

$Z_{ocs}(t)$: mass of carbon in the surface ocean
$Z_{ocd}(t)$: mass of carbon in the deep ocean
$\tau(t)$: ratio stock/out-flow for a reservoir (generally taken over 12 months)

Appendix B: TAlk Equation (22)

Let x=[OH^-]. Using K_{H2O} for the water autoprotolysis constant (i.e. K_w), k_1, k_2 for the first and second dissociation constants of carbonic acid, k_b for the borate dissociation constant, DIC for total dissolved inorganic carbon, and $B_T(S)$ for total boron (possibly scaled with salinity S), the total alkalinity equation can be written as equation (22), where TA (or TAlk) is the total alkalinity. Let's see what's the physical meaning of terms,

- First (fraction) term: carbonate alkalinity contribution from DIC, written in a form using [OH^-] via the relationships between [H^+], [OH^-], and the carbonate equilibria.
- Second term: borate alkalinity = $B_T(S)\times[B(OH)_4^-]$ expressed using [OH^-] (with k_b and K_{H2O} appearing because $[H+]=K_{H2O}/[OH^-]$).
- Third and fourth terms: contributions from water autoprotolysis: $-K_{H2O}/x$ is $-[H^+]$ (since $[H+] = K_{H2O}/[OH-]$), and +x is +[OH^-].

Now let's see what are the Units / dimensions used.

- x has units of $mol\cdot L^{-1}$ (or $mol\cdot m^{-3}$ depending on the concentration units used).
- K_{H2O} has units such that K_{H2O}/x yields a concentration (same units as x). If SI is used: K_{H2O} in $(mol\cdot m^{-3})^2$ so that $[H^+]=K_{H2O}/[OH^-]$ has $mol\cdot m^{-3}$ units, more commonly K_w is given in $(mol\cdot L^{-1})^2$ or $(mol\cdot m^{-3})^2$; One needs to be consistent with DIC and TA units.
- DIC and TA must use the same concentration units as x (e.g. $\mu mol\cdot kg^{-1}$, $mmol\cdot m^{-3}$, etc.).

Solving for x:

- this equation (22) is nonlinear in x. The standard approach is to solve for x numerically (e.g. Newton–Raphson). Use the form above to compute F(x)−TAlk and its derivative for Newton.
- If one prefers to solve for [H^+] instead, substitute $[H^+] = K_{H2O}/x$ and rewrite the equation in h=[H^+]; numerics can sometimes be more stable in h for very small/large values.